

**PERMITTIVITY BIOSENSOR FOR THE RECOGNITION OF SALIVA
SAMPLES OF COPD PATIENTS USING NEUROMORPHIC-BASED
MACHINE LEARNING**

Von der Fakultät 1 – MINT – Mathematik, Informatik, Physik, Elektro- und Informationstechnik der
Brandenburgischen Technischen Universität Cottbus–Senftenberg genehmigte Dissertation zur Erlangung
des akademischen Grades eines

Doktor der Ingenieurwissenschaften (Dr. -Ing.)

vorgelegt von

Pouya Soltani Zarrin

geboren am 29.09.1992 in Tabriz

Vorsitzende: Prof. Dr. Inga A. Fischer

Gutachter: Prof. Dr. Christian Wenger

Gutachter: Prof. Dr. Peter Langendörfer

Gutachter: Prof. Dr. Martin Ziegler

Tag der mündlichen Prüfung: 28.04.2021

**PERMITTIVITY BIOSENSOR FOR THE RECOGNITION OF SALIVA
SAMPLES OF COPD PATIENTS USING NEUROMORPHIC-BASED
MACHINE LEARNING**

Doctoral thesis approved by the faculty of MINT—Mathematics, Computer Science, Physics, Electrical Engineering, and Information Technology—of the Brandenburg University of Technology Cottbus-Senftenberg to obtain the academic degree of
Doctor of Engineering (Dr. -Ing.)

by

Pouya Soltani Zarrin

born on 29.09.1992 in Tabriz

Chairperson: Prof. Dr. Inga A. Fischer

Examiner: Prof. Dr. Christian Wenger

Examiner: Prof. Dr. Peter Langendörfer

Examiner: Prof. Dr. Martin Ziegler

Date of oral exam: 28.04.2021

*Dedicated to my family,
Leonis, Adeleh, Rahim, and Rana,
for their never-ending support along this journey*

Permittivity Biosensor for the Recognition of Saliva Samples of COPD Patients Using Neuromorphic-based Machine Learning

Pouya Soltani Zarrin

Doctor of Engineering Thesis, 2020

Faculty of MINT

The Brandenburg University of Technology

Abstract

Chronic Obstructive Pulmonary Disease (COPD) is an inflammatory lung disease, causing breathing difficulties in patients due to obstructed airflow in lungs. COPD is one of the main leading causes of death worldwide with an annual mortality rate of three million people. Despite the absence of an effective treatment for COPD, an early-stage diagnosis plays a crucial role for the effective management of the disease. However, majority of patients with objective COPD go undiagnosed until late stages of their disease due to the lack of a reliable technology for the recognition and monitoring of COPD in Point-of-Care (PoC).

Alternative diagnostic approaches such as the accurate examination of respiratory tract fluids like saliva can address this issue using a portable biosensor in a home-care environment. Nonetheless, the accurate diagnosis of COPD based on this approach is only possible by concurrent consideration of patients demographic–medical parameters. Therefore, Machine Learning (ML) tools are necessary for the comprehensive recognition of COPD in a PoC setting. On the other hand, drawbacks of cloud-based ML techniques for medical applications such as data safety, immense energy consumption, and enormous computation requirements need to be addressed for this application. Therefore, the objective of this thesis was to develop a ML-equipped system for the management of COPD in a PoC setup. A portable permittivity biosensor was developed in this work and its *in-vitro* performance was evaluated throughout clinical experiments. ML techniques were applied on biosensor results, demonstrating the significant role of these algorithms for the recognition of COPD. Moreover, developed ML models were deployed on a neuromorphic platform for addressing the shortcomings of cloud-based approaches.

Keywords: BiCMOS permittivity biosensors; COPD management; Saliva characterization; Bioneuromorphics; Precision diagnostic; Machine learning in medicine; Neuromorphic AI; Personalized healthcare.

Co-Authorship Statement

The thesis presented here has been written by Pouya Soltani Zarrin under supervision of Prof. Dr. Christian Wenger. Following chapters of this thesis have been published in peer-reviewed journals and conferences, for which I wish to acknowledge the contribution of co-authors.

Studies presented in Chapter 3 have been published as:

- P.S. Zarrin, F.I. Jamal, S. Guha, J. Wessel, D. Kissinger, C. Wenger. “Design and Fabrication of a BiCMOS Dielectric Sensor for Viscosity Measurements: A Possible Solution for Early Detection of COPD,” *Biosensors*, vol. 8, no. 78, 2018.
- P.S. Zarrin, F.I. Jamal, N. Roeckendorf, C. Wenger. “Development of a Portable Dielectric Biosensor for Rapid Detection of Viscosity Variations and Its In-Vitro Evaluations Using Saliva Samples of COPD Patients and Healthy Control,” *Healthcare*, vol. 7, no. 11, 2019.

Studies presented in Chapter 4 have been published as:

- P.S. Zarrin and C. Wenger. “Pattern Recognition for COPD Diagnostics Using an Artificial Neural Network and Its Potential Integration on Hardware-Based Neuromorphic Platforms,” *Springer LNCS (ICANN19)*, Munich, Germany, September, 2019, pp. 284–288.
- P.S. Zarrin, N. Roeckendorf, and C. Wenger. “In-vitro Classification of Saliva Samples of COPD Patients and Healthy Controls Using Machine Learning Tools,” *IEEE Access*, vol. 8, pp. 168053–168060, 2020.
- P.S. Zarrin and C. Wenger. “Implementation of Siamese-based Few-shot Learning Algorithms for the Distinction of COPD and Asthma Subjects,” *Springer LNCS (ICANN20)*, Bratislava, Slovakia, September 2020, pp. 431–440.

The study presented in Chapter 5 is published as:

- P. S. Zarrin, F. Zahari, M.K. Mahadevaiah, E. Perez, H. Kohlstedt, and C. Wenger. “Neuromorphic On-chip Recognition of Saliva Samples of COPD and Healthy Controls Using Memristive Devices,” In *Nature Scientific Reports*, 2020.

The study presented in Chapter 6 has been investigated during a 3-months exchange visit in France and is published as:

- P. S. Zarrin, R. Zimmer, C. Wenger, and T. Masquelier. “Epileptic Seizure Detection Using a Neuromorphic-compatible Deep Spiking Neural Network,” *Springer LNBI (IWBBIO20)*, Granada, Spain, 2020.

Acknowledgements

I would like to express my sincerest gratitude towards my supervisor, Prof. Dr. Christian Wenger, for his constant support and encouragement. This project would not have been possible without his supervision and guidance. I truly admire his way of supervising for providing a perfect balance of freedom and direction, while offering a constant support and guidance at every single step of this work. I could not have asked for a better supervisor.

I have been fortunate to be part of the IHP community with its outstanding personnel and long history of industrial and research excellence. This work would have not been possible without facilities and resources provided for researchers at IHP. I have had the full support from my colleagues with any technical and administrative issues throughout this project. Therefore, I would like to thank all of the staff at IHP for their support and assistance, especially Farabi Jamal, Mamathamba Kalishettyhalli, Eduardo Perez, Rita Winkler, Jan Schäffner, Yvonne Mausolf, Jan Wessel, Frank Popiela, Jay Witthaus, Harald Richter, Jens Lehmann, Rahul Yadav, and all other colleagues who supported me in any respect during the completion of this dissertation. Also, I truly appreciate the support from the IHP's Technology Department for the fabrication of chips.

Initial phase of this work was supported by the Federal Ministry for Education and Research (BMBF) of Germany under Grant No. 13U13862 for the EXASENS project. I would also like to thank the BioMaterialBank Nord (BMB Nord), popgen 2.0 network (P2N), and the German Center for Lung Research for the collection of saliva samples and the staff at FZ Borstel–Leibniz Lung Center for their precious support with the biological aspect of this work, especially Niels Roekendorf and Andreas Frey. I am grateful to the staff at the Nanoelectronics group, Faculty of Engineering of Kiel University, especially Finn Zahari and Hermann Kohlstedt for their precious support with the hardware implementation.

I would like to acknowledge the support from the department of science and technology of the French embassy in Berlin and the French national institute for research in computer science and automation (Inria) for funding the AI-Procope mobility grant, which provided me the possibility to visit CNRS–CerCo institute for a duration of 3 months. I would like to gratefully thank my internship supervisor, Dr. Timothée Masquelier for accepting my visit and supporting my stay at CerCo. I would like to thank all the staff at CNRS–CerCo (Centre de Recherche Cerveau & Cognition) for their support and encouragement during my visit. Though, this mobility project would not have been possible without the initial support of IHP, which encourages its employees to thrive and take advantage of every available opportunity.

Contents

Abstract	iv
Co-Authorship Statement	v
Acknowledgements	vii
Table of Contents	ix
List of Figures	xiii
List of Tables	xvi
Nomenclature and Acronyms	xvii
1 Introduction	1
1.1 Motivation	1
1.2 Research Objectives	2
1.3 Scope of Research	3
1.4 Overview of the Thesis	3
2 Literature Review	6
2.1 Introduction	6
2.2 Diagnosis	9
2.2.1 PoC Technologies for Salivary Biomarker Detection in Primary Care	11
2.3 Treatment	13

2.4	EU Medical Device Approval Regulation	14
2.5	System Design Specifications	15
2.6	Design Objectives and Overview	19
3	Biosensor Development	25
3.1	Design and Fabrication of a BiCMOS Dielectric Sensor	25
3.1.1	Introduction	25
3.1.2	Materials and Methods	29
3.1.2.1	First Generation of the Sensor	29
3.1.2.2	Second Generation of the Sensor	32
3.1.3	Results and Discussions	35
3.1.3.1	Calibration	35
3.1.3.2	Performance Assessment	36
3.1.4	Conclusions and Future Work	39
3.2	Development of a Portable Dielectric Biosensor and Its In-Vitro Evaluations	40
3.2.1	Introduction	40
3.2.2	Sensor Design and Integration	43
3.2.3	Experimental Setup	45
3.2.3.1	Mixture Detection	45
3.2.3.2	Clinical Evaluations	48
3.2.4	Results and Discussion	49
3.2.5	Conclusions and Future Work	54
4	Machine Learning Implementation	61
4.1	Pattern Recognition for COPD Diagnostics Using an Artificial Neural Network	61
4.1.1	Introduction	61
4.1.2	Materials and Methods	63
4.1.3	Results and Discussions	64
4.2	In-vitro Classification of Saliva Samples Using Machine Learning Tools	65
4.2.1	Introduction	66

Contents	xi
<hr/>	
4.2.2	Materials and Methods 68
4.2.2.1	Dielectric Characterization of Saliva Samples 69
4.2.2.2	Machine Learning Implementation for Classifications 70
4.2.3	Results and Discussions 73
4.2.4	Conclusions and Future Work 79
4.3	Implementation of Siamese-based Few-shot Learning Algorithms 80
4.3.1	Introduction 80
4.3.2	Materials and Methods 83
4.3.3	Results and Discussions 86
4.3.4	Conclusions and Future Work 88
5	Hardware Deployment 94
5.1	Neuromorphic On-chip Recognition of Saliva Samples Using Memristive Devices 94
5.1.1	Introduction 94
5.1.2	Materials and Methods 98
5.1.2.1	Data Preparation 98
5.1.2.2	Artificial Neural Network 99
5.1.2.3	Hardware Implementation 100
5.1.2.4	Performance Assessment 105
5.1.3	Results and Discussions 106
5.1.4	Conclusions and Future Work 110
6	Further Potential Applications 117
6.1	Epileptic Seizure Detection Using a Neuromorphic-compatible Spiking Network 117
6.2	BiCMOS Biosensors for the Recognition of SARS-CoV-2 122
7	Concluding Remarks and Future Work 131
7.1	Summary 131
7.2	Future Work 133
Appendices	134

A Technical Drawings and Expanded Views

List of Figures

2.1	Rate of decline in lung function for patients with COPD	7
2.2	Time course of the natural progression of lung function	8
2.3	Mechanisms and biomarkers in COPD pathophysiology	9
2.4	Basic steps to EU compliance	16
3.1	First generation of the dielectric biosensor	29
3.2	Modified chip with ESD-protection elements	30
3.3	Second generation of the biosensor with a quadruple configuration	32
3.4	Biosensor packaging	34
3.5	Measurement setup for the sensor calibration and validation	35
3.6	Calibration fit using the quadratic regression method	36
3.7	Viscosity and permittivity variation of the isopropanol-methanol mixture	38
3.8	Biosensor design schematic	44
3.9	System integration elements	45
3.10	Laptop-shaped foldable packaging of the biosensor	46
3.11	Sensor results for real part of the mixture permittivity	47
3.12	Sensor results for the imaginary part of the mixture permittivity	48
3.13	Clinical samples of saliva collected from HC and COPD patients	49
3.14	Results of m-VROC viscosity measurements	51
3.15	Results of the biosensor measurements for real part of permittivity	51
3.16	Results of biosensor measurements for the imaginary part of permittivity	52

4.1	ANN structure for the COPD pattern recognition and prediction	64
4.2	Measurement setup for the real–imaginary parts of the permittivity of saliva samples	71
4.3	Violin plot of the dataset attributes used for classifications	72
4.4	Hierarchical categorization of saliva samples into extended subgroups	74
4.5	Distribution graph for saliva samples of COPD and HC	75
4.6	Results of the biosensor output for the dielectric characterization	76
4.7	Confusion matrices of the XGBoost algorithm	78
4.8	Four groups of saliva samples available within the Exasens dataset	83
4.9	Required steps for developing a siamese classifier	84
4.10	Zero-shot learning scheme for the recognition of asthma vs. COPD.	85
4.11	One-shot and five-shot learning schemes for training–evaluations.	86
5.1	Conversion of analog attributes into binary bits	98
5.2	ANN simulation topology for the classification of saliva samples	100
5.3	Multilevel thresholding of network analog parameters for hardware implementation	101
5.4	CMOS-integrated RRAM array of IHP	102
5.5	Assignment of memristive devices for the replication of parameters	104
5.6	Conversion of input bits into physical voltage values	105
5.7	Confusion matrices for the recognition of COPD and HC samples	107
6.1	Architecture of the developed deep SNN for the epileptic seizure detection.	120
6.2	Confusion matrix for the SNN performance on unseen test data	121
6.3	Architecture of a neural network for the classification of SARS-CoV-2.	126
A.1	Expanded view of the biosensor packaging	135
A.2	Technical drawing for the sensor holding part	136
A.3	Technical drawing for the microcontroller housing	137
A.4	Technical drawing for the display cover	138
A.5	Expanded view of the laptop-shaped foldable packaging	139
A.6	Technical drawing for the biosensor housing	140

A.7 Technical drawing for the interface housing 141

List of Tables

- 2.1 Various technologies used for the detection of biomarkers in saliva samples. 12

- 3.1 Dielectric constant of utilized materials 35
- 3.2 Results of the sensor verification experiments for methanol dielectric constant. 37
- 3.3 Results of performance evaluation of the second generation of the dielectric sensor. 37
- 3.4 Results of complex permittivity measurements for COPD and HC 50

- 4.1 Performance of ML models for the classification of the first dataset 76
- 4.2 Performance of ML models for the classification of the second dataset 77
- 4.3 Results of zero-, one-, and five-shot learning schemes 87

- 5.1 Performance of the ANN with analog parameters. 105
- 5.2 Performance of the ANN with 10-level resolution. 106
- 5.3 Performance of the memristive neuromorphic chip. 108

- 6.1 Performance of the introduced SNN compared to DNNs. 121
- 6.2 Available RIDTs for the PoC diagnosis of SARS-CoV-2. 124

Nomenclature and Acronyms

Acronyms

1T-1R	1-Transistor-1-Resistor
3D	Three-Dimensional
AI	Artificial Intelligence
AIMDD	Active Implantable Medical Device Directive
ANN	Artificial Neural Network
CA	Competent Authority
COPD	Chronic Obstructive Pulmonary Disease
CMOS	Complementary Metal–Oxide–Semiconductor
CRP	C-reactive Protein
CT	Computerized Tomography
DRE	Drug-Resistant Epileptic
DNN	Deep Neural Network
EC	European Commission
EEG	Electroencephalography
ELISA	Enzyme-linked Immunosorbent Assay
ESD	Electrostatic Discharges
EU	European Union

FEV ₁	Forced Expiratory Volume in 1 second
FN	False Negative
FP	False Positive
FSL	Few-Shot Learning
FVC	Forced Vital Capacity
GNB	Gaussian Naïve Bayes
GOLD	Global initiative for chronic Obstructive Lung Disease
HC	Healthy Controls
HfO ₂	Hafnium(IV) Oxide
HNN	Hardware-based Neural Network
HRS	High Resistivity State
IDC	Interdigitated Capacitors
iEEG	intracranial electroencephalography
IHP	Innovations for High Performance
IL-6	Interleukin 6
IL-8	Interleukin 8
IoT	Internet-of-Things
ISPVA	Incremental Step Pulse with Verify Algorithm
IVDD	In-Vitro Diagnostic Directive
LoC	Lab-on-Chip
LR	Logistic Regression
LRS	Low Resistivity State
MDD	Medical Device Directive
MEMS	Micro Electro Mechanical Systems
ML	Machine Learning
MMP-8	Matrix Metalloproteinase-8

MMP-9	Matrix Metalloproteinase-9
MUT	Material-Under-Test
m-VROC	Microfluidic Viscometer-Rheometer-on-Chip
NB	Naïve Bayes
NE	Neutrophil Elastase
PCB	Printed Circuit Board
PoC	Point-of-Care
RF	Radio Frequency
RIDT	Rapid Influenza Diagnostic Tests
RMS	Root-Mean-Square
RRAM	Resistive Random Access Memory
RT-PCR	Reverse Transcriptase-Polymerase Chain Reaction
SARS-CoV	Severe Acute Respiratory Syndrome Coronavirus
SMU	Source Measurement Unit
SNN	Spiking Neural Network
SNR	Signal-to-Noise Ratio
SOP	Standard Operating Procedure
SVM	Support Vector Machines
TN	True Negative
TNF- α	Tumor Necrosis Factor- α
TORCH	Towards a Revolution in COPD Health
TP	True Positive
WHO	World Health Organization
XGBoost	eXtreme Gradient Boosting

Variables

ε^*	Complex permittivity
ε_∞	High-frequency permittivity limit of a material
ε'_r	Real part of relative permittivity
ε''_r	Imaginary part of relative permittivity
$\varepsilon_{r,eff}$	Effective permittivity
ε_s	Static permittivity
ε_h	Notional high-frequency permittivity limit
σ	Conductivity
σ_{ion}	Ionic conduction of a material
q	Mixing ratio
f	Functioning frequency
f_r	Relaxation frequency of a material
V_{read}	Read-out voltage
X_i	Analog output signal for perceptron i

Units

μA	microamper
cm	centimeters
mm	millimeters
μm	micrometers
nm	nanometers
mm^2	millimeters square
Kg	Kilograms
mg	milligram
ng	nanogram

pg	picogram
mL	milliliter
μL	microliter
KPa	KiloPascals
GPa	GigaPascals
Hz	Hertz
V	Volt
mV	millivolt
s	Seconds
μs	microsecond
h	Hour
mPa·s	millipascal second
$^{\circ}\text{C}$	degree celsius
nJ	nanoJoule

Chapter 1

Introduction

1.1 Motivation

Chronic Obstructive Pulmonary Disease (COPD) is an inflammatory lung disease, causing breathing difficulties in patients due to obstructed airflow in lungs [1]. COPD is one of the main leading causes of death worldwide with an annual mortality rate of three million people [2]. The growth of COPD is significantly due to increase in tobacco use (including active smoking or secondhand smoke) and the air pollution [1]. Apart from its economical burden for healthcare systems, COPD drastically impacts patients' life quality by restricting their physical activities. Despite the absence of an effective treatment for COPD, an early-stage diagnosis plays a crucial role for the effective management of the disease [3]. However, majority of patients with objective COPD go undiagnosed until late stages of their disease due to the absence of necessary Point-of-Care (PoC) technologies. As a result, development of personalized solutions for the COPD management has been significantly promoted by the contemporary healthcare systems for providing patients with appropriate medical assistance in an outpatient clinic or a home-care environment [4]. Analyzing lung capacity of patients using a spirometer is the most common and rudimentary method for diagnosing COPD. However, its bulky size, operation complexity, high cost, and lack of portability limit its application in real-world PoC devices [4]. On the other hand, silicon-based technologies such as Complementary Metal–Oxide–Semiconductor (CMOS) provide countless advantages for PoC applications such as miniaturization, portability, high accuracy, reliability, low cost, low power consumption, and integrability with neuromorphic computing technologies for Artificial Intelligence (AI) approaches [5].

1.2 Research Objectives

In spite of recent advancements in developing biosensors for various biomedical applications, a reliable technology for early diagnosis and monitoring of COPD in a PoC environment is still missing. This is due to the fact that the abovementioned shortcomings of spirometry, the most common method for COPD diagnostic, have limited its application in PoC environments. However, alternative diagnostic approaches such as the accurate examination of respiratory tract fluids like saliva can address this issue by identifying bacterial infections using a portable biosensor in a home-care environment. Hence, regular screening of mechanical and electrical properties of patients' saliva can lead to important information for staging COPD. Nonetheless, the accurate diagnosis of the disease based on this approach is only possible by concurrent consideration of various demographic—medical parameters related to patients. Therefore, advanced AI-based analytical tools are required for the comprehensive recognition of COPD in a PoC setting. On the other hand, drawbacks of cloud-based AI techniques for PoC medical applications such as data safety, immense energy consumption, and enormous computation requirements need to be addressed for real-world applications. For this purpose, neuromorphic platforms can be used for the hardware-based deployment of AI techniques on PoC COPD management devices for the on-chip processing of acquired data without cloud communications. By taking into account these issues, the objectives of this thesis are as follows:

1. To design and develop a CMOS-based permittivity biosensor for the real-time characterization of respiratory tract fluids such as saliva.
2. To integrate the developed permittivity biosensor into a handheld device for the rapid characterization of saliva samples in a PoC environment and to evaluate its *in-vitro* performance using clinical samples of COPD patients and Healthy Controls (HC).
3. To apply Machine Learning (ML) techniques on the data obtained from investigating saliva samples of COPD patients and HC for diagnostic classification and pattern recognition purposes.
4. To implement meta learning models such as few-shot learning for making the system resilient against adversarial diseases like asthma with a similar mechanism to COPD.
5. To deploy the developed ML models on IHP's memristive neuromorphic platform for the on-chip recognition of saliva samples of COPD and HC.

6. To apply the proposed PoC diagnosis approach for the management of other chronic diseases such as the epileptic seizure detection, as the potential application of the technology in the future.

1.3 Scope of Research

Researchers at the Innovations for High Performance (IHP) Microelectronics have been extensively working on the development of CMOS-based sensors and neuromorphic chips for various biomedical and industrial applications. It has been shown that the well-established CMOS technology offers numerous advantages for medical applications such as high accuracy, low-power consumption, reliability, portability, low cost, operation simplicity, and compatibility with label-free measurements [5]. In addition, IHP's neuromorphic chips have provided reliable performance for various real-world applications such as digit recognition [6]. However, this thesis investigates the possibility of using IHP's CMOS-integrated biosensors and neuromorphic chips for the on-chip characterization of saliva samples of COPD and HC subjects. The specific focus of this work is on the development of an AI-equipped system for the management of COPD in a PoC setup. Therefore, a portable permittivity biosensor has been developed in this work and its *in-vitro* performance has been evaluated throughout clinical experiments. A novel dataset reporting the results of these experiments were prepared and reported online for the public use. In addition, various ML techniques have been applied on the obtained results, demonstrating the significant role of AI-based techniques for the management of COPD. Moreover, deployment of these ML models on IHP's neuromorphic platforms has shown the practicality and importance of using neuromorphic chips for biomedical applications.

1.4 Overview of the Thesis

The structure of this thesis is summarized in the outline below:

Chapter 1 Introduction: The introductory chapter.

Chapter 2 Literature Review: Introduces COPD and its biological mechanism as well as the state-of-the-art technologies for COPD diagnosis and treatment.

Chapter 3 Biosensor Development: Presents the development of a permittivity biosensor and its system integration for the characterization of saliva samples of COPD patients and healthy controls.

Chapter 4 Machine Learning Implementation: Presents the implementation of neuromorphic-compatible machine learning tools for the classification of saliva samples on simulation models.

Chapter 5 Hardware Deployment: Presents the hardware implementation of the proposed machine learning simulation models on a memristive neuromorphic platform for on-chip recognition.

Chapter 6 Further Potential Applications: Presents the potential of the introduced technology for further biomedical applications.

Chapter 7 Concluding Remarks and Future Work: Highlights the contributions of this work and required enhancements and discusses the further relevant biomedical applications as future work.

Appendix I Technical Drawings for the System Packaging

Appendix II Permissions and Approvals

Bibliography

- [1] P.J. Barnes. “Mechanisms in COPD: Differences from asthma,” *Journal Chest*, vol. 117, no. 2, pp. 10S—14S, 2000.
- [2] C.D. Mathers, D. Loncar. “Projections of global mortality and burden of disease from 2002 to 2030,” *PLoS Medecine*, vol. 3, no. 442, 2006.
- [3] N.G. Csikesz, E.J. Gartman. “New developments in the assessment of COPD: Early diagnosis is key,” *International Journal Chronic Obstructive Pulmonary Disease*, vol. 9, pp. 277—286, 2014.
- [4] D. Price, A. Crockett, M. Arne, B. Garbe, R. Jones, A. Kaplan, A. Langhammer, S. Williams, B. Yawn. “Spirometry in primary care case-identification, diagnosis and management of COPD,” *Primary Care Respiratory Journal*, vol. 18, no. 216, 2009.
- [5] Y.H. Ghallab, Y. Ismail. “CMOS based lab-on-a-chip: Applications, challenges and future trends,” *IEEE Circuits and Systems Magazine*, vol. 14, no.2, pp. 27—47, 2014.
- [6] C. Wenger, F. Zahari, M.K. Mahadevaiah, E. Perez, I. Beckers, H. Kohlstedt, and M. Ziegler. “Inherent Stochastic Learning in CMOS-Integrated HfO₂ Arrays for Neuromorphic Computing,” *IEEE Electron Device Letters*, vol. 40, no. 4, pp. 639—642, 2019.

Chapter 2

Literature Review

2.1 Introduction

Chronic Obstructive Pulmonary Disease (COPD) is an inflammatory lung disease, causing breathing difficulties in patients due to obstructed airflow in lungs [1]. COPD is one of the main leading causes of death worldwide with an annual mortality rate of three million people [2]. It has been predicted that COPD will be the third leading cause of death in developed countries by 2030 due to its high mortality and morbidity rates [2]. Apart from its economical burden for healthcare systems, COPD drastically impacts patients' life quality by restricting their physical activities. The major cause of COPD, in developed countries, is the long-term exposure of subjects to either tobacco smoke (being an active–secondhand smoker) or other lung-irritants such as air pollution, chemical fumes, or industrial dust [3,4]. However, biomass smoke exposure is independently associated with an increased risk of COPD for non-smoker patients, especially in the developing world [5,6]. Furthermore, in some scarce cases, a genetic condition called alpha-1 antitrypsin deficiency may also contribute to lung damages and COPD [3]. Individuals with objective COPD experience an out of proportion decline in their lung function caused due to the inflammation in the small airways and progressive destruction of lung parenchyma [7]. In addition, patients with COPD experience airway obstruction and mucus hypersecretion; leading to respiratory acidosis, and pulmonary hypertension [8]. The main symptoms of COPD are shortness of breath, chronic coughs, wheezing, chest tightness, and abnormal sputum (mucus) production. However, patients with severe COPD often complain about weight loss, chest pain, and mental deterioration [1]. The manifestations of this disease are heterogeneous,

resulting in a wide range of clinical phenotypes including lung cancer or heart diseases, as reflected in the recent Global initiative for chronic Obstructive Lung Disease (GOLD) guidelines [3,4]. Although an absolute cure for reversing caused lung damages by the disease has yet to be found, an early-stage diagnosis has shown to have a pivotal role for the effective management of COPD [9, 10]. Nevertheless, majority of patients with objective COPD go undiagnosed until late stages of their disease due to the absence of necessary Point-of-Care (PoC) technologies. In fact, COPD is mainly underdiagnosed in younger subjects and overdiagnosed for elderly because of lack of accurate testing among symptomatic patients, resulting in inappropriate therapy and delayed diagnosis of other treatable conditions [11]. As a result, development of personalized solutions for the COPD management has been significantly promoted by contemporary healthcare systems for providing patients with appropriate medical assistance in an outpatient clinic or a home-care environment [3, 9]. In addition, recent studies have shown that the most rapid decline in lung function occurs at early stages of the disease, in contrast to previous reports claiming accelerated decline rate as the disease progressed over time, highlighting the importance of the early recognition of COPD [7]. This fact has been thoroughly studied by Tantucci *et al.* that the mean rate of Forced Expiratory Volume in 1 second (FEV_1) decline is greatest in GOLD Stages II and III COPD and it slows down as COPD advances in its course, as demonstrated in Figure 2.1. As a result, the early identification of patients with

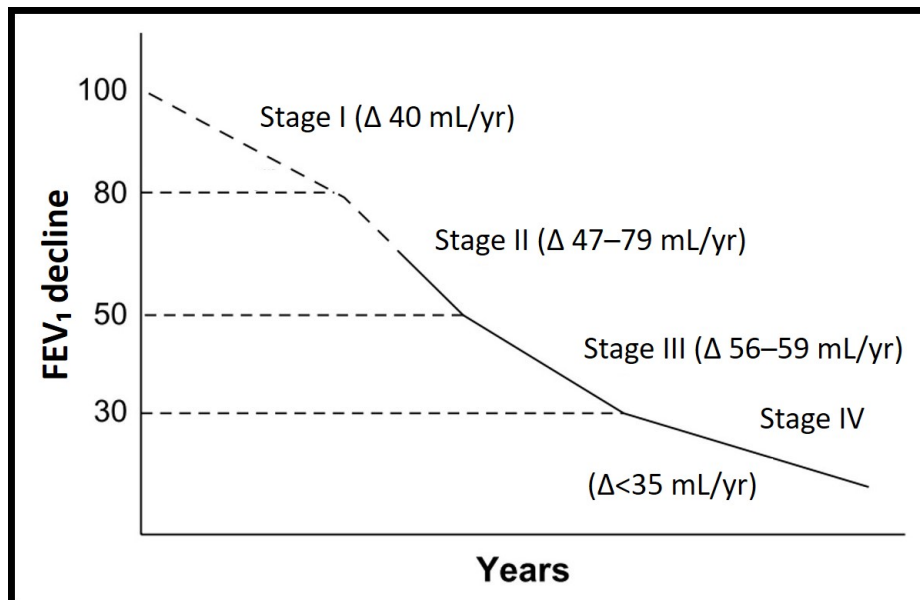


Figure 2.1: Recent evaluation of rate of decline in lung function for patients with COPD demonstrating that the largest decline may occur at early stages of the disease [7].

COPD enables practitioners to appropriately recognize exacerbations of this chronic lung disease, initiating required pharmacologic therapy early in the course of COPD to prevent the disease progression. In addition, as shown in Figure 2.2, susceptible smokers experience a steeper decline in the FEV₁ rate with advancing age, demonstrating the significant impact of smoking cessation at early ages for preventing the disease progress [8]. Therefore, aggressive testing strategies, smoking-cessation efforts, and the initiation of treatments are beneficial and required at early stages of COPD for reducing the extensive morbidity and mortality of this disease [9, 11].

Figure 2.3 represents the pathophysiology of COPD and its mechanisms and biomarkers. Understanding the mechanism of the disease and tracking biomarkers and products related to the evolution of the inflammation caused by COPD can lead to an improved follow-up and outcome prediction for patients. COPD outcomes are result of an enhanced protective response of patients to oxidative stresses caused by cigarette smoking or exposure to other environmental noxious gases [11]. Acute exacerbations represent an even more enhanced response of body to infections such as virus, bacteria, or other inhaled allergens through air pollution. As shown in Figure 2.3, upon the exposure to these agents, patients' body stimulates macrophages and epithelial cells to signal the production of inflammatory products such as IL-6, IL-8, MMP-8, MMP-9, CRP, NE, and TNF- α at the lung parenchyma by the neutrophils [11]. Although these

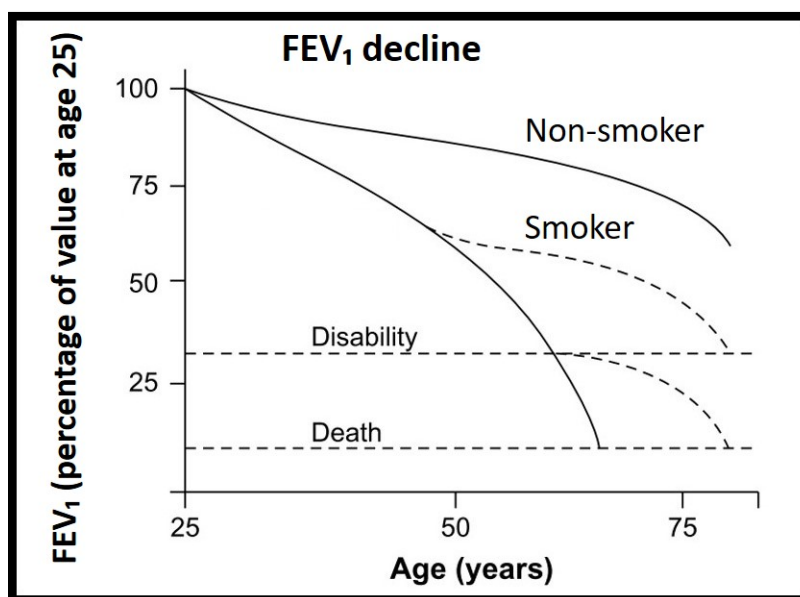


Figure 2.2: Conventionally accepted time course of the natural progression of lung function as a result of exposure to smoking [8].

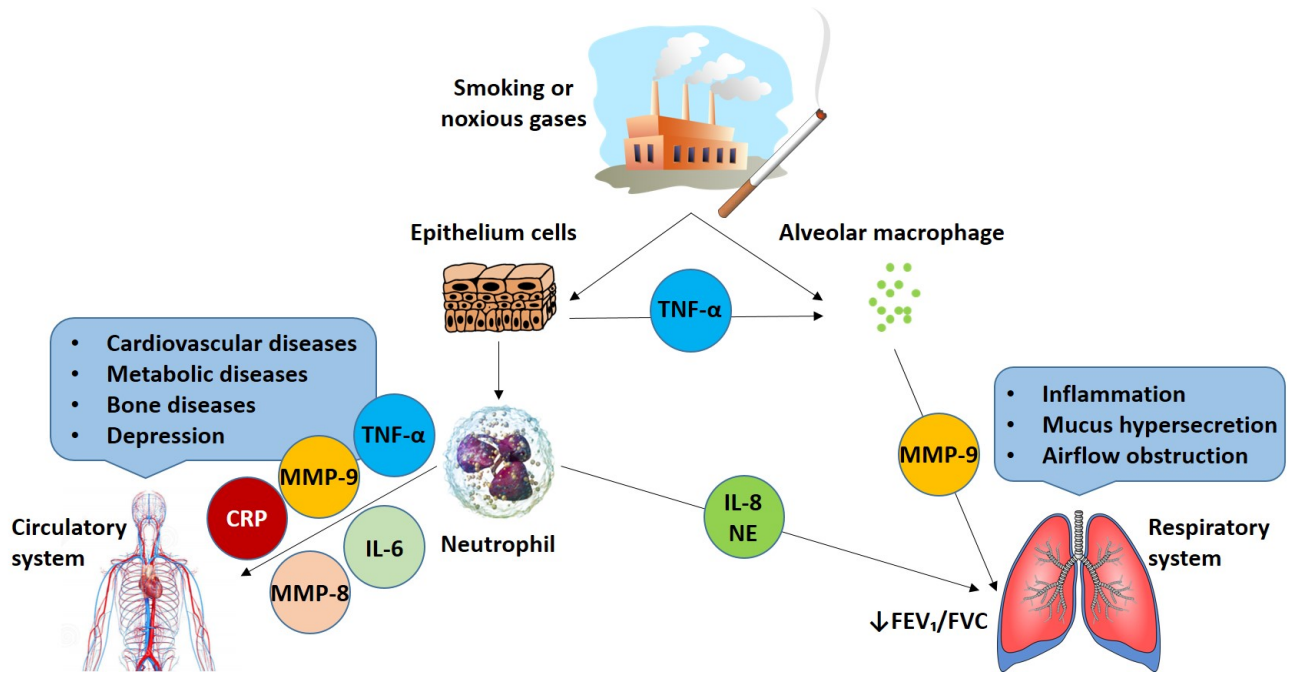


Figure 2.3: Mechanisms and biomarkers in COPD pathophysiology.

biomarkers are also involved in other inflammatory diseases like asthma and idiopathic pulmonary fibrosis, comprehensive analysis of their concentrations and variations can lead to the accurate diagnosis and management of COPD in a PoC environment [11].

2.2 Diagnosis

The clinical ground truth methodology for diagnosing COPD is comprehensively reported within the GOLD guidelines [3]. Among available screening and detection methods, spirometry pulmonary function test is the most rudimentary and systematic method in primary care for the diagnosis of COPD [5, 6]. Along this test, the lung capacity of patients is measured during breathing in–out cycles by considering following indexes: Forced Expiratory Volume in 1 second (FEV_1) and the Forced Vital Capacity (FVC). An $FEV_1/FVC < 0.70$ has been defined as the threshold for the diagnosis of COPD, while the decrease of this ratio is an indicator of the disease progression [5,6]. Using this ratio, healthcare providers diagnose the state of illness in primary and secondary care using well-established analysis criteria for the spirometry method.

Application of spirometry test has been hindered in PoC environments due to following issues: spirometry is highly dependent on skilled operators for the evaluation of the results, considering the quality

and calibration complexity of the utilized device and its sensitivity to environmental temperature variations [5, 9, 11]. In addition, this test is not advised to patients with specific medical conditions such as cardiac problems or dementia, thus limiting its applicability to a broad population of aged users. Furthermore, various error sources can impair the accuracy of exam results such as false start of the test, leakage in the system, coughing, or hesitation during the expiration. Moreover, the main disadvantage of spirometry is its inability to predict patient outcome, making the approach insufficient for preventing acute exacerbations of COPD [5, 9, 11]. Moreover, according to a study by Haroon *et al.*, COPD is widely under-diagnosed due to the limited sensitivity of the spirometry test in the range of 64.5–79.9% [12]. Therefore, the abovementioned shortcomings of spirometry method as well as its bulky size, operation complexity, high cost, and lack of portability make it an inadequate approach for the daily management of COPD in a PoC environment [9, 11].

As an alternative approach, impulse oscillometry and specific airway conductance measurement have been recommended for the early detection of COPD [13–15]. Despite the capability of these techniques for identifying more subtle changes in lung function at early stages compared to traditional spirometry, their operation complexity and lack of portability limit their application for PoC use.

As presented in the literature, imaging techniques such as Computerized Tomography (CT) scan and radiology tools have been widely used for screening respiratory diseases such as lung cancer or COPD [16, 17]. The integration of imaging techniques with advanced machine learning tools enables the accurate prognosis of COPD through this approach. However, the bulky size, high cost, and skilled operator requirements of this method limits its use in PoC setups.

Considering the high correlations between the COPD severity state and protein biomarkers present in body fluids such as blood, sputum, and saliva, accurate analysis and monitoring of these biomarkers can lead to early prediction and identification of COPD and its potential exacerbations [11]. A biomarker, in principal, is a biological molecule found in body fluids or tissues, which is an indicator of the presence of a condition, disease, or a normal–abnormal process. Nonetheless, there are no such a specific molecule in routine clinical use for the diagnosis or management of COPD [9, 11]. Recent studies have investigated the correlation of COPD with combination of several cytokines, chemokines, proteases, and biomarkers and their concentrations in sputum or saliva [18–22]. Although sputum is highly relevant for monitoring lung diseases considering its close proximity to protein, bacterial, and viral agents existing in patient lungs, its

invasive acquisition procedure makes it unfavorable for daily applications [11]. On the other hand, saliva offers a better patient compliance for routine testing of COPD biomarkers on the spot. The presence of biomarkers in saliva occurs from the production of this fluid in highly vascularized salivary glands. Thus, salivary components derive from the blood by passive diffusion or active transport, making it a suitable medium for the recognition of COPD biomarkers in PoC environments. However, drawbacks of using saliva such as presence of lower concentration of targeted biomarkers and the presence of undesired substances in the sample need to be considered for designing detection methods and choosing proper panel of biomarkers for the detection of COPD [11].

The low concentration levels of protein biomarkers in saliva makes their detection extremely challenging, thus requiring precise and sensitive protein detection techniques [11]. For instance, Enzyme-linked Immunosorbent Assay (ELISA) is a standard technique for analyzing protein biomarkers in body fluids with remarkably high accuracy, sensitivity, and specificity. However, its drawbacks in terms of high cost, time consuming procedure, and incapability for miniaturization and automation restrict its PoC application.

As shown in Figure 2.3, combination of a few biomarkers can provide promising results for the diagnose and early-onset detection of COPD exacerbations. These biomarkers include, but not limited to: CRP, IL-8, IL-6, NE, TNF- α , MMP-8, and MMP-9 [11]. Following value ranges have been reported in the literature for these biomarkers for healthy subjects: CRP:0,05—64,3 mg/mL; IL-6:1,3—53,9 pg/mL; IL-8: 54,9—1455,7 pg/mL; MMP-8: 0,531—754 ng/mL; MMP-9: 73,22—195,42 ng/mL; NE: 100—253 ng/mL; TNF- α : 2,7—19,7 pg/mL. On the other hand, according to literature, higher concentrations of MMP-9, CRP, NE, and TNF- α can be found in saliva for COPD patients with an FEV₁/FVC ratio smaller than 70%. Associations between these biomarkers and the severity of the disease can lead to the early staging of COPD through saliva examination [11, 23–26].

2.2.1 PoC Technologies for Salivary Biomarker Detection in Primary Care

Table 2.1 presents various technologies that have been used for the detection of existing biomarkers in saliva samples. These technologies include, but are not limited to, Lab-on-Chip (LoC) biosensors, electrochemical colorimetrics, chemiluminescence, magnet immunosensors, fluorescence-based fiber optic sensors, electrophoresis-based methods. For example, Nie *et al.* has proposed a fluorescence-based LoC biosensor for monitoring IL-8 and MMP-9 in saliva samples [27]. The introduced system required a sam-

Table 2.1: Various technologies used for the detection of biomarkers in saliva samples.

Technology	Biomarker	Sample quantity (μL)	Time (min)
Fluorescence LoC [27]	IL-8/MMP-9	20	70
Fluorescence LoC [30]	CRP	200	30
Colorimetric LoC [31]	CRP	NA	12
Electrophoresis LoC [28]	CRP/IL-6/TNF- α	10	10
Fluorescence optical fiber [32]	IL-6/IL-8	100	150
Electrochemical IL-6 [33]	IL-6	25	245
Colorimetric immunoassay [29]	MMP-8/MMP-9	15	NA

ple volume of 20 μL for measurements and was capable of providing results within 70 minutes. Although the small sample quantity requirement of the setup makes it comfortable for daily use by patients, its time-consuming and complex procedure is a drawback for home-care applications. In a different approach, an electrophoretic immunoassay was designed and developed for monitoring the concentration of salivary CRP, IL-6, TNF- α , and MMP-8 [28]. The developed biosensor was capable of examining patient saliva with sample volume of 10 μL within 10 minutes. Similar to a conventional electrophoresis technique, the system separated molecules by their size and electrical charge through the application of electrical current. Despite its rapid measurement capability, the low accuracy and complicated operation of the system made it inadequate for daily application. Yee *et al.* has introduced a colorimetric immunoassay for the recognition of MMP-8 and MMP-9 in human saliva of periodontal disease patients [29]. In this work, antibodies were injected through a controlled flow and the sample was placed on the sensing area for the biomarker concentration detection through luminescent quantification technique. The setup required a microscope for measurements, revealing its inability for portable applications at home-care.

The following points have been highlighted thorough literature study, which need to be considered for the diagnosis and classification of COPD in a PoC environment:

1. Patient perception of the disease and symptoms merely related to lung function decline are not the best markers for the early recognition of lung destruction during COPD.
2. Considering the enormous crossover between respiratory symptoms and objective diseases, clinical correlation remains of paramount importance, regardless of the intended diagnostic technique.

3. The simplicity, low price, testing time, sample volume, accuracy, and sample preparation requirements are vital points, which need to be taken into consideration for designing PoC diagnostic tools.

2.3 Treatment

Smoking cessation is considered as the initial step for the treatment of COPD, since it slows down the process of lung function decline in patients. Several studies have reported significant improvements for patients' FEV₁ decline over a 5-year period of smoking cessation. In addition, smoking cessation is of ultimate benefit for reducing the mortality of COPD, regardless of the disease severity stage. Although this benefit might root in cardiovascular mortality reduction rather than an effect on respiratory-related mortality, the overall benefit to patients remains the same [34]. Similar to smoking cessation, decreasing or eliminating exposure to biomass or other lung-irritant agents is also of significant impact for the treatment of non-smoking-related COPD patients [35].

Several studies have scrutinized the efficiency of bronchodilator therapy such as tiotropium for treating COPD patients [36]. It has been shown that the inhaled bronchodilators with or without inhaled corticosteroids improve patient outcome by limiting the FEV₁ decline and reducing the disease exacerbations. As an example, a study called Towards a Revolution in COPD Health (TORCH) has investigated the effect of inhaled salmeterol and fluticasone, either alone or in combination, in patients with moderate or severe COPD [37]. This double-blind placebo-controlled trial showed the efficiency of these prescribed treatment for reducing the FEV₁ decline in patients and resulting in fewer acute exacerbations.

As a different approach, anti-inflammatory drugs have been identified for benefiting patients with severe COPD as a steroid-sparing therapy [1, 38]. For instance, a recent trial of high-dose N-acetylcysteine in patients with stable COPD has shown significant reduction in the disease exacerbations and remarkable improvements in the spirometric measurement of small-airway function, without any significant adverse effects [38]. N-acetylcysteine is a well-established drug for the treatment of pulmonary fibrosis, which is known to have both mucolytic effects and anti-inflammatory–antioxidant properties with notable clinical benefits for the prevention of contrast-induced nephropathy and COPD.

In addition to conventional therapies, pulmonary rehabilitation has shown to be beneficial for patients with moderate-to-severe COPD, improving their exercise capacity and health-related quality of life [39,40].

Although, further investigations are necessary to confirm these findings, counseling patients to increase physical activity should likely be an essential component of their therapy for the effective management of newly diagnosed COPD cases.

2.4 EU Medical Device Approval Regulation

According to the regulatory approval process for medical devices in European Union (EU), a medical device is defined as an instrument, apparatus, implant, *in-vitro* reagent, or any similar article which can be used for diagnosing, preventing, or treating diseases and medical conditions [41, 42]. Example of such devices include simple devices such as disposable gloves, thermometers, or tongue depressors as well as advanced instruments used for conducting medical testing, surgical operations, or implants.

The current EU system is governed by three European Commission (EC) directives:

1. Medical Device Directive (MDD): Covering variety of devices such as heart valves, orthopaedic implants, and medical software.
2. *In-Vitro* Diagnostic Directive (IVDD): Including devices used for the examination of bio-specimens taken from the human body such as blood-glucose self-testing strips and pregnancy self-testing devices.
3. Active Implantable Medical Device Directive (AIMDD): This category of devices require external power sources for their function like pacemakers and implantable defibrillators.

General guidelines for approval are laid out in these EC directives, but the final approval systems are coordinated within each country. A medical device manufacturer, seeking to market a new medical device in the EU, selects a proper Competent Authority (CA) within their zone for certifying the new device application. According to the device classification, the CA requests certain materials (e.g. a literature review or clinical data) and performs a quality assessment on the manufacturing process. Upon satisfactory review and approval, a regulatory certificate would be awarded for the device, enabling its access to the EU market [41].

Classification of medical devices through EU regulations is a risk-based system, taking into account the vulnerability of human body to the potential risks associated with the intended device [41]. According to the

Annex IX of the European framework directive, there are four classes of medical devices: Class I, IIa, IIb and III. The medical devices of Class III hold the highest risk with a permanent monitoring requirement for their lifetime duration. Such devices are, as examples, cardiovascular catheters, aneurysm clips, hip joint implants, prosthetic heart valves, and vascular stents. The Class I devices pose the lowest perceived risk to human and depending on their function and sterilization requirements their assessment and approval process differs. Example of such devices are personal protection kits, stethoscopes, corrective glasses, non-sterile wound dressings. Medical devices of Class IIa could be such as surgical gloves, hearing aids, diagnostic ultrasound machines, lancets, and tracheal tubes. This category usually constitutes low to medium risk to users. Patients should use them for a short-term period, any less than 30 days. Similarly, medical devices categorized as Class IIb pose medium to high-risk to their users and are intended for applications longer than 30 days. These devices include long-term corrective contact lenses, surgical lasers, defibrillators, intra-ocular lenses, and surgical lasers. The determination of these classes are performed through various criteria such as the duration of device contact with the user's body, the degree of invasiveness, part of body contacted by device, active vs. non-active functionality of the device, the intended use for the introduced device. Among these criteria the duration of time factor ranges from less than 60 minutes (Transient) to less than 30 days use (Short-term), while more than 30 days represents a device with long-term use. In addition, the degree of invasiveness is determined whether a device is implantable or surgically invasive or non-invasive, and whether it has an application to body surface or an orifice.

Figure 2.4 demonstrates the basic steps for the EU medical device compliance. The overall registration process varies in terms of timeline, complexity, and cost for different classes [42]. The approval time for registering different classes might take 3 to 9 months depending on the device, while the validity of the issued certificate is for a 3-years period regardless of the device's risk class. As a result, a post-market surveillance and vigilance is required for all medical devices sold in the EU.

2.5 System Design Specifications

The World Health Organization (WHO) has defined following criteria as a benchmark for identifying the most appropriate diagnostic tests for resource-constrained settings such as in PoC: Affordable, Sensitive, Specific, User-friendly, Rapid and robust, Equipment-free and Deliverable to end-users (ASSURED). The

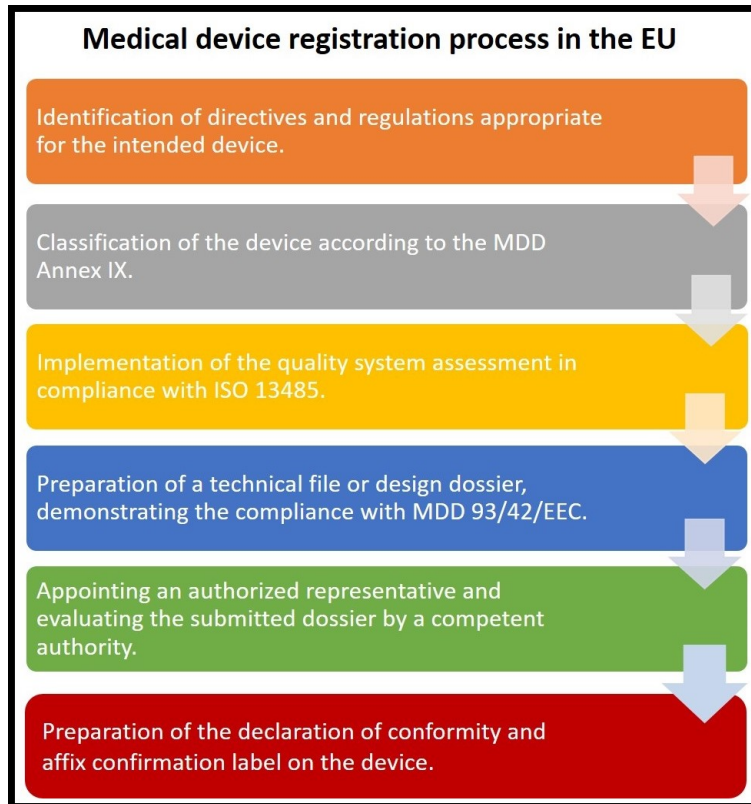


Figure 2.4: Basic steps to EU compliance [41].

ASSURED criteria were proposed for the proper design of PoC diagnostic devices, where laboratory infrastructure is weak. Therefore, following these criteria is necessary for developing a diagnostic device for analyzing saliva and sputum biomarkers near, or at, the point of patient care. Point-of-care testing can significantly improve the COPD management process by optimizing treatment decision-making, avoiding referrals, increasing the efficiency of care, while reducing the ultimate costs. Nevertheless, the ASSURED criteria are generic and need to be adapted to each diagnostic application. Therefore, a list of the most important design requirements for the COPD recognition is provided as follows:

- **Intended Use:** As a design requirement, it is necessary to take into account whether a biosensor is intended to be used for diagnosis, disease monitoring, or verifying a cure presence. In addition, the nature of the condition, whether it is an acute or chronic infection, affects the life cycle and maintenance of the system. Furthermore, for specific applications, where cleaning and sterilization is not possible, it is necessary to design disposable biosensors. The biosensor in this work is intended to be used for the rapid detection and recognition of chronic COPD in a PoC environment for several

usage following a cleaning procedure with ethanol. Therefore, the developed system needs to be portable, light-weight, easy to operate, clean, and maintain, durable with a sustainable battery-life or simple power method like USB.

- **Operational Setting:** The COPD detection system is intended to operate at a PoC or near-patient setting, though its application for professional use in a central laboratory is not necessarily restricted. Therefore, various points such as self-collection of samples, self-testing, self-calibration, end-result analysis, and self-cleaning need to be considered for designing the system. Proper cleaning of the biosensor is crucial for providing accurate results, while preventing any contamination. Ethanol and running water are two most common materials for cleaning medical devices at PoC environments.
- **Test Type:** It is important to take into account whether the test should be quantitative or qualitative. In addition, type of biomarkers which need to be detected such as enzymes, antibodies, and whether it is a single analyte or a multiple analyte which will be investigated. The intended biosensor for the COPD recognition needs to provide quantitative results for characterizing biomarkers in body fluids such as saliva. However, the output of the system could be a qualitative result for the end user for simplifying the operation and providing more meaningful outcome. The biomarkers intended to be monitored in this work are the mechanical (viscosity) and electrical (permittivity) characteristics of saliva samples, as an indicator of COPD progress.
- **Cost:** The system is intended to be used in low- and middle-income countries by end users. Therefore, low cost of the system is of great importance for its affordability by a larger population of patients.
- **Customer:** The end-users of this technology are either patients with COPD or primary health-care workers. In specific cases such as disease control centers at airports, trained laboratory technicians could also benefit from such a PoC sensing device. However, simple operation of the device and ready-to-understand results, provided by AI techniques, are important for general users.
- **Specimen Type:** Various body fluids and specimens can be used for PoC testing including oral fluid, cervical swab, respiratory tract fluids (sputum), nasal swab (self-collection), urine. For the technology introduced in this work, saliva has been chosen as the target specimen considering its non-invasiveness and simplicity to obtain on daily-basis.

- **Performance:** Although a PoC device is merely intended to be used for monitoring a medical condition and not providing a laboratory-comparable diagnosis, the high accuracy and repeatability of the provided results makes it a reliable technology for primary-care.
- **Ergonomic:** Considering the application of the system in a home-care environment, the device need to be made out of biocompatible materials with a comfortable shape without sharp edges. In addition, the portability of device and its light weight is extremely important for such applications.
- **Manufacturing:** Fabricating the packaging of a device in several pieces simplifies its design process and reduces the overall housing costs. In addition, by taking advantage of novel rapid prototyping methods such as 3D printing, building innovative models in a less time-consuming manner is feasible.
- **User-interface** The considered system interface is required to be user-friendly in order to allow the easy operation of the system by users, while providing meaningful testing results for its intended application. In addition, possibility of accessing biosensor results through a personal computer would enable recording system measurements in a long-term use and providing a better overview of patients' progress for physicians.
- **AI-compatibility:** Implementation of AI-based analytical techniques is extremely important for providing real-time and meaningful results for end-users in a PoC setting. AI-based approaches enable the better management of chronic and degenerative conditions and faster prediction of critical-emergency health conditions. However, limitations of cloud-based techniques in terms of data safety and edge-compatibility are required to be addressed using neuromorphic technologies.
- **Robustness:** Robustness of the system has to be considered for different factors. Temperature deviations is one of the main sources of error in PoC technologies, therefore, the developed system needs to be resilient against temperature fluctuations. Furthermore, considering the AI-compatibility of the device for providing advanced analytics for end users, it is important to design robust data transmission techniques for short- and long-range connections. Moreover, securing sensitive medical data against malicious attacks is of great importance for patient privacy. Neuromorphic computing-based platforms can be used for addressing these concerns, while making the system further resilient against data leaks and possible technical errors.

2.6 Design Objectives and Overview

As thoroughly discussed in the literature, recognition of COPD at its early stages plays a pivotal role for the effective treatment of the disease and the coherent prevention of its life-threatening exacerbations. In addition, the early detection of COPD along with pulmonary rehabilitation and smoking cessation can possibly benefit patients by arresting their disease progress and lung function decline. Nevertheless, since the integration of conventional COPD diagnosis methods such as spirometry or CT scan with PoC medical devices has been hindered, approaching alternative paths such as salivary biomarker detection has been highly promoted. However, considering the low concentration of protein biomarkers in saliva, this thesis aims to investigate the mechanical (viscosity) and electrical (permittivity) properties of saliva for the recognition of COPD in a home-care environment. As a result, following chapters will describe the design and development of a CMOS-based permittivity biosensor for the dielectric characterization of saliva samples of COPD patients in a PoC environment and its integration with neuromorphic-compatible machine learning techniques for the real-time analysis of acquired data on-chip. As the first step, Chapter 3 investigates the biosensor development process and its initial and latter performance assessments using controls and clinical saliva samples, respectively. Subsequently, implementation of various machine learning techniques for biosensor output analysis and COPD subjects recognition is discussed in Chapter 4. As a following step, Chapter 5 presents the hardware implementation of the proposed machine learning models on a memristive neuromorphic platform for the on-chip replication of analytical methods and for the post-processing of biosensor data in a secure way. Chapter 6 reports further potential applications of the proposed technology in biomedicine such as the on-chip detection of epileptic seizure in PoC. The final chapter of this thesis, Chapter 7, discusses the concluding remarks and contributions of this thesis and highlights future directions and potential applications of the technology.

Bibliography

- [1] P.J. Barnes. “Mechanisms in COPD: Differences from asthma,” *Journal Chest*, vol. 117, no. 2, pp. 10S—14S, 2000.
- [2] C.D. Mathers, D. Loncar. “Projections of global mortality and burden of disease from 2002 to 2030,” *PLoS Medecine*, vol. 3, no. 442, 2006.
- [3] S. Mirza, R.D. Clay, M.A. Koslow, P.D. Scanlon. “COPD guidelines: a review of the 2018 GOLD report,” *Elsevier Mayo Clinic Proceedings*, vol. 93, pp. 1488–1502, 2018.
- [4] J. Vestbo, S. Hurd, A.G. Agusti, et al. “Global strategy for the diagnosis, management, and prevention of chronic obstructive pulmonary disease: GOLD executive summary,” *Journal of Respiratory and Critical Care Medicine*, vol. 4, no. 187, pp. 347–365, 2013.
- [5] D. Price, A. Crockett, M. Arne, B. Garbe, R. Jones, A. Kaplan, A. Langhammer, S. Williams, B. Yawn. “Spirometry in primary care case-identification, diagnosis and management of COPD,” *Primary Care Respiratory Journal*, vol. 18, no. 216, 2009.
- [6] M.B. Drummond, N.N. Hansel, J.E. Connett, P.D. Scanlon, D.P. Tashkin, R.A. Wise. “Spirometric predictors of lung function decline and mortality in early chronic obstructive pulmonary disease,” *American journal of respiratory and critical care medicine*, vol. 12, no. 185, pp. 1301–1306, 2012.
- [7] C. Tantucci, D. Modina. “Lung function decline in COPD,” *J. Chron Obstruct Pulmon Dis.*, vol. 7, pp. 95–99, 2012.
- [8] C. Fletcher and R. Peto. “The natural history of chronic airflow obstruction,” *BMJ*, vol. 6077, pp. 1645–1648, 1977.

- [9] N.G. Csikesz, E.J. Gartman. “New developments in the assessment of COPD: Early diagnosis is key,” *International Journal Chronic Obstructive Pulmonary Disease*, vol. 9, pp. 277–286, 2014.
- [10] M. Decramer, M. Miravittles, D. Price, et al. “New horizons in early stage COPD – improving knowledge, detection and treatment,” *Respir Med.* vol. 11, no. 105, pp. 1576–1587, 2011.
- [11] T. Dong, S. Santos, Z. Yang, S. Yang, and N.E. Kirkhus. “Sputum and salivary protein biomarkers and point-of-care biosensors for the management of COPD,” *Analyst*, vol. 5, 2020.
- [12] S. Haroon, R. Jordan, Y. Takwoingi, P. Adab. “Diagnostic accuracy of screening tests for COPD: a systematic review and meta-analysis,” *BMJ open*, vol. 5, no. 10, p. e008133, 2015.
- [13] Z.L. Borrill, C.M. Houghton, R. Tal-Singer, et al. “The use of plethysmography and oscillometry to compare long-acting bronchodilators in patients with COPD,” *Br J Clin Pharmacol.*, vol. 2, no. 65, pp. 244–252, 2008.
- [14] Z.L. Borrill, C.M. Houghton, A.A. Woodcock, J. Vestbo, D. Singh. “Measuring bronchodilation in COPD clinical trials,” *British journal of clinical pharmacology*, vol. 59, no. 4, pp. 379–384, 2005.
- [15] S. Frantz, U. Nihlen, M. Dencker, G. Engstrom, C.G. Lofdahl, P. Wollmer. “Impulse oscillometry may be of value in detecting early manifestations of COPD,” *Respir Med.*, vol. 106, no. 8, pp. 1116–1123, 2012.
- [16] O.M. Mets, M. Schmidt, C.F. Buckens, et al. “Diagnosis of chronic obstructive pulmonary disease in lung cancer screening computed tomography scans: independent contribution of emphysema, air trapping and bronchial wall thickening,” *Respiratory Research*, vol. 14, no. 59, 2013.
- [17] A. M. Owrangi, R. Etemad-Rezai, D.G. McCormack, I.A. Cunningham, G. Parraga. “Computed tomography density histogram analysis to evaluate pulmonary emphysema in ex-smokers,” *Acad Radiol.*, vol. 20, no. 5, pp. 537–545, 2013.
- [18] Z. Hollander, M.L. DeMarco, M. Sadatsafavi, B.M. McManus, R.T. Ng, D.D. Sin. “Biomarker development in COPD: moving from P values to products to impact patient care,” *Chest*, vol. 151, no. 2, pp. 455–467, 2017.

- [19] S. Chiappin, G. Antonelli, R. Gatti, F. Elio. “Saliva specimen: a new laboratory tool for diagnostic and basic investigation,” *Clinica chimica acta*, vol. 383, no. 1, pp. 30–40, 2007.
- [20] R.S. Khan, Z. Khurshid, F. Yahya Ibrahim Asiri. “Advancing point-of-care (PoC) testing using human saliva as liquid biopsy,” *Diagnostics*, vol. 7, no. 3, p. 39, 2017.
- [21] S. Williamson, C. Munro, R. Pickler, M. J. Grap and R. K. Elswick. “Comparison of biomarkers in blood and saliva in healthy adults,” *Nursing research and practice*, 2012.
- [22] C. Punyadeera and P. D. Slowey. “Saliva as an emerging biofluid for clinical diagnosis and applications of MEMS/NEMS in salivary diagnostics,” *In Elsevier Nanobiomaterials in Clinical Dentistry*, pp. 543–565, 2019.
- [23] M.T. Lopez-Vidriero, L.d Reid. “Chemical markers of mucous and serum glycoproteins and their relation to viscosity in mucoid and purulent sputum from various hypersecretory diseases,” *American Review of Respiratory Disease*, vol. 117, no. 3, pp. 465–477, 1978.
- [24] M.C. Rose, J.A. Voynow. “Respiratory tract mucin genes and mucin glycoproteins in health and disease,” *Physiological reviews*, vol. 86, no. 1, pp. 245–278, 2006.
- [25] W. Robinson, P. Woolley, R.E.C. Altounyan. “Reduction of sputum viscosity in chronic bronchitis,” *Lancet*, vol. 272, pp. 819–821, 1958.
- [26] S.J. Haward, J.A. Odell, M. Berry, T. Hall. “Extensional rheology of human saliva,” *Rheol. Acta*, vol. 50, pp. 869–879, 2011.
- [27] S. Nie, et al. “An automated integrated platform for rapid and sensitive multiplexed protein profiling using human saliva samples,” *Lab on a Chip*, vol. 14, no. 6, pp. 1087–1098, 2014.
- [28] A.V. Hatch, A.E. Herr, D.J. Throckmorton, J.S. Brennan, A.K. Singh. “Integrated preconcentration SDS–PAGE of proteins in microchips using photopatterned cross-linked polyacrylamide gels,” *Analytical Chemistry*, vol. 78, no. 14, pp. 4976–4984, 2006.
- [29] E.H. Yee, S. Lathwal, P.P. Shah, H.D. Sikes. “Detection of biomarkers of periodontal disease in human saliva using stabilized, vertical flow immunoassays,” *ACS sensors*, vol. 2, no. 11, pp. 1589–1593, 2017.

- [30] J. Park, V. Sunkara, T. H. Kim, H. Hwang and Y. K. Cho. Park, J. “Lab-on-a-disc for fully integrated multiplex immunoassays,” *Analytical chemistry*, vol. 84, no. 5, pp. 2133–2140, 2012.
- [31] N. Christodoulides, et al. “Application of microchip assay system for the measurement of C-reactive protein in human saliva,” *Lab on a Chip*, vol. 5, no. 3, pp. 261–269, 2005.
- [32] T.M. Blicharz, W.L. Siqueira, E.J. Helmerhorst, F.G. Oppenheim, P.J. Wexler, F.F. Little and D.R. Walt. “Fiber-optic microsphere-based antibody array for the analysis of inflammatory cytokines in saliva,” *Analytical chemistry*, vol. 81, no. 6, pp. 2106–2114, 2009.
- [33] I. Ojeda, M. Moreno-Guzmán, A. González-Cortés, P. Yáñez-Sedeño and J. M. Pingarrón. “Electrochemical magnetoimmunosensor for the ultrasensitive determination of interleukin-6 in saliva and urine using poly-HRP streptavidin conjugates as labels for signal amplification,” *Analytical and bio-analytical chemistry*, vol. 406, no. 25, pp. 6363–6371, 2014.
- [34] M. Pelkonen, H. Tukiainen, M. Tervahauta, I.L. Notkola, S.L. Kivelä, Y. Salorinne, A. Nissinen. “Pulmonary function, smoking cessation and 30 year mortality in middle aged Finnish men,” *Thorax*, vol. 55, no. 9, pp. 746–750, 2000.
- [35] R.S. Chapman, X. He, A.E. Blair, Q. Lan. “Improvement in household stoves and risk of chronic obstructive pulmonary disease in Xuanwei, China: retrospective cohort study,” *Bmj*, vol. 331, no. 7524, p. 1050, 2005.
- [36] M. Decramer, B. Celli, S. Kesten, T. Lystig, S. Mehra, D.P. Tashkin. “Effect of tiotropium on outcomes in patients with moderate chronic obstructive pulmonary disease (UPLIFT): a prespecified subgroup analysis of a randomised controlled trial”, *The Lancet*, vol. 374, no. 9696, pp. 1171–1178, 2009.
- [37] C.R. Jenkins, P.W. Jones, P.M. Calverley, B. Celli, J.A. Anderson, G.T. Ferguson, J.C. Yates, L.R. Willits, J. Vestbo. “Efficacy of salmeterol/fluticasone propionate by GOLD stage of chronic obstructive pulmonary disease: analysis from the randomised, placebo-controlled TORCH study,” *Respiratory research*, vol. 10, no. 1, p. 59, 2009.

-
- [38] H.N. Tse, L. Raiteri, K.Y. Wong, et al. “High-dose N-acetylcysteine in stable COPD: the 1-year, double-blind, randomized, placebo-controlled HIACE study,” *Chest*, vol. 144, no. 1, pp. 106–118, 2013.
- [39] B. McCarthy, D. Casey, D. Devane, K. Murphy, E. Murphy, Y. Lacasse. “Pulmonary rehabilitation for chronic obstructive pulmonary disease,” *Cochrane database of systematic reviews*, vol. 2, 2015.
- [40] X.L. Liu, J.Y. Tan, T. Wang, Q. Zhang, M. Zhang, L.Q. Yao, J.X. Chen. “Effectiveness of home-based pulmonary rehabilitation for patients with chronic obstructive pulmonary disease: a meta-analysis of randomized controlled trials,” *Rehabilitation Nursing*, vol. 39, no. 1, pp. 36–59, 2014.
- [41] E. French-Mowat, J. Burnett. “How are medical devices regulated in the European Union?” *Journal of the Royal Society of Medicine*, vol. 105, pp. 22–28, 2012.
- [42] S. Davis, E. Gilbertson, S. Goodall. “EU Medical Device Approval Safety Assessment, A comparative analysis of medical device recalls 2005–2009.”

Chapter 3

Biosensor Development

3.1 Design and Fabrication of a BiCMOS Dielectric Sensor for Viscosity Measurements: A Possible Solution for Early Detection of COPD

Viscosity variation of sputum is a common symptom of the progression of COPD. Since hydration of the sputum defines its viscosity level, dielectric sensors could be used for the characterization of sputum samples collected from patients for early diagnosis of COPD. In this section, a CMOS-based dielectric sensor for real-time monitoring of sputum viscosity is introduced. A proper packaging for the ESD-protection and short-circuit prevention of the sensor was developed. Performance evaluation results show that the radio frequency sensor is capable of measuring dielectric constant of biofluids with an accuracy of 4.17%. Integration of this sensor into a portable system will result in a hand-held device capable of measuring viscosity of sputum samples of COPD-patients for diagnostic purposes, which will be investigated in the next section. This section of the chapter is based on reference [1].

3.1.1 Introduction

COPD is one of the leading causes of death among developed countries [2]. Although studies suggest that early diagnosis could effectively decrease the mortality rate of COPD, many patients go undiagnosed until late stages of their disease [3]. Abnormal sputum, infection, and bronchial spasm are three main syndromes of chronic bronchial disease. Sputum specimens contain saliva, serum transudate, and glycoproteins. Mu-

cus glycoproteins (mucin) are good mediums for bacterial growth and are responsible for viscous properties of mucus. As a result, characterization and rapid screening of mucus could be used for early diagnosis of COPD [4]. Since muco–protein content and hydration of the sputum determine its viscosity level, monitoring viscosity of sputum collected from a patient could provide useful diagnostic information for the disease [4, 5].

Recent advancements in developing viscosity sensors for biofluids are discussed in [6]. A wide range of commercially available viscometers were designed based on piezoelectric sensors. For example, Microvisk (Microvisk Ltd, Oxfordshire, UK), a commercially available viscometer, analyzes glucose concentration in blood for Point-of-Care (PoC) applications using Micro Electro Mechanical Systems (MEMS). Similarly, various research-oriented viscometers have been developed for blood analysis or coagulation monitoring using the MEMS technology [6–8]. The key principle of these piezoelectric-based viscosity sensors is based on the deflection of their piezo material-based cantilevers or beams when they are exposed to the viscous fluid. Deformation of these structures generates an electrical output depending on their readout mechanism. As a result, the generated electrical output indicates viscosity of the fluid exposed to the sensor. Although MEMS-based sensors are one of the most well-established sensing technologies, some drawbacks restrict their application for viscosity measurements. The main disadvantage of these sensors is the resetting of their cantilevers back to the original position, causing calibration and accuracy issues. Moreover, the viscous nature of the sensing fluid causes a considerable amount of damping on the cantilever vibration, impairing sensor's function. Furthermore, there is a significant amount of coupling between the fluid flow and the cantilever vibration that influences acquired results from the sensor. In addition, existing amount of drift in these sensors questions their reliability for long term operations [8]. In a work by Cakmak *et al*, a MEMS-based viscosity sensor was developed on a Complementary Metal Oxide Semiconductor (CMOS) platform. Although miniaturization of the system reduced damping effects and fluid flow rate, no significant improvements in terms of sensor accuracy or drift were achieved [9]. As an alternative technology, a pressure-based viscometer was developed for measuring blood glucose levels [10]. The needle-type glucose sensor consisted of two hollow fibers in which the viscous fluid was pumped up with a constant rate of 5 $\mu\text{L/h}$. In this design, two pressure sensors were placed at both ends of fibers and the pressure difference created by flow determined the viscosity of the sample fluid. Apart from innovative design of the sensor, its long response time (5 to 10 minutes), low resolution, and limited accuracy made its clinical application

unacceptable [10]. In contrast, optical biosensors are known as a well-established modality capable of providing accurate results for clinical applications [11–14]. However, they suffer from a few disadvantages for PoC applications such as high power consumption, high cost, large sample volume requirements, lack of portability, operation complexity, and incapability of label-free measurements. Alternatively, Kuenzi *et al* designed and developed a magnetically actuated rotational microviscometer [15]. The generated viscous friction by the fluid on the rotating magnet affected its rotation speed and angular position which were recorded for viscosity measurements. Although the system was able to provide accurate results, its bulky size limited its use for real-world PoC systems [15].

Silicon-based technologies such as CMOS provide countless advantages for PoC and Internet-of-Things (IoT) applications such as miniaturization, portability, high accuracy, reliability, low cost, high noise immunity, low power consumption, and complete integration with Lab-on-Chip (LoC) systems [16]. Due to these advantages, CMOS-based dielectric sensors have been used in numerous biological applications such as microorganism detection and characterization, neuronal activity detection, dielectric spectroscopy for medical diagnosis, and disease detection [17–19]. Developed biosensors detect and characterize biological targets based on their intrinsic properties or biochemical reactions. These biological parameters include biomarkers, biomolecules, proteins, DNA, pathogenic organisms, hormones, medical analytes such as glucose, and medical parameters like blood pressure [18, 19]. For example, CMOS-based electrochemical sensors have been designed and developed for DNA detection and characterization [20–22]. In these works, Interdigitated Capacitors (IDC) were used to determine biochemical properties of DNA molecules. An IDC sensor is a parallel-plate capacitor whose electrodes are positioned horizontally to provide a single sided access to the Material-Under-Test (MUT). In other words, dielectric constant (relative permittivity) of the MUT defines capacity of the IDC [23]. IDC-based sensors have been used in various studies to detect the dielectric constant of organic fluids as well as characterization of biological cell suspensions [24, 25]. It is noteworthy that the relative permittivity is a frequency-dependent complex number that represents characteristics of a medium in an interaction with electromagnetic fields. Real part of the permittivity is known as dielectric constant, which represents the amount of energy absorbed by a material from an electromagnetic field. For medical applications, measuring real part of the permittivity is useful for medium characterization like estimating glucose concentration or determining ratios of specific mixtures. On the other hand, imaginary part of the permittivity reflects a material's energy loss to an external electric field. For example, conduc-

tivity of a material (which is a feature used for detecting the ratio of dead sperms during semen analysis) is correlated to energy loss [26]. Over recent decades, researchers have investigated the correlation between dielectric properties of biological samples (e.g., blood) and specific diseases at microwave frequencies [27]. It has been shown that biomolecules and biocells existing in analyzed biological samples provide different dielectric characteristics for subjects with diseases compared to healthy ones [19]. The same concept is applicable for sputum samples collected from patients diagnosed with COPD, as previously mentioned. At different stages of COPD, viscosity of sputum varies due to its hydration change. Since dielectric constant (permittivity) of sputum is correlated to its hydration, it is possible to characterize viscosity of sputum by measuring its dielectric constant.

In spite of aforementioned advancements in developing biosensors for various PoC applications, a reliable technology for early diagnosis and monitoring of COPD is still missing. Considering the fact that viscosity of sputum samples collected from a COPD diagnosed patient is a reliable indicator of the disease presence, development of a portable viscometer capable of providing real-time measurements with high accuracy and resolution is significantly important. Therefore, the objective of this step of the work was to design and develop a CMOS-based dielectric sensor for real-time viscosity characterization of controls such as ethanol, methanol, and isopropanol. This step aimed at identifying shortcomings of previous prototypes and develop a newer generation of the dielectric sensor with a proper packaging and improved accuracy [28,29]. Future integration of this biosensor into a medical device can be used for early diagnosis of COPD through viscosity characterization of sputum. The working principle of the intended sensor is based on dielectric measurement of the MUT using capacitance sensors mounted on a CMOS platform. Capacitance changes of the sensor affects the free oscillation frequency of the LC resonant tank which would be used for the readout mechanism. Operating frequency of the sensor is chosen to be in the range of 10–30 GHz, where permittivity of water is considerably high compared to other existing biomaterials in sputum [18]. Due to the existing permittivity contrast in the mentioned frequency range, a better Signal-to-Noise Ratio (SNR) is expected. In addition, a high frequency sensor has generally a small-sized chip which significantly reduces sample volume requirements. Furthermore, the mentioned frequency range provides the most accurate results for dielectric sensing applications considering the fact that the undesired parameter-dependent dispersion mechanism of biological cells, which exists in low-frequency ranges, has negligible effects on the sensor functionality. On the other hand, based on the single Debye's relax-

ation mechanism, dielectric permittivity of water decreases after 17 GHz making extremely high frequency measurements inadequate for the intended application [18].

3.1.2 Materials and Methods

3.1.2.1 First Generation of the Sensor

A first prototype of the CMOS-based dielectric sensor for the detection of viscosity changes in sputum–mucin was presented previously [28, 29]. Details of this prototype along with its modified version are presented below.

Sensor Design and Operation Principle: A CMOS-based Radio Frequency (RF) dielectric sensor for the characterization of sputum–mucin was designed and manufactured, as shown in Figure 3.1(a). The sensor was fabricated through standard 250 nm SiGe:C BiCMOS technology of IHP (IHP, Frankfurt/Oder, Germany) and operated at a frequency of 12 GHz. The working principle of the sensor was based on measuring dielectric constant of liquid samples in order to characterize their viscosity. For this purpose, planar IDC sensors were coupled with inductors forming an LC resonant tank for the CMOS oscillator, as shown in Figure 3.1(b). Capacitance of the IDC varied based on dielectric constant of the MUT, leading to a change in the oscillation frequency. As a result, frequency changes of the oscillator indicated the viscosity variation of the MUT.

Although the developed sensor proved the practicality of the concept of viscosity characterization using dielectric sensors, its susceptibility to Electrostatic Discharges (ESD) made handling of the system

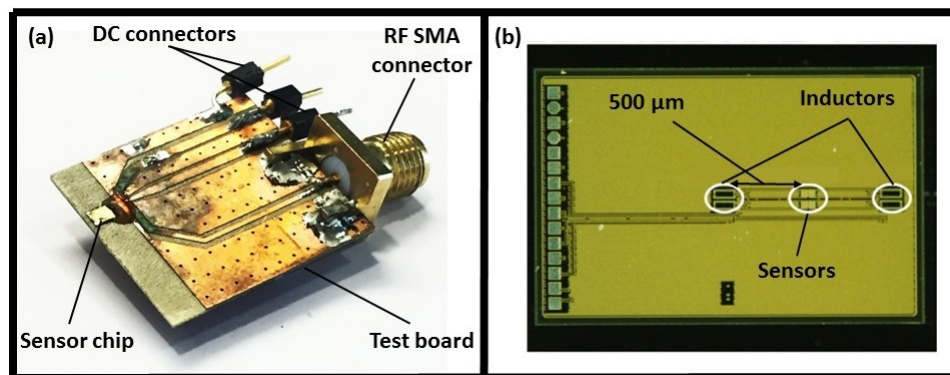


Figure 3.1: (a) First generation of the dielectric sensor, (b) sensor chip showing IDCs and inductors embedded in a CMOS oscillator [28, 29].

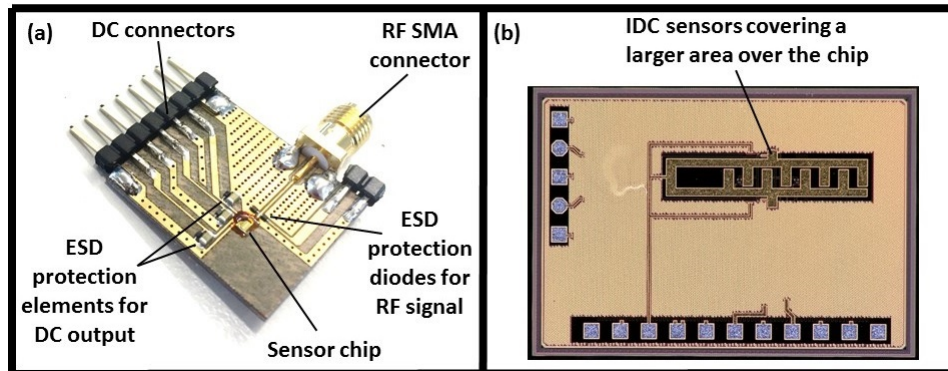


Figure 3.2: (a) ESD-protection elements mounted on the PCB, (b) modified chip with a larger sensing area coverage.

problematic. As a result, ESD-protection diodes (ESD9B, ON Semiconductor, CO, USA) and capacitors (0603 X5R:EIA, Murata Manufacturing Co., Nagaokakyo, Japan) were mounted on a Printed Circuit Board (PCB) in order to reduce the impact of ESD distortions on the sensor functionality, shown in Figure 3.2(a). In order to increase the accuracy and sensitivity of the sensor, a new chip with a larger sensing area coverage (with wider IDC elements) was designed, as demonstrated in Figure 3.2(b). Details of the circuit design is available in [28–30].

Sensor Performance and Required Modifications: The sensor was initially calibrated using ethanol, methanol, acetone, and isopropanol with known permittivity and viscosity values. Following sensor calibration, two sets of experiments were performed to evaluate the sensor. First, two solution mixtures (glycerol–water and glycerol–ethanol) were characterized with varying water and ethanol contents in order to obtain different permittivity and viscosity values. Second, sensor performance was validated by characterizing permittivity of three different biological liquids including: human serum, human saliva, and sputum–mucin clot. The sensor provided an oscillation frequency change of 200 MHz for a change of 60% in sputum–mucin viscosity. Details of assessment methods and its results are available in [28, 29].

The first prototype of the sensor provided promising results and proved the feasibility of the method for measuring viscosity of biological samples using dielectric sensors. However, a few limitations associated with the system restricted its use in real-world applications. These issues are as follows:

1. Even though RF output of the first-generation sensor was useful for conducting pilot experiments and evaluating system during preliminary studies, its numerous drawbacks made it an unfavourable

choice for out-of-the-lab applications. The main drawback of the RF output was the necessity of having costly and bulky spectrum analyzers for signal acquisition which is an unrealistic intention for the development of PoC devices. In addition, RF signal is generally very sensitive to external distortions which causes a considerable amount of noise on the sensor outcome.

2. Due to the lack of an adequate packaging, the sensor was extremely susceptible to ESD-caused damages. As a consequence, handling system during wire bonding process, soldering of PCB elements, and running experiments were significantly inefficient and complicated. Moreover, spreading of conductive liquids on the PCB surface, especially during the characterization of biological samples containing water, caused sensor to short-circuit. Hence, a proper packaging for ESD protection and short-circuit prevention of the system was required.
3. Considering the inhomogeneous nature of biological liquids, including mucin and saliva, a series of sensing elements were required to increase the overall sensing ability of the system and improve its repeatability.
4. Since the sensor measures dielectric constant of a sample, electrical features of a sample determine the sensor outcome rather than its mechanical features. For instance, increasing the concentration of ethanol in an ethanol–glycerol mixture decreases both permittivity and viscosity of the mixture. Conversely, increasing the concentration of water in a water-glycerol mixture increases permittivity of the mixture while decreasing its viscosity. Thus, measured permittivity for a given viscous sample is dependent on constituents of that sample. In other words, it is only permittivity of the solution which is detected by the sensor rather than its absolute viscosity values. This is due to the fact that there is no direct mathematical correlation between viscosity and any electrical quantity. Consequently, different calibrations are required based on intrinsic characteristics of tested samples. This issue causes calibration complexity and makes the viscosity detection of unknown samples impractical. Therefore, a more reliable calibration and validation method is necessary to improve sensor outcome. For this purpose, direct calibration of the sensor using a commercialized viscometer is recommended.

A second generation of the sensor prototype was designed and developed in order to address these shortcomings, as presented in the following section.

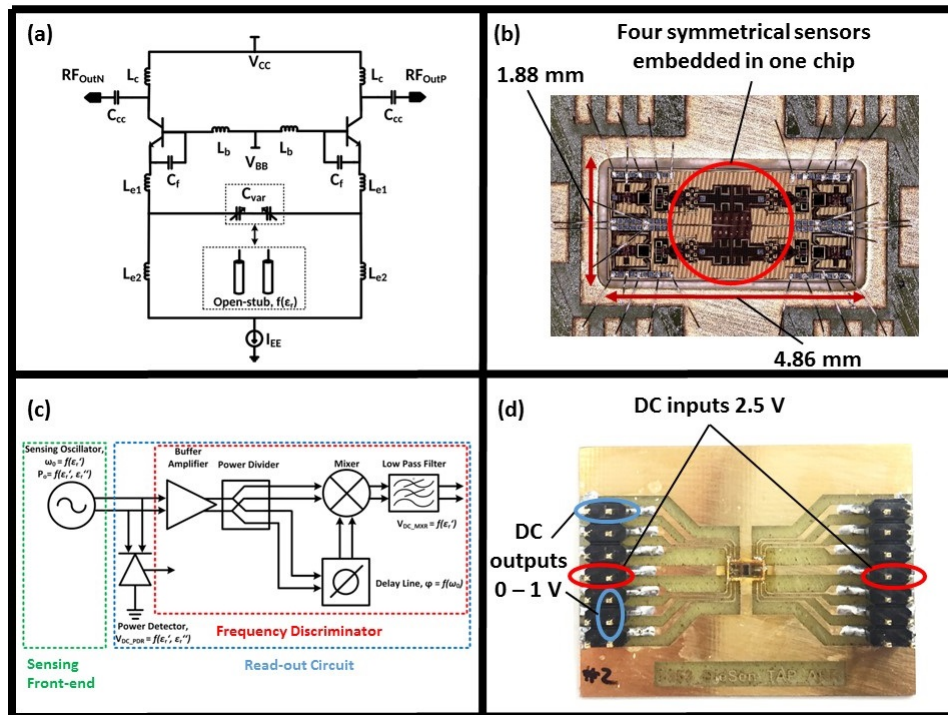


Figure 3.3: (a) Sensor oscillator circuit [31], (b) second-generation chip with a quadruple-sensor configuration, (c) integration of the DC readout circuit and sensor on the CMOS platform [32], (d) test board of the second-generation dielectric sensor with DC inputs and outputs.

3.1.2.2 Second Generation of the Sensor

Functioning on the same sensing principle as the first prototype, a new version of the sensor for the detection of dielectric constant changes due to viscosity variations of sputum–mucin was developed, Figure 3.3. Capacitive elements were coupled with inductors to define the oscillation frequency of the resonator component. In this design, capacitive elements are a pair of microstrip open-stubs with an electrical length below the quarter-wavelength of the sensor operation frequency, as shown in Figure 3.3(a). The operation frequency of the sensor is in the range of 30 GHz, which results in a high SNR [18]. Similar to the previous sensor, 250 nm SiGe:C BiCMOS technology of IHP was used to fabricate the sensor. Limitations of the first prototype were addressed in order to improve the sensor functionality.

Sensor Design and Functionality: As shown in Figure 3.3(b), the second generation of the sensor with a 9.2 mm^2 chip size was designed and fabricated. The larger size of the chip, compared to previous generations, is due to two reasons: quadruple-sensor design for the detection of inhomogeneous samples, Figure

3.3(b)—the full integration of the complementary readout circuit and the sensor on the CMOS platform, Figure 3.3(c).

Unequal dispersion of inhomogeneous fluids over sensing area of the first generation of the sensor led to poor repeatability. In order to address this issue, four analogous sensors were integrated in a quadruple design to increase the sensing area in contact with MUT and to reduce sample dispersion effects on sensor measurements, as shown in Figure 3.3(b). Despite having four sensors, the chip consumes 80 mW power which makes it an appropriate technology for PoC devices.

The readout mechanism for the new generation of the sensor was modified to eliminate noise caused by the RF output. As demonstrated in Figure 3.3(c), a frequency discriminator was implemented into the sensor readout circuit to convert RF information into a DC output. Subsequently, a power detector was used to extract the output power. Therefore, DC signals corresponding to the sensor oscillation frequency were generated as system output. Figure 3.3(d) illustrates inputs and outputs for all four sensors. Two DC inputs of 2.5 V are required for system power source. On the other hand, each sensor provides two DC outputs in a range of 0–1 V for real and imaginary parts of the measured permittivity, as shown in Figure 3.3(d). Further details regarding circuit design are available in [31, 32]. Using DC inputs and outputs, amount of perturbation on the system was diminished and the sensor performance was significantly improved. In addition, low power consumption of sensors and ease of handling DC signals made the integration of the whole system into a compact portable device possible. Packaging process of the system is described in the following section.

System Packaging: Figure 3.4(a) illustrates packaging of the sensor, which was fabricated using a 3D printer at IHP (Keyence Agilista-3200W, Keyence Co., Osaka, Japan). A droplet reservoir was considered for packaging design for holding liquid samples, as shown in Figure 3.4(b). A medical grade biocompatible and electronics-friendly glue (Loctite M-21HP, Henkel AG & Company, KGaA, Dusseldorf, Germany) was used to seal the droplet reservoir thoroughly, as shown in Figure 3.4(c). As a result, short circuit of the sensor due to spreading of conductive liquids on the chip surface was prevented. Additionally, bond wires were covered by a non-conductive biocompatible glue (TNP0400, Kyocera Corporation, Kyoto, Japan) to protect them during assembling packaging and testing samples. Figure 3.4(d) illustrates the remaining sensing area for sample measurements after the gluing process.

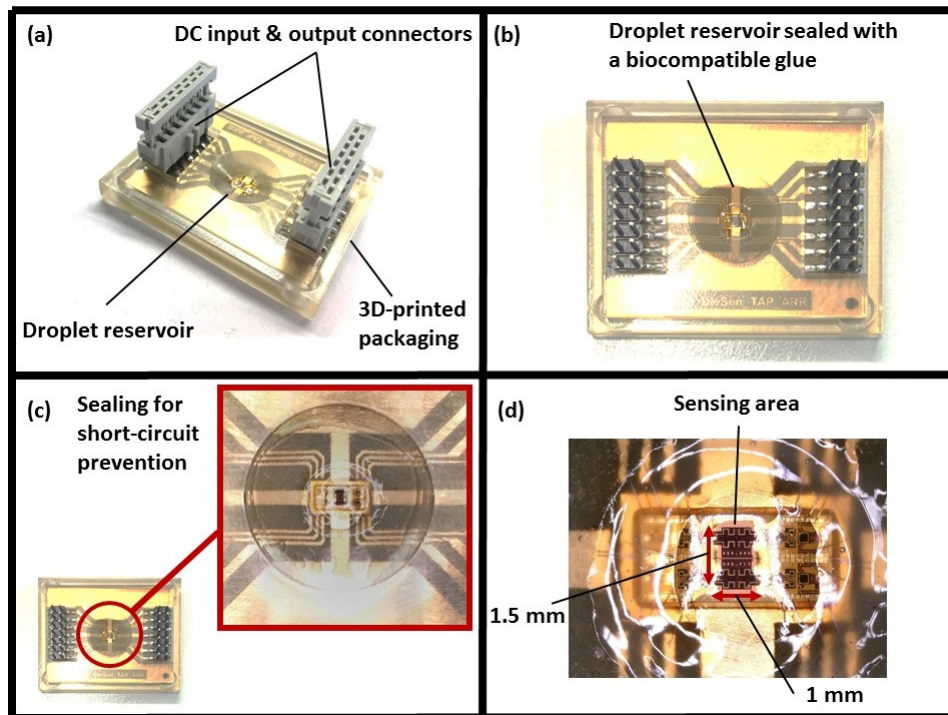


Figure 3.4: (a) The sensor packaging, (b) droplet reservoir, (c) sealing of the reservoir for prevention of liquids spreading, (d) remaining sensing area after the sealing step.

ESD damages caused by direct contact of operators' hands with the test board during conducting experiments were minimized using developed packaging. Moreover, packaging simplified the cleaning process of the chip after conducting measurements, since using conductive liquids such as water for cleaning the sensing area was possible. Therefore, system has become more user-friendly to handle and conduct experiments.

Experimental Setup: Since dielectric constant of materials is highly temperature dependent, all experiments for the sensor calibration and assessments were performed in a lab with a sustained temperature of 21°C , as shown in Figure 3.5. Considering the frequency dispersive behavior of materials, Debye-based relaxation equations were used to calculate dielectric constants of tested materials at 21°C and 30 GHz operating frequency of the sensor, as presented in Table 3.1 [33–36].

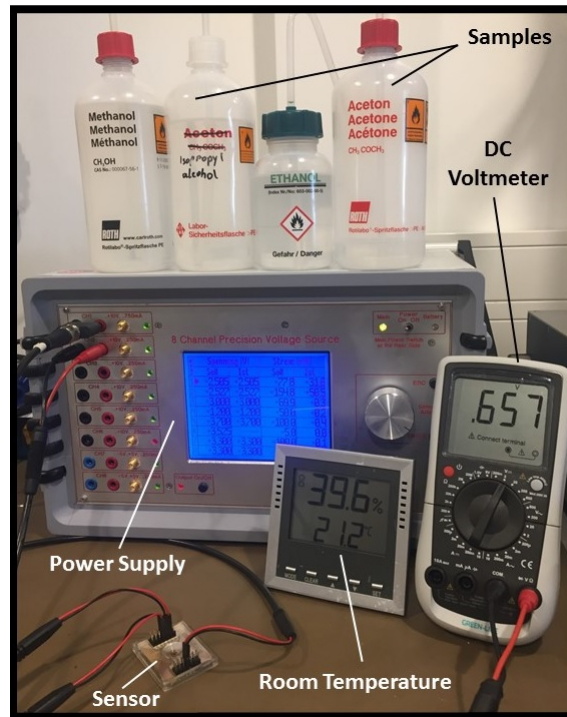


Figure 3.5: Measurement setup for the sensor calibration and validation experiments.

3.1.3 Results and Discussions

3.1.3.1 Calibration

Initial measurements of sensor with no MUT features dielectric characteristics of the surrounding air. As a result, dielectric constants of air, isopropanol, ethanol, and acetone were used to calibrate sensor for dielectric measurements.

The quadratic regression method was used on obtained results to establish a relationship between sensor output and dielectric constant of the corresponding material. As illustrated in Figure 3.6, the calibration

Table 3.1: Dielectric constant of utilized materials at 30 GHz and 21° C [33–36].

Material	Dielectric Constant
Air	1
Isopropanol	3.08
Ethanol	4.51
Methanol	8.2
Acetone	15.4

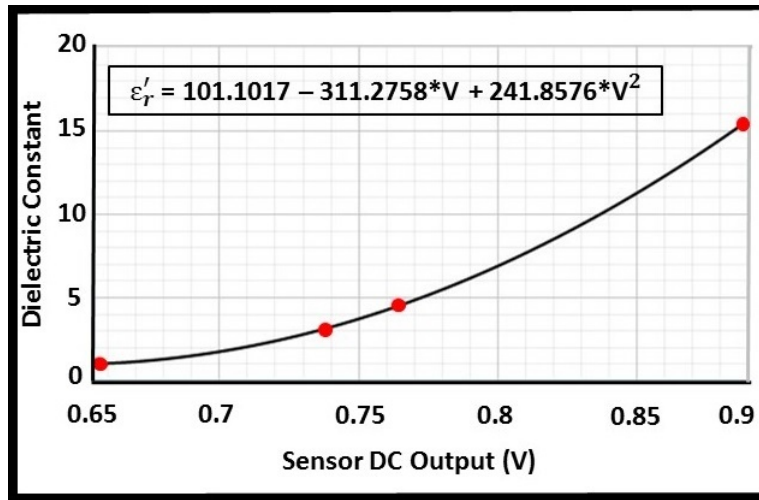


Figure 3.6: Fitted calibration line using the quadratic regression method. In the equation, V represents the corresponding DC output of the sensor in volt and ϵ'_r is the dielectric constant of the MUT.

line was fitted based on calculated coefficients of the quadratic regression expression.

3.1.3.2 Performance Assessment

Following sensor calibration, experiments were performed on methanol to evaluate sensor efficacy. As presented in Table 3.2, experiments were conducted in triplicate and dielectric constant of methanol was calculated using the calibration equation presented in Figure 3.6. Based on obtained results, following performance measures were calculated:

- Accuracy: calculated as the difference between actual and measured values divided by the actual value (relative error). Total error of all three sets of measurements is reported.
- Repeatability: presented as the maximum standard deviation of errors observed during three experiments.
- Hysteresis: calculated as the difference between sensor initial measurements before and after performing an experiment. The highest value of all trials is reported.
- Drift: sensor output with no MUT was recorded from initiation of the system for a time period of 10 minutes. Drift was calculated as the difference between lowest and highest dielectric constant values measured during first and last 10 seconds.

Table 3.2: Results of the sensor verification experiments for methanol dielectric constant.

Methanol	Actual Value	Exp. 1	Exp. 2	Exp. 3
Dielectric Constant (ϵ_r^*)	8.2	8.82	8.14	8.65

- Noise: calculated as the difference between lowest and highest dielectric constant values acquired in a 10 second data set with no MUT.

Functionality of the sensor to detect viscosity variation was evaluated by mixture characterization method. Six mixtures of methanol-isopropanol, ranging from 0% methanol to 100% methanol (in volumes), were prepared. Effective permittivity and viscosity values of mixtures at the working frequency of the sensor were calculated using mixture theories [29, 31, 37]. Theoretical values of mixture permittivity and viscosity are plotted in Figure 3.7. Sensor results for dielectric constant of mixtures were calculated based on the sensor calibration and illustrated in Figure 3.7.

Results of experimental evaluations are presented in Table 3.3. Sensor is capable of measuring dielectric constant of the MUT with an accuracy of 4.17% and a repeatability of 5.36%. Therefore, results of the second-generation sensor are more reliable compared to the first prototype. Furthermore, a hysteresis value of 2 mV was observed to have a negligible effect on the sensor measurements.

Issues related to the susceptibility of the RF signal to external distortions were addressed and a more stable system with DC readout mechanism was developed. Therefore, level of noise existing in the system has been remarkably reduced (1 mV) compared to the first-generation sensor. In addition, the sensor shows a low amount of drift (5 mV) which results in a calibration consistency during long term measurements. Low drift and hysteresis characteristics of the sensor make it a more reliable technology for real-world applications.

Short-circuiting issues of the sensor was addressed using sensor packaging. Droplet reservoir of the packaging was thoroughly sealed in order to prevent spreading of conductive samples on the board during experiments. Furthermore, packaging prevented the direct contact of operators' hands with the board for

Table 3.3: Results of performance evaluation of the second generation of the dielectric sensor.

	Accuracy	Repeatability	Hysteresis	Drift	Noise
$\epsilon_r^* /(\text{mV})$	4.17%	5.36%	0.014 (2 mV)	0.038 (5 mV)	0.006 (1 mV)

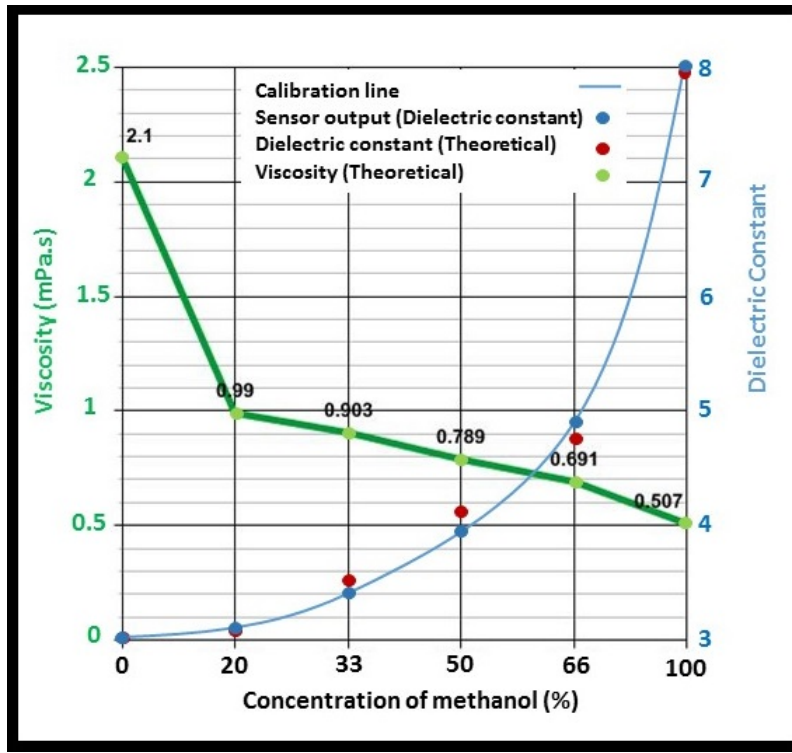


Figure 3.7: Viscosity and permittivity variation of the isopropanol-methanol mixture with respect to methanol content.

ESD-protection.

Quadruple design of the chip improved the overall sensing ability of the system and therefore, more repeatable and consistent results were achieved. Further investigation to evaluate sensor performance during characterization of inhomogeneous fluids is required.

Figure 3.7 shows variation of the viscosity and dielectric constant of isopropanol-methanol mixtures with respect to concentration of methanol. It is shown that with the addition of methanol, viscosity of the resultant mixture decreases due to the low viscosity of methanol. Conversely, permittivity of the solution increases considering the high permittivity of methanol. As a result, the sensor is able to detect viscosity variation of solutions based on their permittivity changes. However, it should be noted that it is required to know dielectric characteristics of mixture's constituents to be able to detect its viscosity variation. Estimation of absolute viscosity values using a dielectric sensor is not feasible since there is no direct mathematical correlation between viscosity and an electrical quantity.

Although capabilities of the system were evaluated through the characterization of control liquids with

known dielectric constant values, a direct viscosity calibration and validation method is still missing. Our team is currently investigating this approach using a commercialized viscometer (m-VROC, RheoSense Inc., San Ramon, CA, USA) to correlate absolute viscosity values of saliva and sputum samples to sensor results. However, complexity of viscosity measurements of non-Newtonian fluids make it a challenging approach. These investigations are still ongoing.

The second generation of the sensor was able to address limitations of the previous design. Drawbacks related to the RF output of the sensor were addressed and a portable low-cost system with a high accuracy and repeatability was developed. 3D-printed packaging of the sensor prevented damages previously caused by short-circuiting and ESD. Designed sensor consisted of four symmetrical sensing elements to eliminate effects of local concentration of particles in inhomogeneous liquids on sensor measurements. Calibration issues with viscosity measurements caused by the indirect verification of sensor results is still under investigation.

3.1.4 Conclusions and Future Work

In this section, the concept of viscosity measurement of sputum samples for early diagnosis of COPD using a dielectric sensor was investigated. Two prototypes of dielectric sensors were designed and fabricated using CMOS technology. Sensors measured permittivity variations of MUT which was correlated to their viscosity changes. Limitations of the first prototype were identified and addressed and a newer version of the sensor was developed. The sensor performance for detecting viscosity of liquids was evaluated using controls and through mixture characterization method. The sensor assessment results show that the RF sensor is capable of measuring dielectric constant of liquids with an accuracy and a repeatability of 4.17% and 5.36%, respectively. Moreover, low amounts of noise and drift were observed during measurements, providing reliable results for long-term medical applications. In addition, packaging of the sensor simplified system handling during operation. The DC readout mechanism of the second prototype as well as its compact size and low power consumption made it a suitable technology for PoC applications. Ease of cleaning, portability, low cost, and capability of rapid detection of viscosity are among main novelties of this biosensor for clinical applications.

As a next step, the sensor will be calibrated using a commercialized viscometer and its performance will be evaluated during the characterization of non-Newtonian fluids. Considering the practical application of

this sensor, providing absolute viscosity values is necessary for COPD diagnostics. In addition, the developed sensor will be incorporated into a complete hand-held device suitable for PoC and IoT applications.

3.2 Development of a Portable Dielectric Biosensor for Rapid Detection of Viscosity Variations and Its In-Vitro Evaluations Using Saliva Samples of COPD Patients and Healthy Control

As extensively discussed in the previous section, literature studies suggest that regular screening of sputum viscosity could provide important information for COPD management. Since viscosity of sputum is mainly defined by its mucin–protein and water contents, dielectric biosensors can be used for the detection of viscosity variations by screening changes in sputum’s contents. However, the previous section only investigated the performance of the developed biosensor on characterizing non-conductive controls. Therefore, the objective of this section was to integrate the developed dielectric biosensor into a handheld system for the characterization of conductive water-based mixtures and to evaluate its clinical performance for evaluating viscosity differences of saliva samples collected from COPD patients and Healthy Control (HC). For this purpose, a handheld dielectric biosensor, capable of providing real-time measurements, was developed. The sensor performance for dielectric characterization of mediums with high water content, such as saliva, was evaluated using isopropanol–water mixtures. Subsequently, saliva samples, collected from COPD patients and HC, were investigated for clinical assessments. The radio frequency biosensor provided high repeatability of 1.1% throughout experiments. High repeatability, ease of cleaning, low-cost, and portability of the biosensor made it a suitable technology for its intended point-of-care application. This section of the chapter is based on reference [38].

3.2.1 Introduction

COPD is a life-threatening lung disease affecting millions of people worldwide [39]. It has been predicted that COPD will be the third leading cause of death in developed countries by 2030 [39]. The growth of COPD is significantly due to increase in tobacco use (including active smoking or secondhand smoke) and air pollution [2]. Although many cases of COPD are considered to be treatable, early diagnosis is the key

factor in their effective prevention and control [3]. COPD is an umbrella term describing chronic lung diseases that cause airflow constraints in lungs. The main symptoms of COPD are breathlessness, chronic cough, and abnormal sputum production [2]. Analyzing lung capacity of patients using a spirometer is the most common and rudimentary method for diagnosing COPD. However, sputum examination may be required for a more accurate diagnostics and identification of bacterial infections [40]. Sputum produced by lungs mainly consists of mucin, water, epithelial cells of airway mucosa, and salts (in physiological concentrations). In addition, sputum could be contaminated with saliva during sampling. Since viscosity of sputum is mainly defined by its mucin (mucus glycoproteins) and water contents, regular monitoring of sputum viscosity could provide important information for early and fast detection of COPD [4,5]. However, it is not feasible to obtain sputum samples non-invasively in PoC environments or from healthy controls on a daily basis. On the other hand, saliva is easily obtainable on a daily basis, in a non-invasive manner, with a better patient compliance. Therefore, in this thesis, it was aimed to investigate whether viscosity of saliva samples is a proper biomarker for COPD, despite the fact that their viscosity differences are less distinct compared to sputum samples [5,41].

A broad range of technologies have been used for viscosity measurements of biofluids in medical applications [6]. Nonetheless, commercially available viscometers are mainly designed based on MEMS. For example, Microfluidic Viscometer-Rheometer-on-Chip (m-VROC) is a MEMS-based pressure sensor array integrated into a microfluidic channel to measure the viscosity of Newtonian and non-Newtonian fluids. In this device, the test fluid is loaded in a micro-syringe and pumped inside the microfluidic. The pressure drop through the channel is measured by the sensor array and correlated to the fluid viscosity. The high accuracy and repeatability, small sample volume requirements, and the temperature control capability of the device make it an adequate technology for medical applications. However, its high cost, bulkiness, and cleaning complexity limit its use for PoC applications. Similarly, Microvisk (Microvisk Ltd., Oxfordshire, UK) is a commercially available viscometer for blood coagulation monitoring, functioning based on MEMS technology. In this device, piezoelectric elements pulsate steadily in the sample, characterizing its viscosity. The working principle of MEMS is based on the deflation of their cantilevers upon exposure to viscous fluid, which generates an electrical impulse. Many advantages of MEMS, such as high sensitivity and low cost, make them a well-established sensing technology for PoC [6–8]. However, their application for viscosity measurements is limited due to some drawbacks. The main limitation is the coupling between

the fluid flow rate and its viscosity, impairing accuracy. In addition, the amount of drift, caused by resetting of sensor cantilevers back to their original position, is considerably high, which makes the calibration and accuracy of MEMS questionable in long term. Moreover, a complicated cleaning process is required to remove stuck biological particles, such as protein molecules, from sensor surface or capillary [8].

Apart from MEMS, other sensing technologies such as optical-sensors, pressure-sensors, and magnetic-sensors are moderately used for viscosity characterization of biofluids. However, their bulky size, operation-cleaning complexity, high cost, and lack of portability limit their application in real-world PoC devices [10–15]. In contrast, silicon-based technologies such as CMOS have been widely used for the characterization of biological samples considering their high accuracy, miniaturization, robustness, and low cost [16]. These applications cover various dielectric spectroscopy methods for medical diagnosis and detection [17–19]. In addition, CMOS-based microorganism characterization using biochemical–biological markers is reported in the literature [20–22, 25]. As an example, Stagni et al. developed a CMOS-based capacitive sensor for the detection of DNA molecules. In this work, the presence of DNA molecules are detected by capacitance variations of the sensor [20]. A similar detection principle was implemented to characterize various biological cell suspensions in organic fluids using dielectric biosensors [24]. It is shown that dielectric characteristics of biological samples (blood, semen, and saliva) at microwave frequencies differ for patients with diseases compared to healthy subjects [19, 26, 27]. The relative permittivity (dielectric constant) of a medium is a dimensionless frequency-dependent complex number, real (ϵ'_r) and imaginary (ϵ''_r) parts of which represent a material's energy absorption and energy loss, respectively, in an interaction with an electromagnetic field [27]. Therefore, conductivity (σ), which accounts for losses in a material, is definable using the following equation:

$$\sigma = \sigma_{ion} + f\epsilon''_r(f), \quad (3.1)$$

where σ_{ion} is the material's ionic conduction and ϵ''_r is imaginary part of the permittivity at the functioning frequency of f .

Despite advancements in development of bio-viscometers, a reliable technology for screening viscosity of sputum or saliva for rapid detection of COPD, at early stages, is still missing. Since viscosity variations of sputum, at different stages of COPD, are caused by changes in its water and mucin contents, dielectric

sensors could potentially be used for screening viscosity changes for rapid monitoring of COPD. Previously, the concept of viscosity measurements using dielectric sensors was investigated [1, 28, 29]. Our previously developed BiCMOS dielectric sensor provided promising results for dielectric characterization of compounds such as ethanol, methanol, and isopropanol as well as mixtures (i.e., ethanol–methanol mixture). Additionally, dielectric characteristics of mixtures were correlated to their viscosity measures and sensor’s capability for detecting viscosity changes was assessed [1, 28, 29]. However, the sensor integration into a portable device for PoC applications and its clinical performance evaluations were missing. Therefore, the objective of this part of thesis was to integrate our previously designed dielectric sensor into a handheld device for rapid characterization of saliva viscosity and to evaluate its *in-vitro* performance for distinguishing viscosity differences of saliva samples of COPD patients and Healthy Control (HC). For this purpose, proper packaging of the system and development of a user-friendly interface were essential. In addition, a commercially available viscometer, with high accuracy and reliability, was required for the sensor performance evaluations during clinical trials. The following sections elaborate upon technical design of the device and its clinical evaluations.

3.2.2 Sensor Design and Integration

As previously reported [1], the functioning principle of the sensor is based on permittivity measurements of the MUT using capacitive elements (or more specifically four pairs of microstrip open-stubs), as shown in Figure 3.8(a). These capacitive elements are coupled with inductors, defining oscillation frequency of the LC resonant tank, Figure 3.8(b). As a result, permittivity characteristics of the MUT alter the capacitance of sensing elements, leading to a frequency shift in the resonator. As illustrated in Figure 3.8(c), frequency information of the oscillator is converted into DC signals, using a frequency discriminator, and extracted as sensor output for real part of the permittivity of the MUT. Moreover, output power of the oscillator was detected using a power detector, providing information on imaginary part of the permittivity of the MUT.

The sensor chip, with a 9.2 mm² size and 80 mW power consumption, was fabricated using the 250 nm SiGe:C BiCMOS technology of IHP. The operation frequency of the sensor is in the range of 30 GHz, where a high signal-to-noise ratio is expected [18]. This is due to the fact that, based on the single Debye’s relaxation mechanism, permittivity of water at 17 GHz is significantly high relative to other biological particles, making 10–30 GHz frequencies the most adequate range for dielectric spectroscopy applications [18].

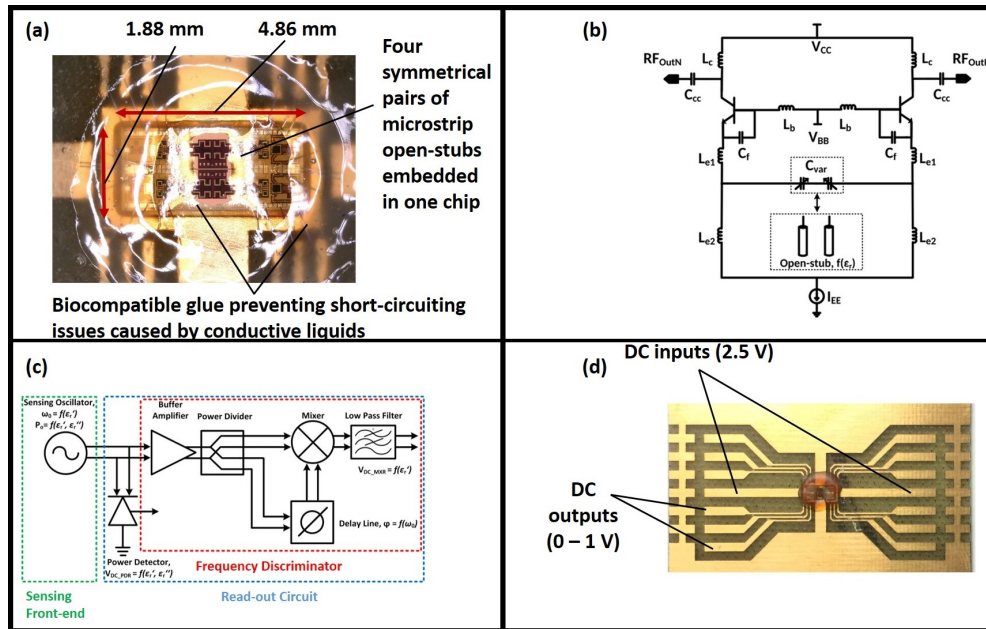


Figure 3.8: (a) capacitive elements, four pairs of microstrip open-stubs, used for permittivity characterization of the MUT; (b) sensor oscillator circuit, illustrating inductors coupled with capacitive elements; (c) DC read-out schematic, elaborating frequency discriminator and power detector; and (d) DC inputs and outputs of the sensor chip embedded on a PCB.

In addition, the undesired parameter-dependent dispersion mechanism of biological cells, existing in low-frequency ranges, has negligible effects on sensor measurements at its functioning frequency [18]. As shown in Figure 3.8(d), DC readout, small size, and low power consumption of the sensor have made its fully integration into a handheld device possible.

Figure 3.9(a) illustrates required parts for the full integration of the biosensor. The packaging of the device was fabricated out of a transparent resin (AR-M2) using a 3D printer (Keyence Agilista-3200W, Keyence Co., Osaka, Japan). The droplet reservoir, emplaced over the sensor area, was designed to access the MUT, while preventing sample spread over the Printed Circuit Board (PCB). Proper sealing of the reservoir was necessary for short-circuit prevention during handling conductive liquids, as shown in Figure 3.8(a). Further details on sealing and packaging of the sensor are available in [1]. A 1.8" display (Raspberry PI, ST7735, SIMAC Electronics GmbH, Neukirchen-Vluyn, Germany) was used to provide measurement results to users, as shown in Figure 3.9(b). In addition, an Arduino microcontroller (Mega 2560, SIMAC Electronics GmbH, Neukirchen-Vluyn, Germany) was used to supply DC power inputs, in order to acquire sensor outputs for post-processing, and to display processed results on the interface display. Portability,

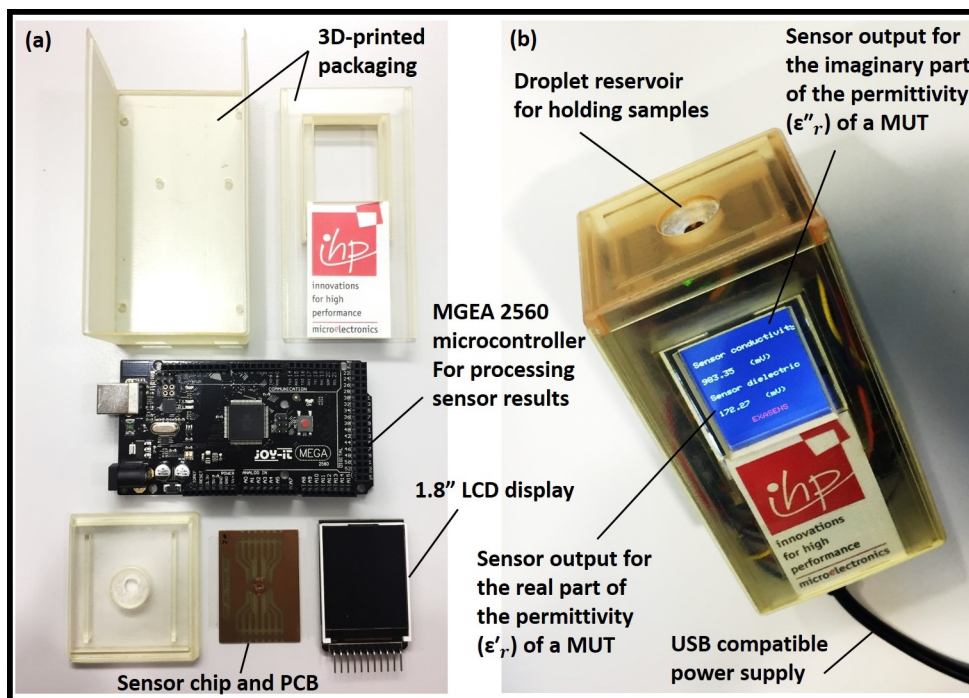


Figure 3.9: (a) Various parts required for the fully integration of the biosensor into a handheld device including a microcontroller, an LCD display, and a 3D-printed packaging; (b) assembled device working with a USB power supply.

ease of cleaning, low-cost, rapid detection possibility, and small sample requirements of the USB-powered device made it a suitable technology for home-care and PoC applications.

As shown in Figure 3.10(a), a second version of the prototype, powered with four rechargeable batteries (1.2 V–1900 mAh, Fujitsu Ltd., Tokyo, Japan) and a simpler user interface (0.28" LED voltage panels, Seeed Technology Co., Shenzhen, China) was developed. Independency of this prototype from a USB power supply makes it a suitable technology for remote applications. The laptop-shape design of the packaging secures the sensor surface in remote–harsh environments, as shown in Figure 3.10(b).

3.2.3 Experimental Setup

3.2.3.1 Mixture Detection

As reported in the previous section, the sensor provided an accuracy of 4.17% for dielectric characterization of low-conductive liquids such as ethanol [1]. In addition, it was able to accurately distinguish isopropanol–methanol mixtures with various methanol concentrations. However, considering water as the

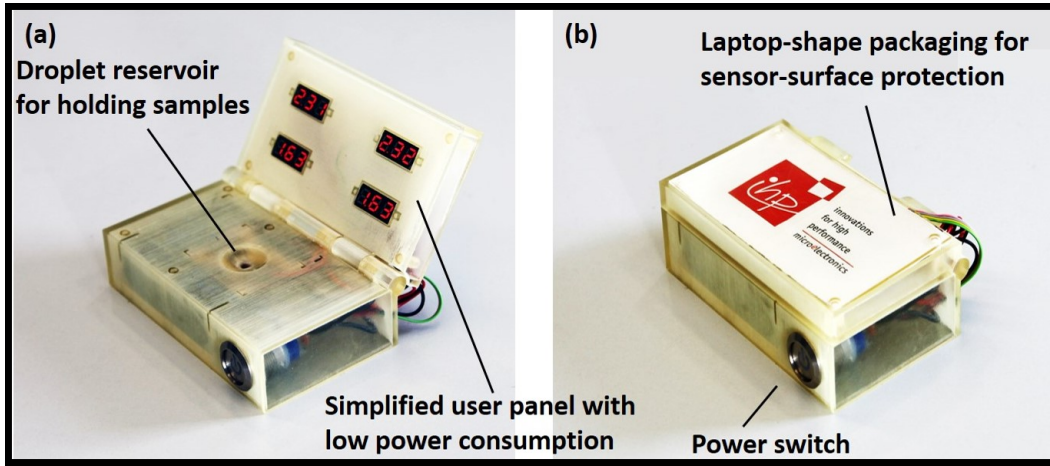


Figure 3.10: (a) battery-powered version of the biosensor suitable for harsh and remote environments with a limited access to a USB power supply; (b) laptop-shaped foldable packaging suitable for sensor-surface protection.

major component of saliva [42], it was critical to evaluate the sensor performance in characterizing conductive mixtures prior to its clinical assessment. Water is a highly conductive lossy material that impairs the dielectric sensor's function.

For this purpose, mixtures of isopropanol–water (deionized water), ranging from 0–100% water (in volumes), were prepared and used for sensor performance assessments. Effective permittivity of these mixtures at different steps were calculated using mixture theories [37]. The effective permittivity ($\epsilon_{r,eff}$) of a binary isotropic mixture, with mixing ratios of $1 - q$ and q for its host (the dominant content, $\epsilon_{r,h}$) and guest ($\epsilon_{r,g}$) constituents, is calculable using the following equation:

$$\epsilon_{r,eff} = \frac{\epsilon_{r,g}(2q + 1) + 2\epsilon_{r,h}(1 - q)}{(2 + q) + \frac{\epsilon_{r,g}}{\epsilon_{r,h}}(1 - q)}. \quad (3.2)$$

Debye-based relaxation equations, for modeling the frequency dispersive behavior of materials, were required to calculate the complex permittivity of water and isopropanol at 30 °C and 27 GHz for the operating temperature and frequency of the sensor, respectively [34–36]. The double-Debye relaxation equation, with high accuracy for modeling materials with two dielectric relaxations, was used for the complex permittivity ($\epsilon^* = \epsilon'_r - j\epsilon''_r$) calculations, Equation (3.3).

$$\epsilon^* = \epsilon_\infty + \frac{\epsilon_s - \epsilon_h}{1 + jf/f_{r1}} + \frac{\epsilon_h - \epsilon_\infty}{1 + jf/f_{r2}}. \quad (3.3)$$

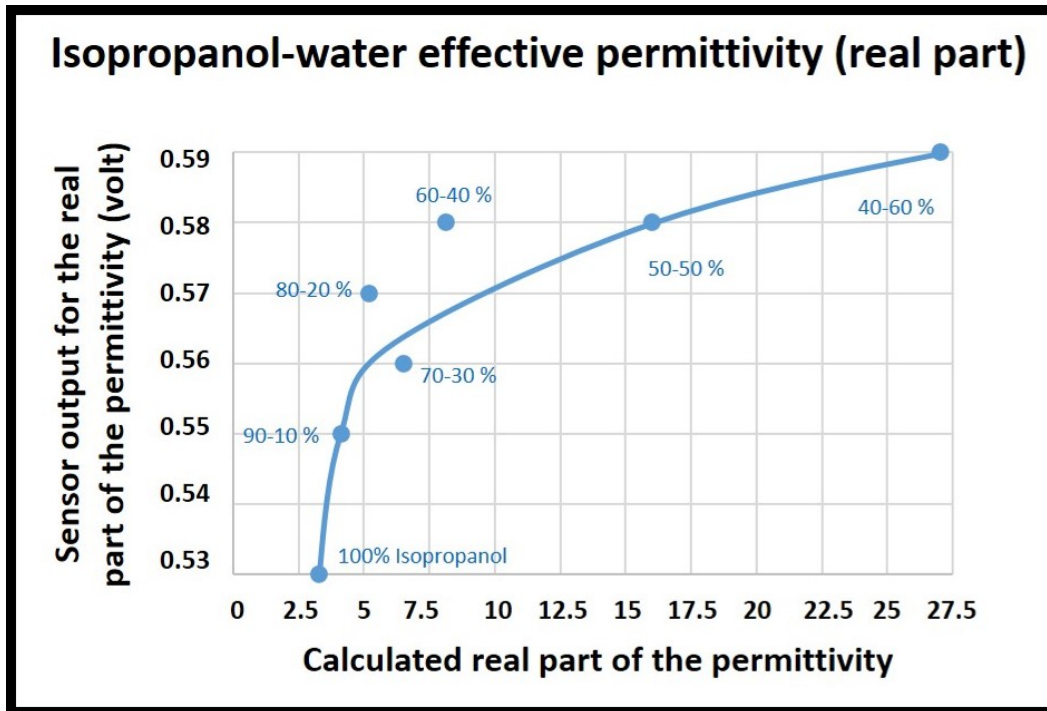


Figure 3.11: Sensor results for real (ϵ'_r) part of the effective permittivity of isopropanol–water mixtures compared to its theoretical values calculated using mixture theories.

In this equation, f_{r1} and f_{r2} are relaxation frequencies of the material's two dielectric relaxations. The high-frequency permittivity limit of the material is ϵ_∞ ; however, ϵ_s and ϵ_h are representing static permittivity and notional high-frequency permittivity limit of the lower frequency relaxation, respectively. Calculated theoretical values for real (ϵ'_r) and imaginary (ϵ''_r) parts of the complex permittivity of these mixtures were recorded and compared to biosensor results, as presented in Figures 3.11 and 3.12.

Figure 3.11 shows the sensor output for the real (ϵ'_r) part of effective permittivities of mixtures and their theoretical values. It is shown that, by adding water into mixtures, both output voltage of the sensor and dielectric constant values of mixtures increase. This is along with the functioning principle of the sensor, since increasing the water content of mixtures (higher dielectric constant) triggers the input capacitance of the sensor, leading to a higher output voltage. However, after the 50–50% step, water becomes the dominant content of the mixture, stopping the sensor from functioning adequately.

The sensor outcome for imaginary (ϵ''_r) part of the effective permittivities of mixtures and their theoretical values are illustrated in Figure 3.12. Increase in the water content (higher conductivity) of mixtures leads to a greater energy leakage and a decline in the output power of the oscillator. Similar to acquired

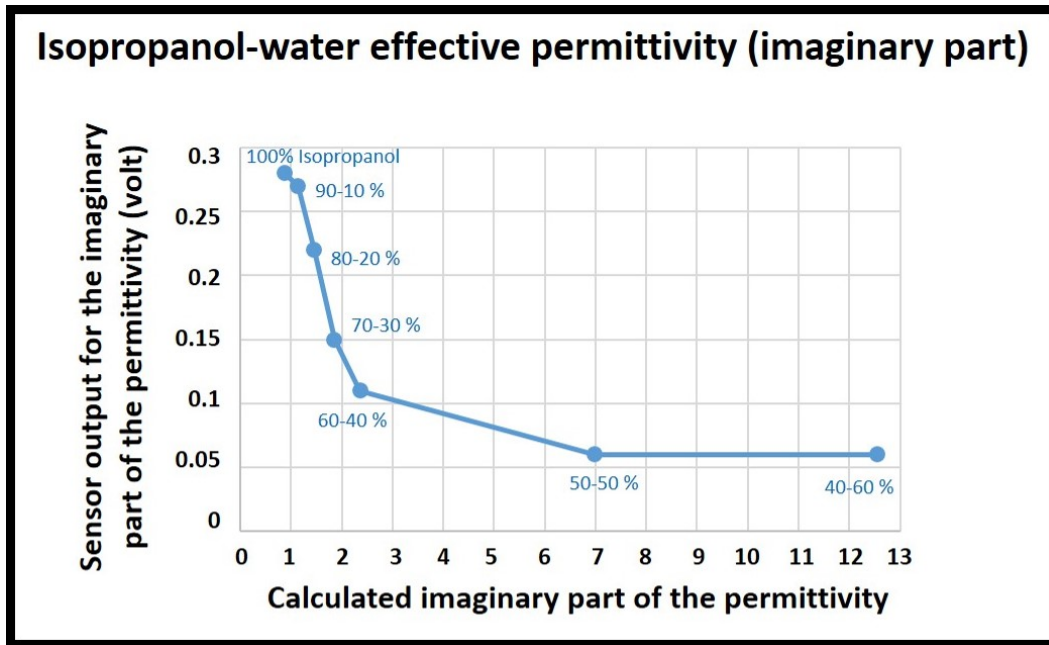


Figure 3.12: Sensor results for the imaginary (ϵ_r'') part of the effective permittivity of isopropanol–water mixtures compared to its theoretical values calculated using mixture theories.

results for ϵ_r' , the sensor stops functioning properly after the water dominance in the mixture. This is due to the fact that, after the 50–50% step, the energy leakage in the system is so high (so lossy) that the sensor cannot track the input changes accordingly and, consequently, the sensor output remains constant (Figure 3.12).

3.2.3.2 Clinical Evaluations

An m-VROC viscometer (m-VROC, RheoSense Inc., San Ramon, CA, USA), capable of viscosity characterization of non-Newtonian biofluids, was used for sensor performance evaluations. Two groups of saliva samples, collected from HC and COPD patients (five samples for each group), were de-frozen and prepared for measurements, as illustrated in Figure 3.13(a). It should be noted that the sampling of saliva samples was approved by the local ethics committee of the University of Luebeck (approval no. 16-167) and a written informed consent was obtained from all patients. A commercialized centrifuge (Eppendorf centrifuge 5415R, Eppendorf Inc., Hamburg, Germany) was used to separate and remove particulate pallets from saliva samples, as shown in Figure 3.13(b). The process was conducted at 4 °C and 4000 RPM for 5 min. After the centrifugation process, the viscosity and complex permittivity of samples were simultaneously

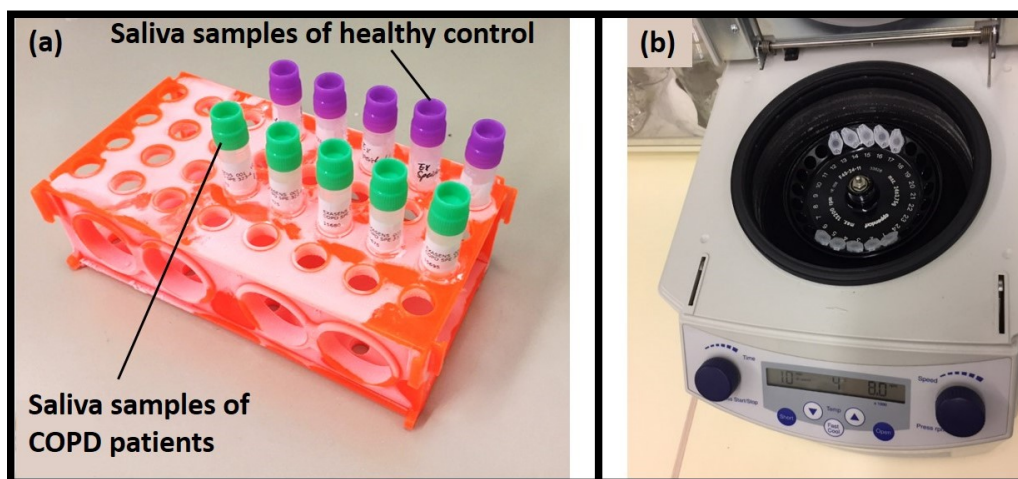


Figure 3.13: (a) two groups of saliva samples collected from HC and COPD patients (five samples for each group); (b) centrifuging saliva samples for particulate pallets separation and removing.

measured using m-VROC and the dielectric sensor, respectively. Experiments were conducted in triplicate following cleaning (using Aquet) and primary steps required for m-VROC measurements. Average values of three measurements were calculated and reported for every sample, as shown in Figure 3.14. During last two sets of experiments, the micro-capillary of m-VROC was blocked by particulate matters existing in saliva (such as protein molecules). As a consequence, m-VROC viscosity results for these measurements were inaccurate and, therefore, were excluded from calculations and the report, as shown in Figure 3.14. Inaccuracy and unreliability of these measurements were evident considering their low r-square values, provided for their slope-fit by m-VROC, as well as their irrelevancy with respect to the expected viscosity range for saliva samples (1.5 mPa·s) [41].

Figures 3.15 and 3.16 show biosensor results for complex permittivity measurements of saliva samples collected from COPD patients and HC. Real part of the permittivity indicates the energy absorption capability of these two groups of samples; however, imaginary part of the permittivity represents energy loss differences in them. Moreover, by taking Equation (3.1) into account, imaginary part of the permittivity (energy loss) could indicate conductivity characteristics of samples.

3.2.4 Results and Discussion

Table 3.4 presents results of the complex permittivity and viscosity measurements acquired by the dielectric biosensor and m-VROC for COPD patients and HC. The relative standard deviation method was

implemented on acquired results to determine repeatability characteristics of sensors. Repeatability values of 1.3% and 1.1% were calculated for m-VROC and the biosensor, respectively.

Viscosity measurements by m-VROC provided important information on physical properties of saliva samples of COPD patients and HC, beneficial for disease diagnosis. As shown in Figure 3.14, the average viscosity of saliva samples is approximately 0.15 mPa·s greater for COPD patients compared to HC. However, considering this extremely small difference, it is crucial to take into account effects of measurement conditions on results. For example, temperature fluctuations can significantly affect the sensor performance. Therefore, temperature compensation methods are necessary to improve sensor accuracy for real-world applications. Furthermore, the sample fraction from which the saliva was collected (after the centrifugation process) determines its density level. As a result, saliva samples from different fractions might show slightly different viscosity characteristics.

On the other hand, the developed biosensor provided valuable information on electrical properties of saliva samples of COPD and HC groups by distinguishing between their complex permittivity values, as illustrated in Figures 3.15 and 3.16. As shown in Figure 3.15, the average sensor output for real part of the permittivity were shown to be 0.65 (V) and 0.58 (V) for COPD and HC, respectively. Therefore, COPD samples provided better dielectric characteristics (energy absorption capability) compared to HC. However, considering the biosensor results for permittivity characterization of isopropanol–water mixture (Figure 3.11), measured values for real part of the permittivity of COPD samples are out of the expected measurement range. This issue could be caused due to the presence of highly dielectric materials such as salt or other biological particles in COPD samples. Therefore, further investigations from a biological point of view are required to identify the main cause behind this phenomenon, which is out of the scope of this thesis. As illustrated in Figure 3.16, the average sensor output for imaginary part of the permittivity of COPD and HC were shown to be 0.071 (V) and 0.064 (V), respectively. Due to a greater energy leakage (energy

Table 3.4: Results of complex permittivity and viscosity measurements for COPD and HC patients.

Samples	m-VROC (mPa·s)	Biosensor ϵ'_r (Volt)	Biosensor ϵ''_r (Volt)
COPD	1.61	0.65	0.071
HC	1.46	0.58	0.064

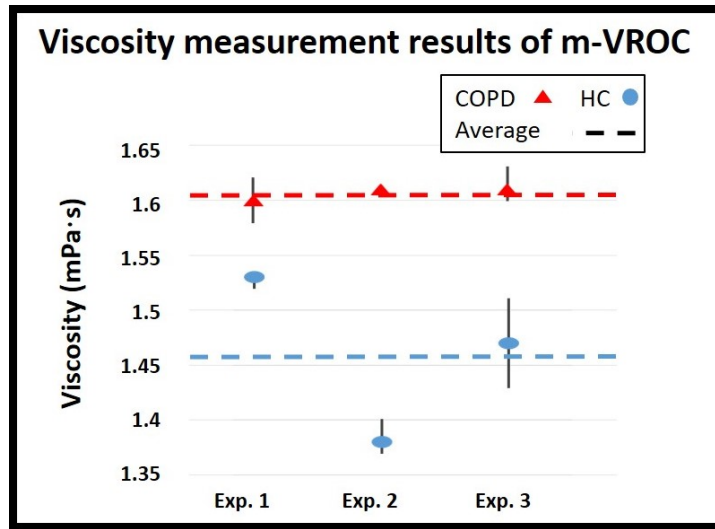


Figure 3.14: Results of m-VROC viscosity measurements for saliva samples of COPD patients and HC.

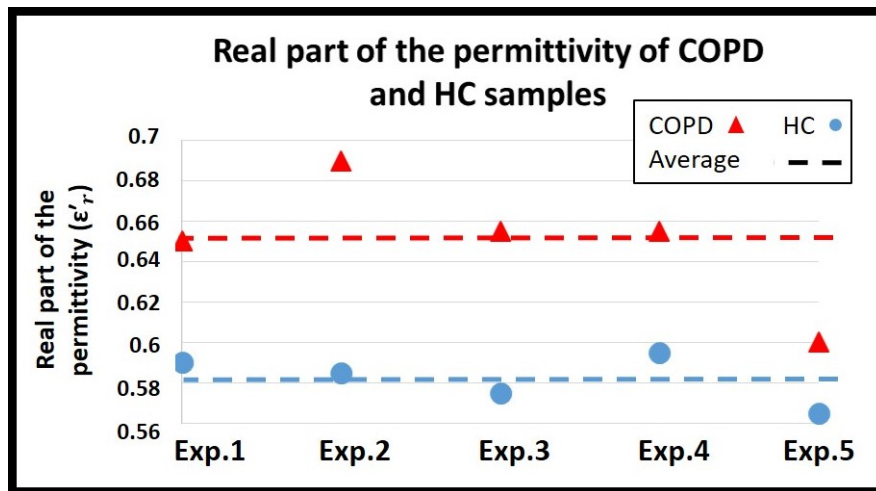


Figure 3.15: Results of the biosensor measurements for real part of the permittivity indicating the energy absorption capability of saliva samples of COPD and HC.

loss) in HC samples, imaginary part of the permittivity of these samples is lower than COPD. As discussed in Figure 3.12, lower values for imaginary part of the permittivity are representing higher conductivity features. Therefore, saliva samples of HC presented better conductivity characteristics compared to COPD, which could be due to the presence of a greater water content in HC samples. Since the greater water content of saliva represents its lower viscosity level, sensor results suggest higher viscosity values for COPD samples relative to HC. This conclusion goes along with viscosity results acquired from m-VROC.

Although no direct theoretical correlation between viscosity (mechanical properties) and dielectric con-

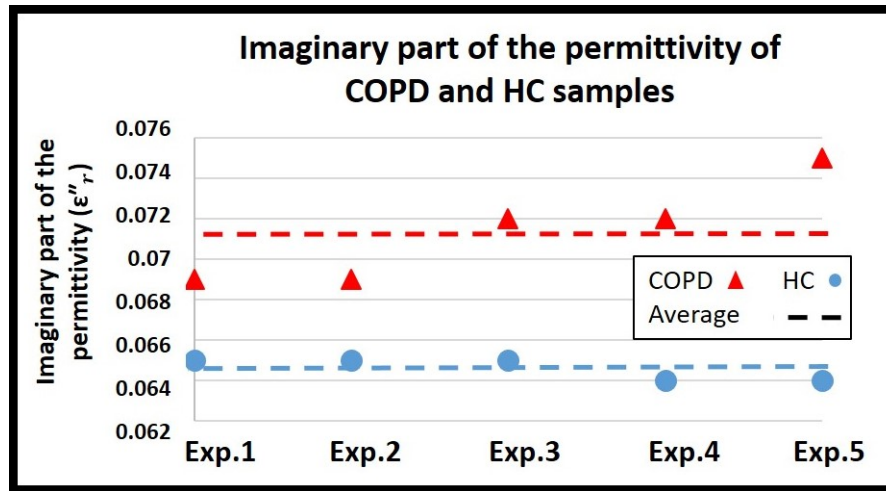


Figure 3.16: Results of the biosensor measurements for imaginary part of the permittivity represents the energy loss differences in COPD samples compared to HC.

stant (electrical properties) of a medium exists, m-VROC and the biosensor were able to identically track variations of these two features in saliva samples of COPD and HC. In other words, the dielectric biosensor was able to detect viscosity differences between saliva samples of COPD and HC by identifying their complex permittivity differences. However, considering the functioning principle of a dielectric sensor, providing absolute viscosity values of these samples was not possible.

Considering the high water content of saliva and notably small viscosity differences of COPD and HC samples, detection of dielectric constant variations in these samples requires an extremely accurate and sensitive sensing technology. Therefore, modifications are required to improve the accuracy and sensitivity of the dielectric sensor for characterization of these kinds of samples. Since the developed biosensor is able to characterize dielectric properties of a MUT from millimeter distances, locating sensor a few millimeter distanced from droplet reservoir could potentially address issues related to the extensive energy loss caused by highly conductive liquids such as water. However, the trade-off between sensor resolution and its distance from the MUT need to be taken into account. In addition, using bottom fractions of the centrifuged saliva (the high-density region with less water) for measurements could possibly improve the sensor performance.

It is noteworthy that the goal of this step was to show the feasibility of the concept in a preclinical setting. However, further investigations, with a large number of saliva samples (preferably 50 or more), are required in the future to show the precise and accurate trend in viscosity variations for COPD and HC groups. Upon unavailability of clinical samples in such a large number, artificially simulated saliva

samples could be used for these investigations. However, it should be taken into account that the spiking volume of external substances, added for increasing viscosity of specific samples, should not exceed 5% of the artificial saliva. In addition, it needs to be mentioned that the variability of saliva as a sample matrix, due to various factors such as a patient's diet, could potentially affect viscosity properties of samples and, consequently, the accuracy of clinical assessments. Therefore, a standard operating procedure (SOP) was implemented in our sampling method to reduce potential differences in our sample pool and in between samples. However, viscosity differences of saliva samples cannot be the one and only parameter for determining the absolute state of the disease, but a broader panel of COPD biomarkers, such as cytokine levels and pathogen load of samples, is required for an accurate diagnosis. As a result, the low reliability level of saliva, considering its variability, is among the main caveats of this assay procedure for clinical assessments. On the other hand, main advantages of using saliva as a sample matrix are its availability in PoC environments and the possibility of obtaining samples non-invasively on a daily basis. Future enhancements required for efficiency of the testing procedure include using artificially simulated saliva and modifying the cleaning–calibration processes of the system for conducting large number of experiments in a shorter period of time.

A major advantage of the developed biosensor was its capability for static characterization of non-Newtonian liquids with no fluid flow requirements. This feature of the device made its cleaning process relatively faster and simpler compared to microfluidic-based systems such as m-VROC, in which removing protein molecules stuck inside its capillary is very challenging and time consuming. Moreover, the cost-effectiveness of the system, due to its simplified design and packaging, as well as its notably short response time are among its main advantages compared to other emerging technologies. Considering these advantages, the biosensor could potentially be used in the future for other bioanalytical applications and biomarkers detection such as micro-organisms characterization, medical spectroscopy, glucose concentration monitoring, cerebra spinal fluid characterization, DNA detection, and sperms identification for semen analysis.

As previously mentioned, ambient conditions such as temperature can notably affect samples viscosity characteristics and, consequently, the biosensor outcome. However, this issue could be problematic from a medical–diagnostic point of view. To address this issue, acquired results from the biosensor need to be sent to a web-enabled (cloud-connected) smart device, such as a smartphone or a tablet, for further com-

parison with available patient records. Development of diagnostic algorithms based on different ambient conditions is essential for this purpose. Training neural networks for optimizing these diagnostic algorithms using available medical records will pave the way towards an artificial intelligence-based diagnostic method. Nevertheless, this complex method requires further investigations, which will be discussed in the subsequent chapters.

3.2.5 Conclusions and Future Work

In this section, a dielectric biosensor was developed for the rapid detection of viscosity variations of biofluids. The sensor was fully integrated into a handheld device and provided rapid and real-time measurements for users. Low-cost, simplified packaging, ease of cleaning, portability, and rapid detection capability of the biosensor made it a suitable technology for PoC applications.

The sensor efficacy for dielectric characterization of water-based mediums was assessed using isopropanol–water mixtures. The sensor showed promising results for complex permittivity characterizations of mixtures up to a point where water dominated solutions.

In-vitro performance of the biosensor was evaluated using a commercialized m-VROC viscometer. Viscosity and complex permittivity of saliva samples, collected from COPD patients and HC, were characterized and capability of the biosensor to detect their viscosity differences was evaluated. Throughout these experiments, COPD samples provided higher viscosity compared to HC. Similarly, greater values for real part of the complex permittivity of COPD samples, representing their better dielectric features, were recorded. In contrast, imaginary part of the permittivity of HC, which indicates conductivity characteristics, were shown to be greater compared to the COPD group. Further investigations are required to clarify biological causes on obtained results.

The biosensor showed promising results for the detection of viscosity differences of saliva samples of COPD and HC through detecting their permittivity variations. In addition, capability of the biosensor to distinguish between electrical properties of COPD and HC saliva samples, opened up a new window into different methodologies for early and rapid detection of COPD. High repeatability of 1.1% was reported for the biosensor, making it a reliable technology for medical diagnostics. Nevertheless, future modifications are required to compensate temperature effects on measurements and to make the biosensor more compatible to mediums with a high water content. In addition, considering the recent trend in medical

technologies towards the internet of things for smart healthcare systems [43, 44], the next generation of the biosensor will be interfaced with a smartphone to enable physicians with a continuous monitoring of the disease progress. Furthermore, by sending collected data to the cloud, it will be possible to implement machine learning methods for precision diagnostic purposes. The next chapter of the thesis will investigate the use of machine learning techniques for advanced analytics.

Bibliography

- [1] P.S. Zarrin, F.I. Jamal, S. Guha, J. Wessel, D. Kissinger, C. Wenger. “Design and Fabrication of a BiCMOS Dielectric Sensor for Viscosity Measurements: A Possible Solution for Early Detection of COPD,” *Biosensors*, vol. 8, no. 78, 2018.
- [2] P.J. Barnes. “Mechanisms in COPD: Differences from asthma,” *Journal Chest*, vol. 117, no. 2, pp. 10S—14S, 2000.
- [3] N.G. Csikesz, E.J. Gartman. “New developments in the assessment of COPD: Early diagnosis is key,” *International Journal Chronic Obstructive Pulmonary Disease*, vol. 9, pp. 277–286, 2014.
- [4] W. Robinson, P. Woolley, R.E.C. Altounyan. “Reduction of sputum viscosity in chronic bronchitis,” *Lancet*, vol. 272, pp. 819–821, 1958.
- [5] M.T. Lopez-Vidriero, L.d Reid. “Chemical markers of mucous and serum glycoproteins and their relation to viscosity in mucoid and purulent sputum from various hypersecretory diseases,” *American Review of Respiratory Disease*, vol. 117, no. 3, pp. 465–477, 1978.
- [6] C. Boss, E. Meurville, J.M. Sallese, P. Ryser. “A viscosity-dependent affinity sensor for continuous monitoring of glucose in biological fluids,” *Biosensors and Bioelectronics*, vol. 30, no. 1, pp. 223–228, 2011.
- [7] B.J. Kim, S.Y. Lee, S. Jee, A. Atajanov, S. Yang. “Micro-Viscometer for Measuring Shear-Varying Blood Viscosity over a Wide-Ranging Shear Rate,” *Sensors*, vol. 17, p. 1442, 2017.
- [8] Y. Zhao, S. Li, A. Davidson, B. Yang, Q. Wang, Q. Lin. “A MEMS viscometric sensor for continuous glucose monitoring,” *Journal of Micromechanics and Microengineering*, vol. 17, p. 2528, 2007.

- [9] O. Cakmak, E. Ermeke, N. Kilinc, I. Baris, I.H. Kavakli, G. Yaralioglu, H. Urey. “Microcantilever based LoC system for coagulation measurements,” In *Proceedings of the 18th International Conference on Miniaturized Systems for Chemistry and Life Sciences*, San Antonio, TX, USA, 26–30 October 2014; pp. 2050–2052.
- [10] U. Beyer, D. Schafer, A. Thomas, H. Aulich, U. Haueter, B. Reihl, R. Ehwald. “Recording of subcutaneous glucose dynamics by a viscometric affinity sensor,” *Diabetologia*, vol. 44, pp. 416–423, 2001.
- [11] L.M. Lee, X. Cui, C. Yang. “The application of on-chip optofluidic microscopy for imaging *Giardia lamblia* trophozoites and cysts,” *Biomedical Microdevices*, vol. 11, p. 951, 2009.
- [12] P.S. Zarrin, A. Escoto, R. Xu, R.V. Patel, M.D. Naish, A.L. Trejos. “Development of an optical fiber-based sensor for grasping and axial force sensing,” In *Proceedings of the International Conference on Robotics and Automation (ICRA)*, Singapore, 29 May–3 June 2017, pp. 939–944.
- [13] J.S. Daniels, N. Pourmand. “Label-free impedance biosensors: Opportunities and challenges,” *Electroanalysis*, vol. 19, pp. 1239–1257, 2007.
- [14] P.S. Zarrin, A. Escoto, R. Xu, R.V. Patel, M.D. Naish, A.L. Trejos. “Development of a 2-DOF Sensorized Surgical Grasper for Grasping and Axial Force Measurements,” *IEEE Sensors Journal*, vol. 18, no. 7, pp. 2816–2826, 2018.
- [15] S. Kuenzi. “Implantable Glucose Sensor: An Approach Based on a Rotating Microviscometer Combined with a Sensitive Liquid Containing Dextran and Concanavalin A,” *EPFL University: Lausanne*, Switzerland, 2007.
- [16] Y.H. Ghallab, Y. Ismail. “CMOS based lab-on-a-chip: Applications, challenges and future trends,” *IEEE Circuits and Systems Magazine*, vol. 14, no.2, pp. 27–47, 2014.
- [17] M.N. Gulari, M. Ghannad-Rezaie, N. Chronis. “A compact, optofluidic system for measuring red blood cell concentration,” In *Proceedings of the 17th International Conference on Solid-State Sensors, Actuators and Microsystems*, Barcelona, Spain, 16–20 June 2013, pp. 2552–2555.

- [18] S. Guha, F.I. Jamal, C. Wenger. “A Review on Passive and Integrated Near-Field Microwave Biosensors,” *Biosensors*, vol. 7, p. 42, 2017.
- [19] K. Entesari, A.A. Helmy, M. Moslehi-Bajestan. “Integrated Systems for Biomedical Applications: Silicon-Based RF/Microwave Dielectric Spectroscopy and Sensing,” *IEEE Microwave Magazine*, vol. 18, pp. 57–72, 2017.
- [20] C. Stagni, C. Guiducci, L. Benini, B. Ricco, S. Carrara, B. Samori, C. Paulus, M. Schienle, M. Augustyniak, R. Thewes. “CMOS DNA sensor array with integrated A/D conversion based on label-free capacitance measurement,” *IEEE Journal of Solid-State Circuits*, vol. 41, pp. 2956–2964, 2006.
- [21] E. Ghafar-Zadeh, M. Sawan. “A hybrid microfluidic/CMOS capacitive sensor dedicated to lab-on-chip applications,” *IEEE Transactions on Biomedical Circuits and Systems*, vol. 1, pp. 270–277, 2007.
- [22] E. Ghafar-Zadeh, M. Sawan. “Charge-based capacitive sensor array for CMOS-based laboratory-on-chip applications,” *IEEE Sensors Journal*, vol. 8, pp. 325–332, 2008.
- [23] J.W. Kim. “Development of Interdigitated Capacitor Sensors for Direct and Wireless Measurements of the Dielectric Properties of Liquids,” *The University of Texas at Austin: Austin, TX, USA*, 2008.
- [24] S. Guha, K. Schmalz, C. Meliani, C. Wenger. “CMOS based sensor for dielectric spectroscopy of biological cell suspension,” *Journal of Physics: Conference Series*, vol. 434, p. 012017, 2013.
- [25] S. Guha, F.I. Jamal, K. Schmalz, C. Wenger, C. Meliani. “CMOS lab on a chip device for dielectric characterization of cell suspensions based on a 6 GHz oscillator,” In *Proceedings of the European Microwave Conference (EuMC)*, Nuremberg, Germany, 6–10 October 2013, pp. 471–474.
- [26] A. Lonappan, A.V. Kumar, G. Bindu, V. Thomas, K.T. Mathew. “Qualitative analysis of human semen using microwaves,” In *Proceedings of the Progress in Electromagnetics Research Symposium*, Cambridge, MA, USA, 26–29 March 2006, pp. 110–114.
- [27] A. Helmy, H.J. Jeon, Y.C. Lo, A.J. Larsson, R. Kulkarni, J. Kim, J. Silva-Martinez, K. Entesari. “A self-sustained CMOS microwave chemical sensor using a frequency synthesizer,” *IEEE Journal of Solid-State Circuits*, vol. 47, pp. 2467–2483, 2012.

- [28] S. Guha, K. Ramaker, T. Krause, C. Wenger. “A CMOS radio frequency biosensor for rapid detection and screening of sputum-mucin viscosity,” In *Proceedings of the SENSORS, Glasgow, UK*, 29 October–1 November 2017, pp. 1–3.
- [29] S. Guha, C. Wenger. “Radio frequency CMOS chem-bio Viscosity sensors based on dielectric spectroscopy,” In *Proceedings of the 10th International Joint Conference on Biomedical Engineering Systems and Technologies (BIOSTEC)*, Porto, Portugal, 21–23 February 2017, pp. 142–148.
- [30] S. Guha, K. Schmalz, C. Wenger, F. Herzel. “Self-calibrating highly sensitive dynamic capacitance sensor: Towards rapid sensing and counting of particles in laminar flow systems,” *Analyst*, vol. 140, pp. 3262–3272, 2015.
- [31] F.I. Jamal, S. Guha, M. Eissa, J. Wessel, D. Kissinger. “A Fully Integrated Low-Power 30 GHz Complex Dielectric Sensor in a 0.25- μm BiCMOS Technology,” *IEEE Journal of Electromagnetics, RF and Microwaves in Medicine and Biology*, vol. 2, no. 3, pp. 163–171, 2018.
- [32] F.I. Jamal, S. Guha, M. Eissa, J. Borngräber, C. Meliani, H. Jalli, D. Kissinger, J. Wessel. “Low-Power Miniature K-Band Sensors for Dielectric Characterization of Biomaterials,” *IEEE Transactions on Microwave Theory Technology*, vol. 65, pp. 1012–1023, 2017.
- [33] J.V. Hughes, H.L. Armstrong. “The dielectric constant of dry air,” *Journal of Applied Physics*, vol. 23, pp. 501–504, 1952.
- [34] A.P. Gregory, R.N. Clarke. “Tables of the Complex Permittivity of Dielectric Reference Liquids at Frequencies Up to 5 GHz,” *National Physical Laboratory: Teddington, UK*, 2001.
- [35] F. Buckley, A. Maryott. “Tables of Dielectric Dispersion Data for Pure Liquids and Dilute Solutions,” *National Bureau of Standards circular*, U.S. Dept. of Commerce, vol. 589, November, 1958.
- [36] A. Megriche, A. Belhadj, A. Mgaidi. “Microwave dielectric properties of binary solvent wateralcohol, alcohol-alcohol mixtures at temperatures between $-35\text{ }^{\circ}\text{C}$ and $+35\text{ }^{\circ}\text{C}$ and dielectric relaxation studies,” *Mediterranean Journal of Chemistry*, vol. 1, no. 4, pp. 200–209, 2012.
- [37] A. Sihvola. “Mixing rules with complex dielectric coefficients,” *Subsurface sensing technologies and applications*, vol. 1, pp. 393–415, 2000.

- [38] P.S. Zarrin, F.I. Jamal, N. Roeckendorf, C. Wenger. “Development of a Portable Dielectric Biosensor for Rapid Detection of Viscosity Variations and Its In-Vitro Evaluations Using Saliva Samples of COPD Patients and Healthy Control,” *Healthcare*, vol. 7, no. 11, 2019.
- [39] C.D Mathers, D. Loncar. “Projections of global mortality and burden of disease from 2002 to 2030,” *PLoS Med.*, vol. 3, p. 442, 2006.
- [40] D. Price, A. Crockett, M. Arne, B. Garbe, R. Jones, A. Kaplan, A. Langhammer, S. Williams, B. Yawn. “Spirometry in primary care case-identification, diagnosis and management of COPD,” *Primary Care Respiratory Journal*, vol. 18, no. 216, 2009.
- [41] S.J. Haward, J.A. Odell, M. Berry, T. Hall. “Extensional rheology of human saliva,” *Rheologica acta*, vol. 50, pp. 869–879, 2011.
- [42] D.P. Lima, D.G. Diniz, S.A.S. Moimaz, D.H. Sumida, A.C. Okamoto. “Saliva: reflection of the body,” *International Journal of Infected Disease*, vol. 14, pp. 184–188, 2010.
- [43] S.K. Vashist, P.B. Lupta, L.Y. Yeo, A. Ozcan, J.H. Luong. “Emerging technologies for next-generation point-of-care testing,” *Trends in Biotechnology*, vol. 33, pp. 692–705, 2015.
- [44] S. B. Baker, W. Xiang, I. Atkinson. “Internet of Things for Smart Healthcare: Technologies, Challenges, and Opportunities,” *IEEE Access*, vol. 5, pp. 26521–26544, 2017.

Chapter 4

Machine Learning Implementation

4.1 Pattern Recognition for COPD Diagnostics Using an Artificial Neural Network and Its Potential Integration on Hardware-based Neuromorphic Platforms

This section of the thesis presents the development of an Artificial Neural Network (ANN) model for pattern recognition for COPD diagnosis. As discussed previously, recent advancements in healthcare devices and availability of numerous medical data have facilitated the management of chronic diseases. In addition, machine learning tools have made the management and diagnostic of a chronic illness more efficient by converting collected medical data from biosensors into meaningful clinical information. However, securing sensitive medical data, collected from patients, is still a challenging task. Hardware-based neural networks address this data safety concern by on-chip processing of acquired data, without cloud communications. Therefore, the presented ANN model was designed to comply with the intrinsic structure of neuromorphic platforms for future integrations. Materials presented in this section of the chapter is based on reference [1].

4.1.1 Introduction

With the expansion of IoT and wearable technologies in healthcare, constant and remote monitoring of patients has become a reality. Recent advances in point-of-care medical devices have facilitated the early detection, prevention, and treatment of various diseases [2]. In addition, availability of numerous clinical

data, thanks to medical IoT, has paved the way towards the better management of chronic disease [3]. For example, various technologies have widely been used for monitoring blood glucose levels in diabetic patients, heart activity tracking in elderly, and gait pattern observations of Parkinson's diseased patients [2]. However, without analytical insight, collected data from medical sensors are merely raw data with low clinical value. For instance, in the previous section, a portable biosensor for the management of COPD in home-care environments was presented [4]. The developed biosensor was capable to characterize the viscosity of saliva samples for diagnostic purposes. However, viscosity properties of saliva samples is one parameter out of various parameters which are required for COPD detection. In addition, ambient conditions such as temperature considerably affect the viscosity of samples, causing diagnostic complexities. In other words, two identical samples collected from a single patient could be diagnosed as diseased and healthy in low and high temperatures, respectively. This issue is not a measurement error (to be addressed using a temperature compensation sensor), but an environmental parameter affecting samples. Therefore, various parameters including ambient conditions, patients medical background, smoking history, gender, and age are required for the disease diagnosis. As a result, upon viscosity measurements by the developed biosensor, a sophisticated diagnostic algorithm, by concurrent consideration of all essential parameters, is required for the detection of COPD. Therefore, machine learning tools, or more specifically pattern recognition methods, could make the diagnostic procedure more efficient by converting collected data from medical sensors into meaningful clinical information. Moreover, machine learning can be used for identifying diagnostic links between symptoms and diseases, which have been previously unknown, and providing treatment plans and recommendations to the healthcare specialists. Therefore, the objective of this section was to develop an ANN for pattern recognitions for COPD diagnosis. Nevertheless, the end goal of this approach is to transfer the modeled ANN onto the previously developed neuromorphic platform [5]. As reported in [5], a new learning algorithm for neuromorphic systems was implemented based on the inherent stochasticity of CMOS integrated HfO₂-based Resistive Random Access Memory (RRAM) devices. For the implementation of the learning algorithm, the RRAM array was integrated into a mixed-signal neuromorphic circuit with software-based neurons [5]. The hardware-based approach provides many advantages over the ANN such as low energy consumption. In addition, the main advantage of the hardware-based platforms, which is the main incentive behind this approach, is the possibility of securing sensitive medical data by processing them on-chip, without requiring any cloud communication or backend post-processing.

Although, advantages of neuromorphic platforms for medical applications are briefly discussed at the end of this section, the focus of this part is to present the hardware-compatible simulation model using an ANN.

4.1.2 Materials and Methods

Prior to modeling the ANN, required clinical parameters for diagnosing COPD and their respected ranges for diseased and healthy subjects were identified. Apart from sensor measurements on viscosity of saliva samples, the ambient temperature, patients smoking background, cytokine level, pathogen load, mucin combinations, gender, and age are among the eight fundamental parameters required for the diagnosis of COPD [6]. Since, at this stage of the project, actual medical records for training the neural network were unavailable, synthetic data were generated for thousand subjects. For clinical relevancy, synthetic data for various parameters were created with respect to reported ranges in previous studies [6–9]. For example, patients with severe COPD have shown a lower cytokine level of $\text{TNF}\alpha$ compared with controls (COPD: 0–20 pg/ml and controls: 0–40 pg/ml) [7]. Additionally, viscosity of saliva was investigated to be greater in COPD samples (1.6–2 mPa·s) compared to healthy controls (1–1.5 mPa·s) [4, 8, 9]. Further information regarding clinical parameters and their ranges for different stages of COPD is available in the literature [6–9]. By taking into account the literature information for synthesizing data, first 300 subjects were considered as COPD diseased patients and were labeled as 3; whereas, the last 300 were chosen to be healthy subjects with the label 0. Labels 2 and 1 indicated patients (200 subjects for each label) with high and low probabilities of containing COPD, respectively. In a similar manner, 200 additional data for test subjects were created to evaluate the ANN's performance after training it. Generated data for train and test samples were normalized separately, to the range of 0–1, to improve network's performance. As shown in Figure 4.1(a), a dense ANN with a single hidden layer was modeled on the JupyterLab environment using Python and Keras. The input layer of the network consisted of 8 neurons, considering abovementioned clinical parameters. Considering intrinsic structure and characteristics of the neuromorphic platform (64×64 grid structure of the memristor), a hidden layer with 64 neurons and a sigmoid activation function was modeled. The output layer, with a sigmoid activation function, consisted of 4 neurons for four potential outcomes. Adam optimization algorithm, with a 0.0001 learning rate, and the cross entropy error function were used for training and optimizing network parameters. A dropout, with 20% probability, was implemented for overfitting prevention. After modeling the ANN, generated data were fed into the network for 150 training

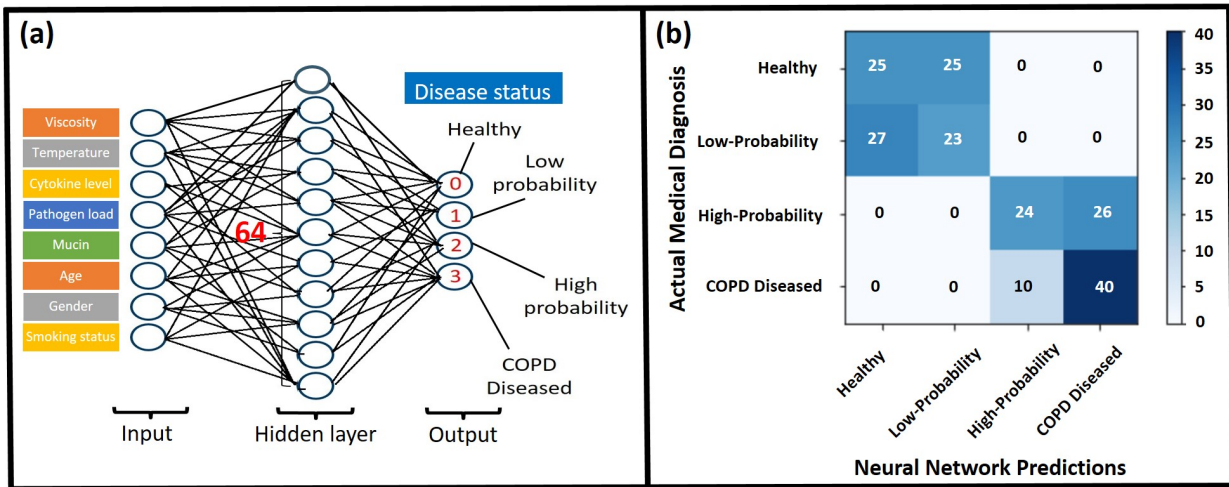


Figure 4.1: (a) the structure of the ANN developed for pattern recognition for COPD diagnostics; (b) ANN predictions for the test subjects compared to their actual status.

epochs with a batch size of 10. During training the network, 10% of the data were split for validation purposes. The trained network was used to predict labels of the generated test data.

4.1.3 Results and Discussions

The developed ANN provided accuracies of 65% and 72% for the network and validation performances, respectively. The synthetic nature of the generated data, used for training the network, could possibly be the main reason behind ANN's limited accuracy. Using actual medical records, therefore, will potentially improve the accuracy in the future. After the training procedure, generated test data were fed into the network for performance evaluations. The ANN was able to precisely predict the status of 112 samples (out of 200), as presented in Figure 4.1(b). Moreover, no diseased patient was diagnosed as healthy or vice versa, representing ANN's reliability for medical applications.

Machine learning provides promising results for diagnosing various diseases and identifying trends in medical data. It fills the gap between patients, in remote locations, and the medical staff by providing accurate and real-time predictions on their health status or disease progress. Furthermore, it assists healthcare professionals by recommending treatment plans and medical prescriptions. Machine learning will play a pivotal role in the future for assisting patients with degenerative conditions, management of chronic conditions, monitoring patients rehabilitation progress, and predicting critical and emergency health conditions. Although machine learning is of a great importance for healthcare, various drawbacks and challenges of

this approach have limited its real-world applications. The main drawback of this method is the security risk related to handling sensitive medical data which concerns patients' privacy. Precise security regulations need to be considered for designing short-range (device to smartphone via bluetooth) and long-range (smartphone to backend using internet) communications for transferring data from medical devices to the backend. In addition, storage of the collected medical data in a single database increases the potential risk for malicious attacks [2]. Furthermore, acquired data require pre-processing and data curation–compression to comply with the broadband communications specifications, prior to their extraction from the device towards the backend. Moreover, enormous computational power with significant energy consumption is required for post-processing and analyzing collected data at the backend to provide meaningful and real-time information to users and the medical staff.

The abovementioned limitations of machine learning in healthcare can possibly be addressed using neuromorphic platforms. A neuromorphic unit offers a hardware-based imitation of neural networks by using actual electrical components as neurons and synapses. By bringing data post-processing from the backend onto a chip, real-time analysis of data in a less time consuming manner with a smaller time delay is feasible [10]. Furthermore, securing sensitive medical data on a single chip, without external communications, is far more practical. In addition, energy-efficient neuromorphic platforms are relatively better immune against false operations and, therefore, offer a large fault tolerance for medical applications [11]. Therefore, the integration of the presented ANN model, for diagnosing COPD, on previously developed hardware-based neuromorphic platform is a necessary step, which will be discussed in the next chapter.

4.2 In-vitro Classification of Saliva Samples of COPD Patients and Healthy Controls Using Machine Learning Tools

As previously discussed, the accurate examination of respiratory tract fluids like saliva is a promising approach for staging COPD and predicting its upcoming exacerbations in a PoC environment. However, the concurrent consideration of patients' demographic and medical parameters is necessary for achieving accurate outcomes. Therefore, Machine Learning (ML) tools can play an important role for analyzing patient data and providing comprehensive results for the recognition of COPD in a PoC setting. As a result, the goal of this section is to implement ML tools on the data acquired from characterizing saliva samples of

COPD patients and healthy controls as well as their demographic information for the PoC recognition of the disease. For this purpose, the previously introduced permittivity biosensor was used to characterize dielectric properties of saliva samples and, subsequently, ML tools were applied on the acquired data for classification. The XGBoost gradient boosting algorithm provided a high classification accuracy and sensitivity of 91.25% and 100%, respectively, making it a promising model for COPD evaluation. Integration of this model on a neuromorphic chip, will enable the real-time assessment of COPD in PoC, with low cost, low energy consumption, and high patient privacy. In addition, constant monitoring of COPD in a near-patient setup will enable the better management of the disease exacerbations. This section is based on reference [12].

4.2.1 Introduction

COPD, as one of the most prevalent lung diseases worldwide, runs a perfidious course with an often long-lasting undiagnosed initial phase. Clinical treatment approaches for COPD result in repeated clinical visits and extended hospitalization for patients. This fact, apart from being an economical burden for healthcare infrastructures, drastically impacts patients' life quality. To address this issue, contemporary healthcare systems have encouraged the development of personalized solutions, through which patients can receive appropriate medical assistance in an outpatient clinic or a home-care environment [13].

The clinical ground truth methodology for diagnosing COPD is comprehensively reported within the GOLD guidelines [14]. Among available screening and detection methods, spirometry pulmonary function test is the most rudimentary and systematic method in primary care for the diagnosis of COPD. Along this test, lung capacity of patients is measured during breathing in–out cycles [15]. According to a study by Haroon *et al.*, COPD is widely under-diagnosed due to the limited sensitivity of the spirometry test in the range of 64.5–79.9% [16]. As a result, examining mucin, present in sputum or saliva samples, provides more reliable information on the course of the disease which can be affected by bacterial infections [15]. Sputum and saliva are both mucosal secretions, their composition is affected by changes in health conditions of individuals suffering from inflammatory lung diseases such as COPD [13, 17]. Alterations in the mucin production during the course of COPD, which impacts the viscosity of mucosal secretions, has long been studied [18]. In addition, the expression of aquaporin-5 has found to be decreased in some COPD patients, affecting dielectric properties of their respiratory tract fluids [19]. The main contents of sputum, produced

by lungs, are mucin, water, epithelial cells of the airway mucosa, and salt (in physiological concentrations). Salt concentrations in epithelial lining fluid was investigated by Effros *et al.*, indicating its effect on the dielectric properties of the fluid [20]. However, a direct correlation of dielectric properties with COPD was not stated in their work [20]. Therefore, investigating dielectric and supramolecular properties of sputum can provide useful information for staging COPD [9]. This is due to the fact that supramolecular properties of mucin gels are considerably affected by water content variations at different stages of the disease [9]. Upon the entry of water into mucin's gels matrix, there is a considerable amount of proton release resulting from cations exchange (particularly Ca and Na), which drastically changes the dielectric permittivity properties of mucin samples [9]. In other words, sputum samples collected from COPD patients are expected to have different permittivity characteristics compared to samples of HC, which could be used as a biomarker for the assessment of the disease in a PoC environment [4, 8]. However, due to the complexities of obtaining sputum samples non-invasively on a daily-basis, saliva could be an alternative with better patient compliance for PoC applications [21].

Although the dielectric characterization of saliva samples can potentially shine a spotlight onto the detection of COPD in a PoC setting, the comprehensive diagnosis of the disease requires a sophisticated algorithm by concurrent consideration of all essential parameters related to a patient's personal and medical backgrounds [4]. These demographic parameters include, but are not limited to, age, gender, weight, cytokine level, pathogen load, and the smoking background of subjects [4]. Therefore, without analytical insight, information obtained on one specific parameter has a low clinical value for the disease diagnosis [2]. As a result, implementation of ML tools is crucial for the conversion of collected raw data from subjects into meaningful clinical–diagnostic information [3, 22, 23]. Furthermore, advanced ML analytics could make the management of COPD in PoC applications more efficient. Therefore, the novel hypothesis of this part of the thesis was to scrutinize whether dielectric properties of saliva change upon the development of a COPD; and whether ML tools, applied on this information together with demographic parameters, can identify the diagnostic status of patients.

Among various ML classifiers, Artificial Neural Networks (ANNs), Support Vector Machines (SVMs), principal component analysis, Logistic Regression (LR), eXtreme Gradient Boosting (XGBoost) algorithm, and Naïve Bayes (NB) are among the most common models used for the classification of medical data [24–27]. Although ANNs generally provide acceptable performance for classifying data, their sensitiv-

ity to outliers— especially in small datasets—causes overfitting issues, thus degrading their accuracy [28]. On the other hand, non-perceptron classifiers such as XGBoost or SVM are less prone to overfitting and less sensitive to outliers, thus performing notably better in applications with a small-sized dataset. In addition, unlike ANNs, non-perceptron classifiers are computationally more efficient since their computational complexity does not depend on the dimension of the input space, making them an appropriate tool for edge computing applications [28]. Therefore, energy–computation efficiency of non-perceptron classifiers make them a suitable choice for medical data classifications in PoC applications.

The objective of this section was to apply machine learning tools on the data obtained from characterizing saliva samples of COPD patients and HC for diagnostic classifications. This part is the extension of the previous section, which introduced a neuromorphic-compatible ANN for COPD pattern recognition using synthesized data [1]. However, the current part deals with real data collected from COPD patients and HC in a clinical setting. The high performance of the XGBoost algorithm for classifying saliva samples, with relatively a small number of data points, and its less susceptibility to overfitting made it an adequate tool for clinical analytics. Although the presented research in this thesis targets the PoC detection of COPD in a personalized care scheme, the introduced ML techniques can be used in the future for the enhancement of conventional clinical-based standard of care methods, available for the diagnosis and staging of COPD.

4.2.2 Materials and Methods

Two groups of saliva samples, 160 for HC and 79 for COPD patients, were collected in the frame of a joint research project Exasens at the Research Center Borstel, BioMaterialBank Nord (Borstel, Germany). Patient materials were collected between November 2016 and February 2018 and were anonymized prior to accessibility. The sampling procedure of the saliva samples was approved by the local ethics committee of the University of Luebeck under the approval number AZ-16-167 and a written informed consent was obtained from all patients. The COPD subjects of the study were patients who had been previously hospitalized in the pulmonary clinic Borstel (Borstel, Germany) and several outpatients. Therefore, the inclusion criterion for enrolling patients into the COPD group was a diagnosed COPD without acute respiratory infection, with respect to the GOLD guidelines [14]. Inclusion criteria for the healthy group were the absence of a diagnosed COPD or asthma affections. Demographic information—including gender, age, smoking status (smoker, ex-smoker, and non-smoker), the date of probing, sampling conditions, and special notes

regarding the contamination of saliva with blood—were collected at the recruitment, based on patients' self-declarations. Saliva sampling (5 ml) after mouth wash was induced using a chewing gum (GC Corporation, Leuven, Belgium). The collected samples were aliquoted and snap frozen in liquid nitrogen immediately after receipt and were stored at $-80\text{ }^{\circ}\text{C}$. To avoid frequent freeze–thaw cycles, samples were thawed and transferred onto the sensor immediately before dielectric measurements, as recommended in standard operating procedures for keeping the integrity of human biospecimens such as saliva [29]. Although effects of freezing and de-freezing saliva samples on their dielectric properties have yet to be investigated, all characterized samples in this work have exactly gone through a one-freeze–one-thaw cycle. As a result, possible effects of freezing samples have not been considered as a model variable for ML models. Measurements on dielectric properties of saliva samples were conducted *in-vitro* at the Research Center Borstel, Leibniz lung center.

4.2.2.1 Dielectric Characterization of Saliva Samples

Prior to measurements, saliva samples of COPD and HC (40 samples for each group) were defrozen and centrifuged for removing insoluble matter. The centrifugation process was conducted using a commercialized centrifuge (Eppendorf centrifuge 5415R, Eppendorf Inc., Hamburg, Germany) at $4\text{ }^{\circ}\text{C}$ and 4000 RPM for a duration of 5 minutes. As shown in Figure 4.2, a previously developed permittivity biosensor (IHP Microelectronics, Frankfurt Oder, Germany) was used for the dielectric characterization of the saliva samples [4, 8]. The output of the biosensor was extracted into an Excel file using a user-friendly data acquisition (PLX-DAQ) interface, as demonstrated in Figure 4.2. It is noteworthy that calibration inconsistency and performance degradation, caused by frequent cleaning cycles, can impair the long-term functioning of the developed biosensor, thus restricting the sample population size which can be characterized in stable and reliable circumstances. As a consequence, only 80 samples out of the available 239 were dielectrically characterized in this study. As extensively reported in the previous section, the developed biosensor is capable of measuring both real and imaginary parts of the permittivity of a material-under-test [4, 8]. From a physical point of view, real part of the permittivity represents a material's energy absorption (dielectric properties) in an interaction with an electromagnetic field; while imaginary part of it is an indicator of the material's energy loss (conductivity properties). After the sample preparation process, a droplet of $5\text{ }\mu\text{L}$ was taken and located over the sensing area of the device. Upon the presence of a sample droplet, the output

voltage of the biosensor notably drops from its calibration level, depending on the permittivity properties of the introduced sample. All measurements were conducted in a lab environment with a controlled room temperature following a primary cleaning procedure using ethanol and compressed air for the removal of extraneous particles from the sensor surface. It is noteworthy that temperature fluctuations can possibly impair the biosensor performance in real-world applications as part of measurement uncertainties associated with this system [4, 8]. As a solution, the ambient temperature can be introduced as an input variable into the ML model [1]. Nonetheless, considering the consistency of the ambient temperature throughout experiments, this parameter was not considered in this ML approach. Furthermore, uncertainties associated with the calibration and cleaning of the biosensor need to be addressed in the future for the performance enhancements in long-term applications. To obtain reliable results, experiments were repeated three times for every sample and the average (for the duration of the sample's presence over the sensing area) and minimum values of the observed results for each experiment were recorded. Subsequently, the absolute minimum and the overall average of the all three trials were reported for the final results of the real and imaginary parts of the permittivity of every sample. While the average value of observations represents the overall dielectric characteristic of a sample, the minimum value could be an indicator of the presence of some specific suspending particles inside a sample. Further information on the working principle of the dielectric biosensor is presented in details in previous sections [4, 8].

4.2.2.2 Machine Learning Implementation for Classifications

Data Preparation: As discussed in the previous section, the dielectric characterizations were conducted on only 80 samples out of the available 239, due to the limited life-cycle of the biosensor. However, to highlight the important role of demographic features in COPD detection, analysis were performed on both datasets with and without dielectric properties. The first dataset includes information on the 80 characterized saliva samples (40 samples for each group of COPD and HC). The attributes of this dataset include both the demographic features—or more specifically gender, age, and the smoking status of patients—and the permittivity properties of the saliva samples obtained through measurements, as shown in Figure 4.3. On the other hand, the second dataset includes only the demographic information of all 239 saliva samples with the following attributes: gender, age, and the smoking status of patients. For computational purposes, the non-quantitative attributes—diagnosis, gender, and smoking status—were converted into numerical values

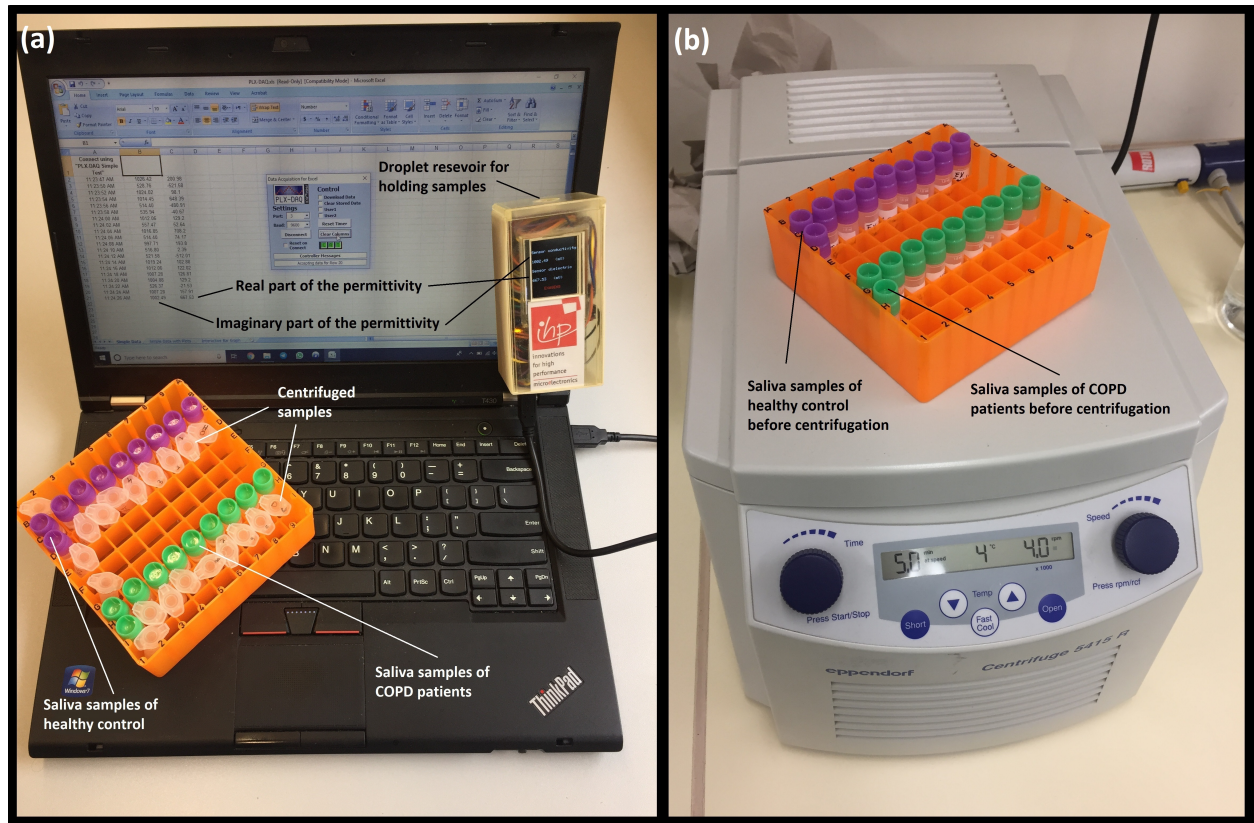


Figure 4.2: (a) the measurement setup demonstrating the biosensor output for the real–imaginary parts of the permittivity of saliva samples; (b) the centrifugation process for saliva samples collected from healthy controls and COPD patients.

using the following labels: diagnosis (COPD (1)–HC (0)), gender (male (1)–female (0)), smoking status (smoker (3)–ex-smoker (2)–non-smoker (1)). Sections of the data, used for analytics in this thesis, are publicly available at <http://iee-dataport.org/2361> [30]. To improve the performance of ML models, the first and second datasets were normalized and standardized to the Gaussian standard normal distribution with zero mean and unit variance, respectively, as presented in Figure 4.3. Standardization of datasets is significantly important for improving the performance of many machine learning classifiers, since the objective function of their learning algorithm considers all attributes of a dataset to be centered around zero with a variance in a similar order of magnitude. Data preparations and ML implementations were performed on the JupyterLab environment using Keras 2.2.5 and Scikit-learn 0.22 libraries of Python [27].

Analytical Tools: Non-perceptron machine learning classifiers including Gaussian NB (GNB), SVM, and LR—provided by the Scikit-learn 0.22 library [27]—as well as the powerful decision tree algorithm,

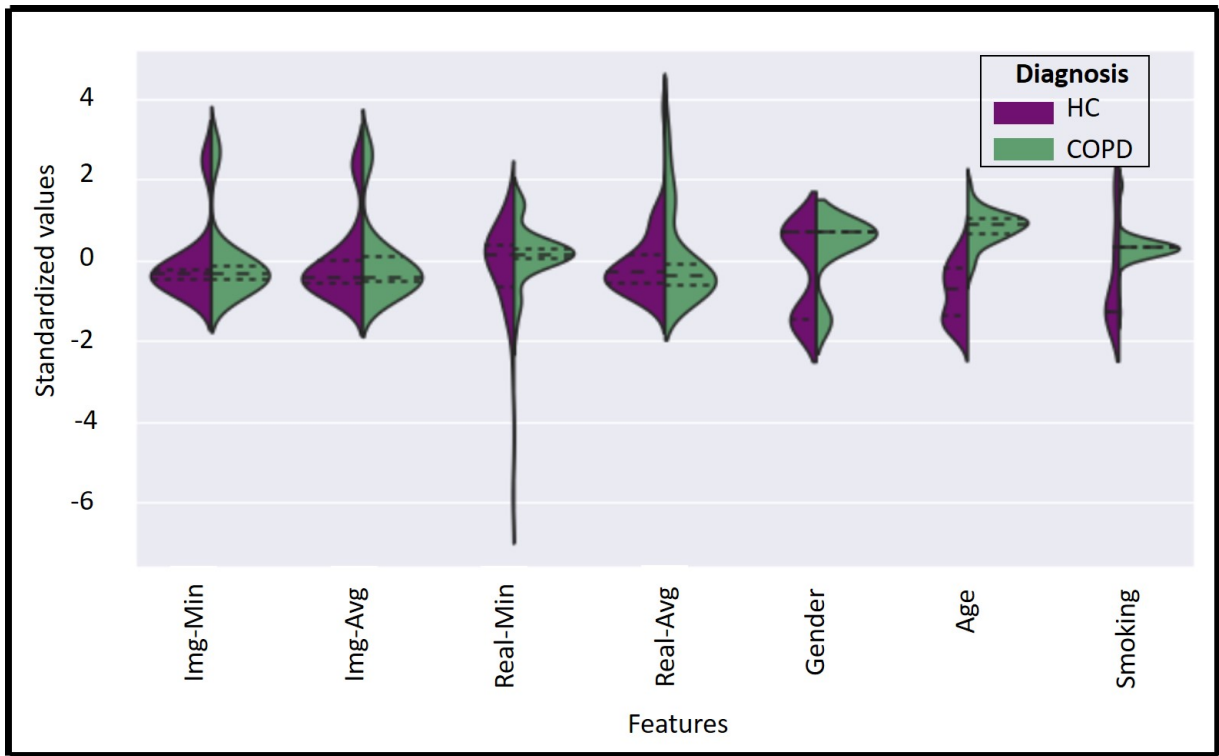


Figure 4.3: Violin plot of the dataset attributes used for classifications, representing the Gaussian standard normal distribution of features with zero mean and unit variance.

XGBoost [25], were used for the classification of saliva samples of COPD and HC. In addition, a dense ANN with one hidden-layer and one read-out layer was developed for the classification of COPD and HC samples. To replicate the intrinsic structure of a neuromorphic platform, a hidden layer with 4 neurons and a sigmoid activation function was modeled. The read-out layer, with a sigmoid activation function, consisted of two neurons for the two possible classes of COPD and HC. A dropout with 20% probability was applied to the hidden-layer for the overfitting prevention. Adam optimization algorithm, with 0.0001 learning rate, and a cross entropy error function were used for training the network in the backend using the Google Colab GPU platform. The simple architecture of the developed ANN was chosen for the integration compatibility with the intended neuromorphic hardware. For the proposed SVM model, a radial basis function kernel was chosen with a gamma and cost parameters of 0.1 and 1000, respectively. For the LR algorithm, a limited-memory Broyden–Fletcher–Goldfarb–Shanno optimization algorithm was used for the parameter estimation with a multinomial loss fit across the entire probability distribution. The XGBoost model was fine tuned with a learning rate and random state values of 0.01 and 1, respectively. In

addition, its number of trees in the forest was chosen as 100 with a maximum depth of 3 for every tree. A multiclass log loss function and minimum weighted leaf fraction of 0 were chosen as recommended in its default instruction [25]. XGBoost is an optimized distributed gradient boosting decision tree framework, providing high efficiency and flexibility for portable applications. The parallelization of tree construction in its algorithm leads to efficiency of compute time and memory resources, thus making XGBoost an adequate tool for edge computing applications such as PoC diagnostic devices. All metrics and models used in this study are available in details at <https://github.com/Pouya-SZ/HCOPD>.

Considering the small size of the investigated COPD data set, k-fold cross-validation method was implemented for the evaluation of the models, thus preventing overfitting circumstances. Hence, relevant tools provided at the Scikit-learn 0.22 library were used for the 5-fold cross-validation of models [27]. The average of five cross-validation iterations was reported as the 5-fold accuracy (5-fold Acc.) performance of models, as shown in Tables 4.1 and 4.2. Sensitivity (recall), specificity, and precision measures for models were calculated on a single-fold iteration with the best accuracy. Since for every cross-validation iteration, the dataset was split into test–train subsets with a ratio of 20–80%, the test-fraction, with unseen data points during model training, was considered as an external validation dataset for the evaluation of models. The sensitivity (recall) of a model was calculated as the proportion of the true positives out of all diseased cases; while the specificity value shows the number of true negatives over number of true negatives and false positives. Precision criterion shows the ratio of true positives over true plus false positives.

4.2.3 Results and Discussions

Figure 4.4 demonstrates a hierarchy chart, categorizing the collected saliva samples into extended sub-groups with respect to their diagnosis, gender, and smoking status. As reported, more than two-thirds of the COPD diagnosed subjects are male patients. Although this phenomenon could be explained considering the fact that smoking tobacco, and consequently COPD, is more prevalent among men, some studies suggest a more complex interpretation by taking into account various gender-specific factors such as differential susceptibility to tobacco, anatomic and hormonal differences, behavioral differences, and differences in response to available therapeutic modalities [31]. In addition, according to the observations reported in Figure 4.4, 81% of COPD diagnosed patients are holding an ex-smoker status, while only 13% are active smokers. This could possibly be due to the reason that some of the ex-smoker subjects have already reached

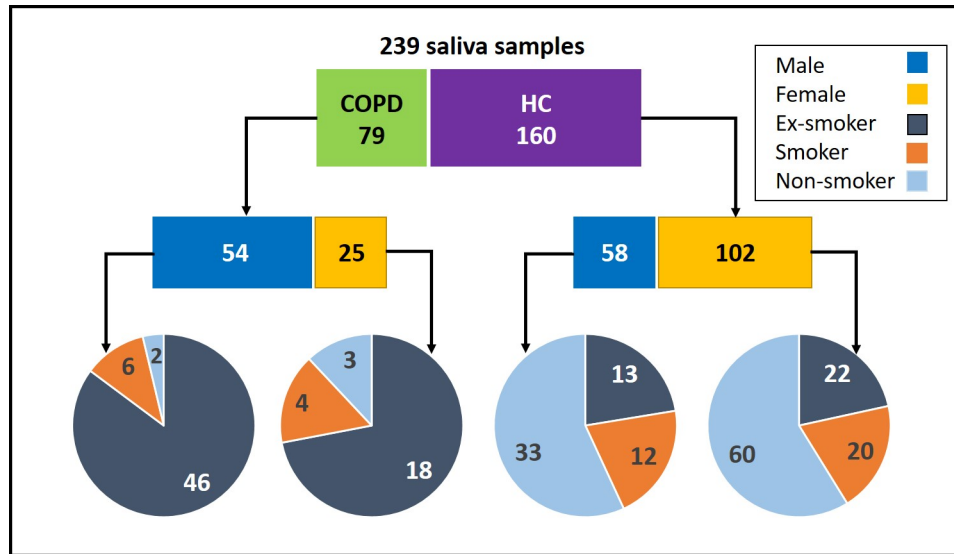


Figure 4.4: Hierarchical categorization of collected saliva samples into extended subgroups with respect to their diagnosis, gender, and smoking status.

a severe stage of COPD before making a decision to quit smoking. This point is also noticeable in Figure 4.5, which presents the distribution of the saliva samples with respect to age, diagnosis, and the smoking status of subjects. Furthermore, as shown in Figure 4.5, in most cases, the COPD diagnosed patients are middle-aged or older adults. This observation complies with the fact that, increasing age means a longer exposure of subjects to the risk factors and, consequently, further damages to their lungs. Moreover, as the body ages, the recovery process of the damaged lung cells becomes more difficult, making a subject more susceptible to COPD [32].

Figure 4.6 presents the results of the biosensor output for the dielectric characterization of saliva samples (the minimum values of the real part of the permittivity). The presented box-plot provides distributional information including minimum–maximum, median, and the first–third quartile values for the obtained results on both categories of COPD and HC. The reported results in this figure represent the output voltage drop of the biosensor, after calibration with respect to the dielectric properties of the surrounding air, representing the dielectric properties of the tested samples, as explained in previous sections [4,8]. As illustrated in Figure 4.6, the minimum values of the real part of the permittivity (dielectric features) for HC samples has a greater standard deviation value (21.86) compared to the COPD group (16.77), making it a useful feature for clustering data points using ML classifiers. In contrast, the imaginary part of the permittivity of saliva has a symmetric distribution for both HC and COPD patients, as shown in Figure 4.3, thus lacking

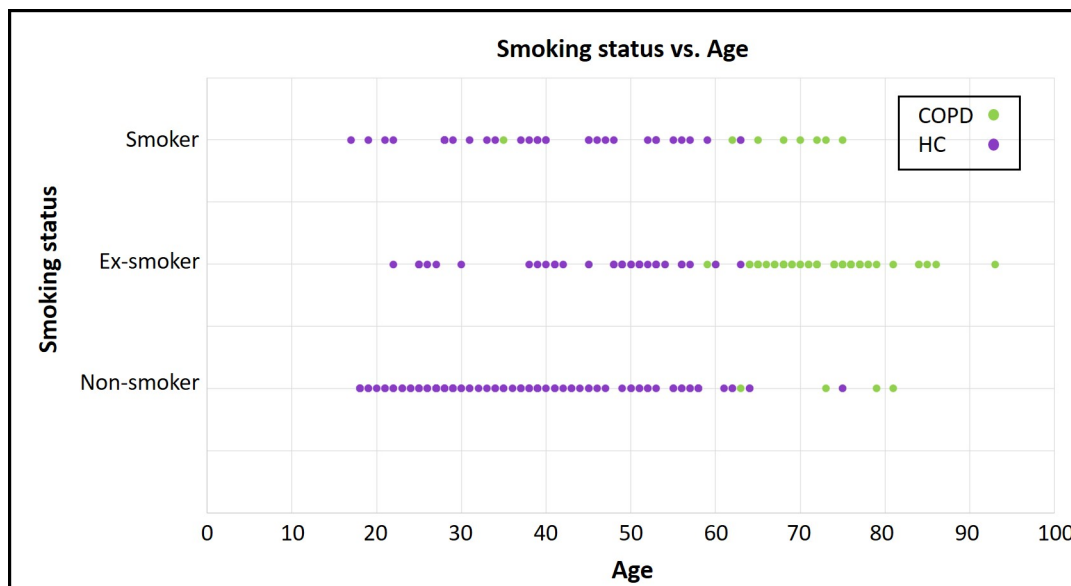


Figure 4.5: Distribution of saliva samples of COPD and HC with respect to age and the smoking status of the subjects.

valuable information for data segregation.

Due to the dependent nature of the aforementioned attributes, implementation of ML methods was crucial for the realistic classification of the samples by concurrent consideration of all parameters. Tables 4.1 and 4.2 present the performance of the proposed ML models including XGBoost, SVM, GNB, LR, and ANN for the classification of the first and second datasets with 80 and 239 saliva samples, respectively. These results indicate the high performance of ML-based analytical tools for the classification of saliva samples of COPD and HC. Especially, among the introduced methods, the XGBoost decision tree algorithm provided the best performance in terms of accuracy, sensitivity, specificity, and precision, thus making it a suitable model for this work. As reported in Table 4.1, XGBoost classifier has exceeded other models by providing accuracy, sensitivity, specificity, and precision values of 91.25%, 100%, 88.89%, and 87.5%, respectively, for the classification of saliva samples with respect to their dielectric and demographic properties. The acquired results illustrate the practicality of the concept of applying ML tools for classifying saliva samples of COPD and HC, which was proposed as a hypothesis for this part of the thesis. The current study is an important cornerstone, presenting the fact that the dielectric properties of saliva together with the demographic information on the respective patients can be analyzed using ML tools for the discrimination of patients affected by COPD from healthy controls. Moreover, results presented in Table 4.2 indicate

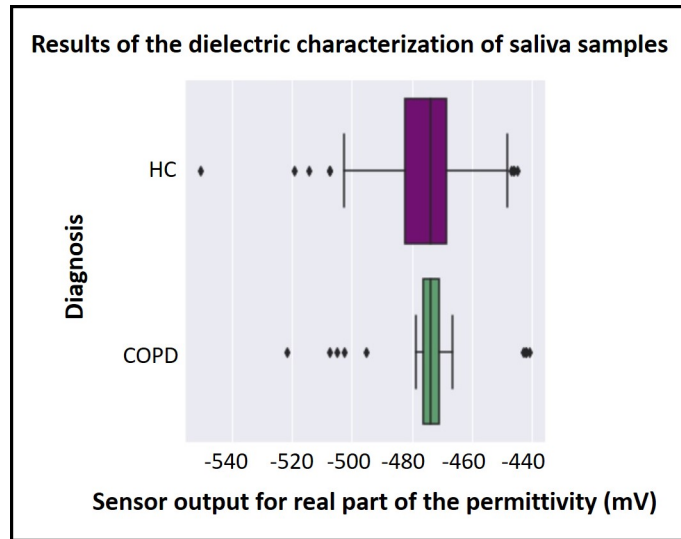


Figure 4.6: Results of the biosensor output for the dielectric characterization (minimum values of the real part of the permittivity) of saliva samples, providing distributional information including minimum–maximum, median, and the first–third quartile values.

the superiority of XGBoost performance for the classification of samples based on merely demographic information with accuracy, sensitivity, specificity, and precision values of 92.05%, 95.24%, 100%, and 100%, respectively. The remarkable performance of classifiers based on only demographic attributes—age, gender, and smoking status—indicates the significant role of demographic information for the detection of COPD. In contrast to non-perceptron classifiers, the proposed ANN provided a poor performance due to its sensitivity to outliers and overfitting in small-sized datasets.

Table 4.1: Performance of ML models for the classification of the first dataset with 80 saliva samples (64 training and 16 test data).

Classifier	5-fold Acc.	Sensitivity	Specificity	Precision
XGBoost	91.25%	100%	88.89%	87.5%
SVM	91.25%	100%	77.78%	77.78%
GNB	87.5%	85.71%	100%	100%
LR	90%	100%	11.11%	46.66%
ANN	73.75%	100%	44.45%	58.33%

Figures 4.7(a) and (b) demonstrate the confusion matrices of the XGBoost algorithm for predicting the diagnostic status of the unseen test samples. As shown in these figures, the XGBoost model, at its best

performance (with threshold values of 0.66 and 0.53), was capable to predict the status of the unseen test subjects for the first and second datasets with only one false-positive and one false-negative and accuracies of 93.75% and 97.92%, respectively. The precision-recall curves for these confusion matrices are shown in figures 4.7(c) and (d), demonstrating the trade-off between precision and recall (sensitivity) for different thresholds. The XGBoost classifier provided the best performance for the classification of first and second datasets at threshold values of 0.66 and 0.53, respectively. The high accuracy, sensitivity, specificity, and precision of the XGBoost algorithm make it an adequate model for COPD classifications using edge devices [33].

The high accuracy of the proposed ML models compared to the ground truth spirometry method, with a sensitivity range of 64.5–79.9% [16], make them a promising tool for the management of COPD in PoC environments. However, this thesis has only investigated the practicality of COPD classification in *in-vitro* circumstances, whereas, for the real-world predictions on the progression of COPD and its exacerbations, real-time analysis of the dielectric properties of saliva on a daily basis is required.

Generalizability to a larger population, as the main limitation with any ML study on a small-sized novel dataset, is a fundamental concern for this study, demanding extensive investigation. Nonetheless, to the best of author’s knowledge, there is no other comprehensive dataset for the COPD classifications available up to date, which can be used for training and evaluating the introduced ML models in this work. Therefore, this study is considered as a stepping stone to future studies in the field, while endorsing the necessity for further data collections and advanced-analytical implementations for the COPD management.

The results of this section imply the capability of ML tools for enhancing the quality of personalized healthcare solutions by facilitating the management of chronic diseases through performing complex di-

Table 4.2: Performance of ML models for the classification of the second dataset with 239 saliva samples (191 training and 48 test data).

Classifier	5-fold Acc.	Sensitivity	Specificity	Precision
XGBoost	92.05%	95.24%	100%	100%
SVM	92.05%	90.47%	100%	100%
GNB	92.89%	95.24%	100%	100%
LR	91.65%	95.24%	96.3%	95.24%
ANN	93.33%	90.47%	96.3%	95%

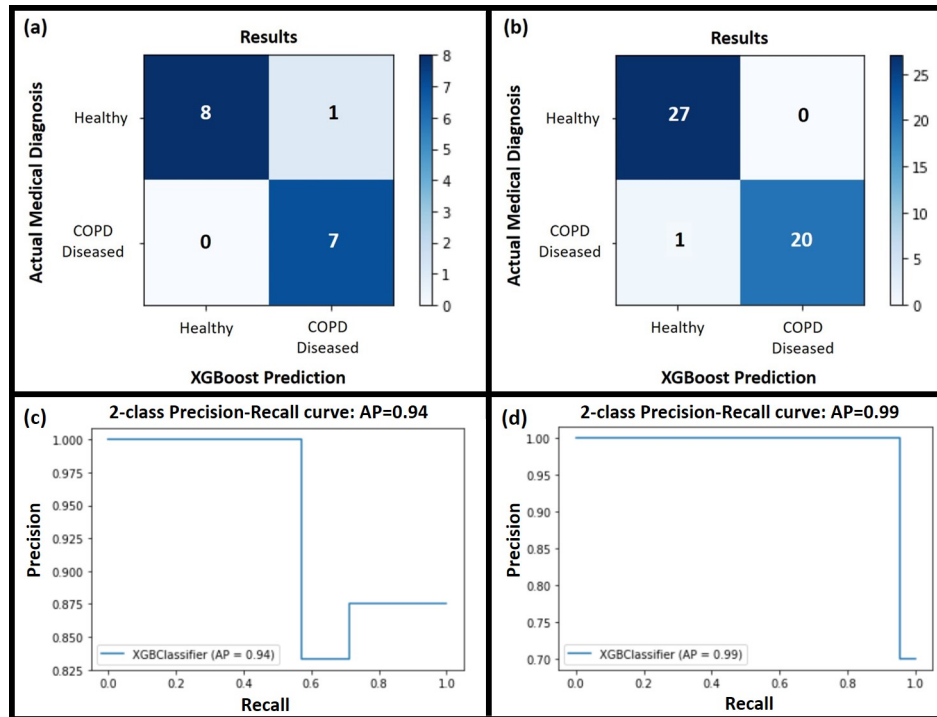


Figure 4.7: Confusion matrices of the XGBoost algorithm, presenting the prediction performance of the model on the unseen test samples and the precision-recall curve, demonstrating the trade-off between precision and recall for different thresholds: (a) and (c) first dataset with 80 saliva samples (64 training and 16 test data); (b) and (d) second dataset with 239 saliva samples (191 training and 48 test data).

agnosis. The scope of ML tools goes far beyond classical statistical analyses performed in healthcare. Therefore, ML methods, or the Artificial Intelligence (AI) from a broader scope, is expected to revolutionize healthcare in the near future by providing accurate and real-time predictions on the health status of patients or the progress of their diseases. Especially, AI will play a pivotal role in the future for assisting patients in remote locations with the management of chronic and degenerative conditions, monitoring their rehabilitation progress, and predicting critical-emergency health conditions. In addition, availability of numerous health-related data, thanks to the advancements in wearable technologies and biosensors, will facilitate the better integration of AI with healthcare devices in PoC environments. However, all of the mentioned astonishing capabilities of ML tools come at the cost of immense energy consumption and enormous computational power. In addition, complexities associated with cloud communications such as robustness against interference, wide bandwidth requirements, low latency, and data security limit the application of AI in sensitive fields such as medicine. As a result, the trade-off between mentioned benefits

and risks related to securing sensitive medical data is, still, an on-going challenge. To address this concern, low-power neuromorphic platforms could be integrated into medical devices for locally processing of computations required for ML algorithms [34]. Neuromorphic chips have been successfully implemented in different studies for matrix-multiplications required for non-perceptron and perceptron-based ML methods [5, 35]. By bringing data post-processing from the backend onto a chip, real-time analysis of data in a less time consuming manner with a smaller time delay is feasible. Furthermore, sensitive medical data are better protected by being processed locally on a chip without external communications. In addition, the energy-efficient neuromorphic platforms offer a large fault tolerance for sensitive applications such as in healthcare [11]. Therefore, implementation of the presented ML models on a neuromorphic platform, for the on-chip classification of saliva, will be investigated in the following chapter.

Although the introduced ML model was capable to accurately classify the saliva samples based on a few attributes, further demographic information on the medical-personal background of patients' (such cytokine level, blood pressure history, or pathogen) could possibly improve the performance of the model in terms of accuracy and generalizability. However, accessing such a sensitive medical information is highly restricted through governmental data protection policies and, thus, requires an appropriate approval from the ethics committee, prior to acquisitions. In addition, investigating novel ML algorithms, such as a few-shot learning, with better performance on small-sized datasets could pave the way towards more accurate and generalizable models for medical applications with limited data availability [36].

4.2.4 Conclusions and Future Work

This section investigated the *in-vitro* classification of saliva samples of COPD and HC using machine learning techniques. Saliva samples were initially collected from different subjects in a clinical setting and demographic information regarding the age, gender, and smoking status of patients were recorded. In addition, dielectric characteristics of a smaller subset of collected samples were measured using a permittivity biosensor. Various ML tools including XGBoost, SVM, NB, LR, and ANN were applied for classifying collected samples into COPD and HC categories. The XGBoost algorithm provided the best performance, among other methods, for classifying and predicting saliva samples of COPD and HC with respect to their dielectric and demographic properties. Although implementation of ML tools enables the fast and efficient diagnosis of COPD, the existing shortcomings in terms of data availability, data safety, and computation

cost limit their application in real-world. Therefore, further data collection is necessary in the future for enhancing the performance of the proposed models. Moreover, as the next step, deployment of the introduced ML models on hardware-based neuromorphic platforms will enable the on-chip recognition of COPD with low energy consumption and high patient privacy.

4.3 Implementation of Siamese-based Few-shot Learning Algorithms for the Distinction of COPD and Asthma Subjects

This section investigates the practicality of applying brain-inspired Few-Shot Learning (FSL) algorithms for addressing shortcomings of ML methods in medicine with limited data availability. As a proof of concept, the application of ML for the detection of COPD patients was investigated. The complexities associated with the distinction of COPD and asthma patients and the lack of sufficient training data for asthma subjects impair the performance of conventional ML models for the recognition of COPD. Therefore, the objective of this part of the thesis was to implement FSL methods for the distinction of COPD and asthma subjects with a few available data points. The proposed FSL models in this section were capable of recognizing asthma and COPD patients with 100% accuracy, demonstrating the feasibility of the approach for applications such as medicine with insufficient data availability. Materials introduced in this section has been published in [36].

4.3.1 Introduction

Artificial Intelligence (AI), with its galloping progress, has revolutionized various aspects of our data-driven world [37]. A broad spectrum of AI's applications has been introduced in recent years, covering many aspects of science from robotics to medicine [37]. The astonishing performance of AI-oriented ML methods for exceeding human capabilities in medical recognition and classification tasks has already been demonstrated [3]. However, the significant dependence of these methods, especially deep learning, on the availability of a vast training dataset has hindered their far-reaching application in many areas of medicine with limited data availability [38]. A training dataset in this scope is defined as properly-labeled data points which can be used for training ML-based models. Some of the causes behind the scarcity of ML-friendly datasets in medicine include, but are not limited to, the following: First, incomplete, incorrect, inaccurate,

and heterogeneous nature of old medical records, due to the inconsistency in their acquisition methods and vocabulary, degrade their labeling and usability for ML. In addition, generating ground-truth labels is generally an expensive and time-consuming process, which has been neglected until recently. Second, the AI-oriented data collection for various medical applications, especially rare diseases or novel treatments, is still at its infancy. For instance, genetic engineering, drug discovery, or surgical robotics are exemplary domains where extensive data collections are still required for the enhancement of their performances [22, 23, 39, 40]. Third, different standardization methods, ethical concerns, and strict privacy regulations have hindered the data sharing in medicine, further restricting their availability. Last but not least, data acquisitions through invasive and complex medical operations is extremely challenging, if not impossible, thus restricting the size of the available data in this realm [38]. The intracranial electrode placement for the prediction and management of the drug-resistant epilepsy is an example of this kind, where very few data points are available due to safety concerns [34, 41]. The lack of sufficient data for training ML models for the mentioned applications not only limits their performance and accuracy but also questions their generalizability to a larger population of patients or medical cases [34, 38]. Patient-to-patient variability is a challenging concern for the development of medical–diagnostic solutions in personal healthcare [42]. As an example, the discussed epileptic seizure management setup requires the implantation of numerous electrodes within a patient’s skull for the monitoring of the brain’s electrical activities. However, the exact location of the implanted electrodes, the number of functioning–active electrode channels after the operation, and the specific area of a patient’s brain where the excessive electrical discharges occur make the developed ML models for this application strongly patient specific [34]. This is significantly problematic for the development of a generalizable healthcare solution for the management of epilepsy. Furthermore, despite the availability of vast sources of epilepsy data from canine, with a similar seizure mechanism to human, generalization of the developed models based on the canine data to the human is still hampered. Similarly, ML models developed for the diagnostic classification of COPD patients from HC suffer from generalization to a broader group of respiratory disease such as asthma [1, 30]. Patients suffering from asthma or COPD develop similar symptoms due to the analogous mechanism of the diseases and a significant overlap between them, causing diagnostic complexities [43, 44]. On the other hand, the lack of sufficient training data is a significant hurdle for improving the performance of the developed ML models for the COPD detection [1, 30]. Therefore, due to the lack of data availability, ML-models need

to be re-trained from scratch to provide a comparable performance for every individual patient or disease case in spite of an identical task. This is a significant drawback of these models for real-world applications, where rapid adaptation and learning is essential [45]. Examples of these applications include autonomous driving, surgical robotics, medical mechatronics, personalized medicine, precision diagnostic, etc., where online learning of a ML-enabled system with the least possible computation for the interaction with external circumstances is crucially important. Therefore, implementation of novel brain-inspired meta-learning algorithms such as few-shot learning, possibly on neuromorphic platforms, could be a solution for the real-world learning and rapid adaptations with fewer data points [45].

Few-shot Learning (FSL), a novel ML method, falls under a broader umbrella term known as meta-learning which aims for bridging the gap between AI and human-like learning by learning the meta information of classes–tasks rather than merely the data [45, 46]. Therefore, by using prior–meta knowledge, FSL can rapidly learn from fewer data points and can better generalize a model to new tasks with the least supervision [45]. As a result, FSL could possibly relieve the burden of collecting large-scale labelled-data for medical applications [45]. Since FSL denotes learning out of a few data points per class, upon the availability of only one example per class the method would be called as one-shot learning, while zero-shot learning represents a scenario where no data points are available for learning a new class of inputs. Siamese networks are among the most popular and simple models used in FSL algorithms with potential applications in areas such as disease diagnosis, object tracking, one-shot robotic imitation, visual navigation, and drug discovery [47].

The objective of this part of the thesis was to implement siamese-based zero-shot, one-shot, and five-shot learning models for the distinction of COPD subjects from asthma, with a few available data points. Differentiation of COPD patients from asthma, at an early stage of the disease, is significantly important from a medical perspective for the efficiency of the treatment [43]. However, due to the lack of sufficient data from asthma subjects, the classification performance of conventional methods is significantly limited. As a result, implementation of the FSL-based approaches for the distinction of COPD patients from asthma can possibly address the generalization problem with the current available ML models for this application. Therefore, in the continuum, the practicality of applying FSL methods for enhancing the performance of ML models in applications such as medicine—with limited availability of large-scale, high-quality, and correctly labelled training data—will be investigated.

4.3.2 Materials and Methods

The open access Exasens dataset, available at the UCI machine learning repository (<https://archive.ics.uci.edu/ml/datasets/Exasens>), was used in this study for the classification and distinction of saliva samples of COPD and asthma patients, as well as HC. This novel dataset contains information on hundred saliva samples collected from four groups of respiratory patients including: COPD (40 samples), HC (40 samples), asthma (10 samples), and respiratory infected subjects without COPD or asthma (10 samples), as shown in Figure 4.8 [30]. The attributes of the dataset used for the classification of subjects include demographic information of patients (age, gender, and smoking status) as well as the dielectric properties of the characterized saliva samples for every class [4, 8]. Despite the high performance of classifiers for the segregation of COPD and HC samples, simultaneous classification of all three classes of COPD, HC, and asthma led to a deficient accuracy of 55%, due to the extremely small-size of the asthma population. Therefore, the FSL method was applied for the distinction of COPD and asthma subjects to make the developed COPD diagnosis models further resilient against adversarial samples like asthma, thus making the ML-based classification of COPD more reliable and valuable for real-world applications.

Prior to analytics, the analog values of these four attributes were thresholded and converted into 23 binary bits (Gender (1), smoking status (3), age (9), dielectric (10)), as shown in Figure 4.8. Binarization of the attributes of this small-sized dataset has shown to reduce overfitting and noise, and to improve the

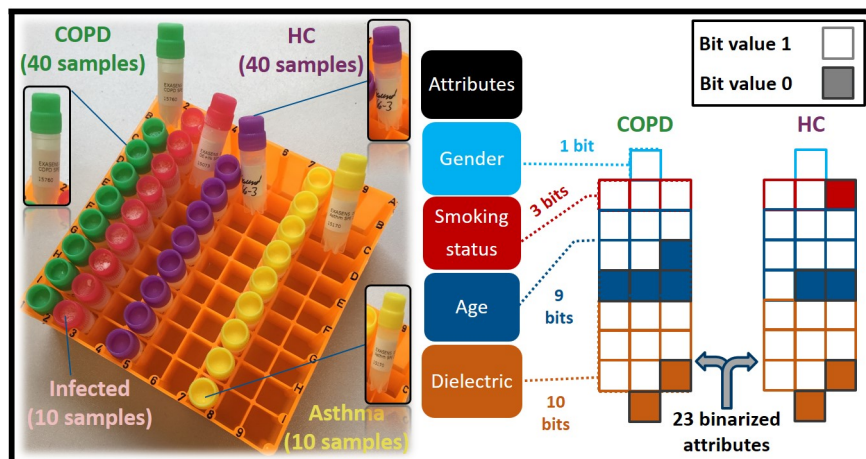


Figure 4.8: Four groups of saliva samples available within the Exasens dataset.

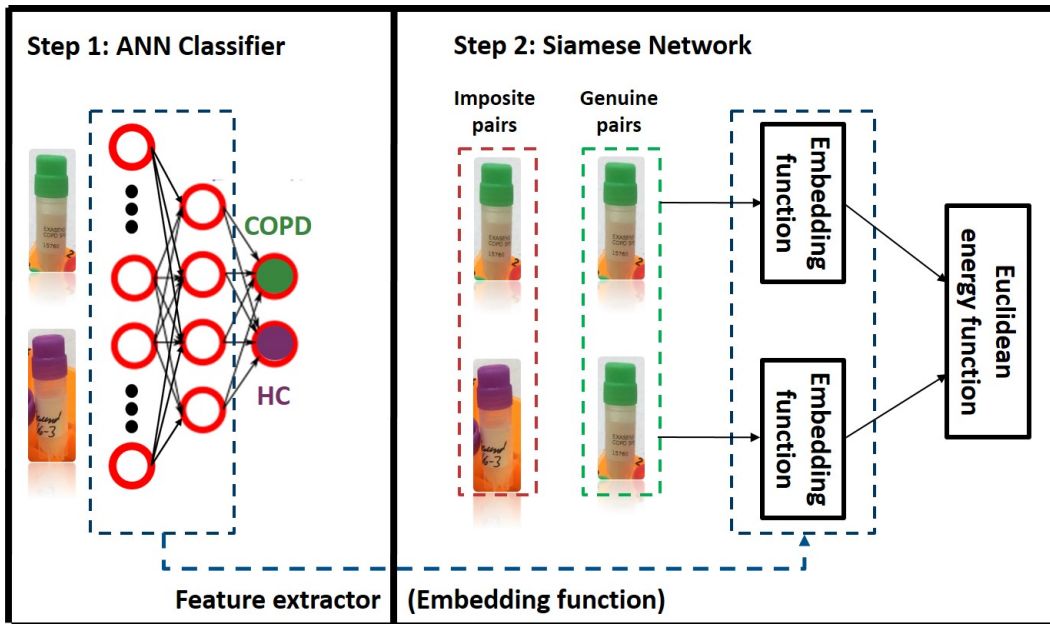


Figure 4.9: Required steps for developing a classifier (left) and a siamese network (right).

performance of ML tools for the classification of COPD and HC samples [30]. In addition, considering the small size of the investigated dataset, 5-fold cross-validation method was implemented for the evaluation of models, thus preventing overfitting and providing reliable and generalizable results. After data preparations, as the first step, an Artificial Neural Network (ANN), with one hidden-layer and one read-out layer, was developed for the classification of COPD and HC samples, as shown in Figure 4.9(left). The hidden-layer consisted of four neurons with a rectified linear unit activation function, while the read-out layer determined the two possible classes using softmax. A dropout of 20% was implemented on the hidden-layer for the overfitting prevention. Adam optimization algorithm, with a 0.0001 learning rate, and a cross entropy error function were used for training and optimizing the network parameters. The compiled network was trained for 4000 epochs and a 5-fold cross-validation was applied for the network performance evaluations. After training the initial ANN classifier, the network structure without the readout layer (up to the output of the hidden-layer) was used as an embedding function for extracting the feature vectors of input samples, determining their unique footprints. Next, this feature-extracting network (embedding function) was integrated into a siamese architecture for the recognition of identical input pairs, as shown in Figure 4.9(right). A Euclidean distance function was used as an energy function to calculate the similarities between the feature vectors of the input pairs. Subsequently, a contrastive loss function, with a margin value of one, was used

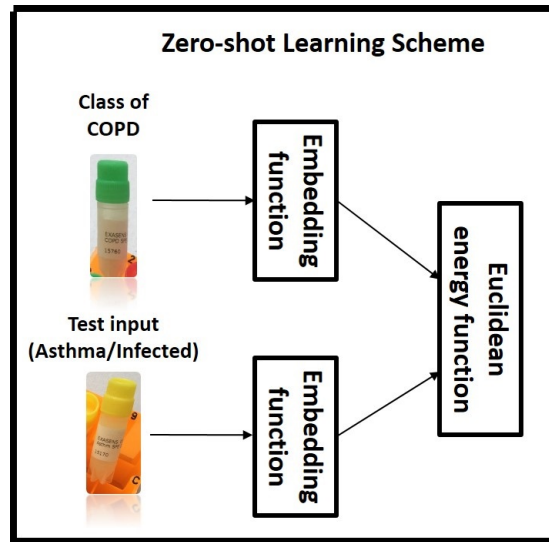


Figure 4.10: Zero-shot learning scheme for the recognition of asthma vs. COPD.

for training the siamese network and minimizing the calculated Euclidean error. For training the developed siamese network, two datasets of genuine and imposite pairs were prepared. The genuine dataset included 20 pairs of COPD–COPD samples, while the imposite dataset consisted of 20 pairs of COPD–HC samples. The data were fed into the siamese network for 1000 training epochs and a 5-fold cross-validation was performed for assessing the model performance. After the successful distinction of genuine COPD inputs from the imposite input pairs, the model was used in a zero-shot learning scheme to distinguish COPD subjects from asthma, as demonstrated in Figure 4.10. Through this approach, the feature vector of a test input was extracted and compared to the feature vector of the class of COPD using the Euclidean error function. In case of a smaller than margin distance of the feature vector of the test input, it was determined as a COPD sample, while inputs with greater margin distances belonged to the adversarial samples class (either asthma or infected). However, to improve the recognition performance of the model and to make it more resilient against other adversarial inputs like infected, the developed siamese network was re-trained for an additional 500 epochs using one and five COPD–asthma imposite pairs (along with COPD–COPD genuine pairs) for one- and five-shot learning schemes, respectively, as shown in Figure 4.11. Similar procedure, as for the zero-shot learning testing, was performed for evaluating the performance of the one- and five-shot learning models for distinguishing asthma subjects from COPD. The data preparations and ML implementations were performed on the JupyterLab environment using Keras 2.2.5 and Scikit-learn 0.22 libraries of Python [27]. The metrics and data used in this study are publicly available at <https://github.com/Pouya->

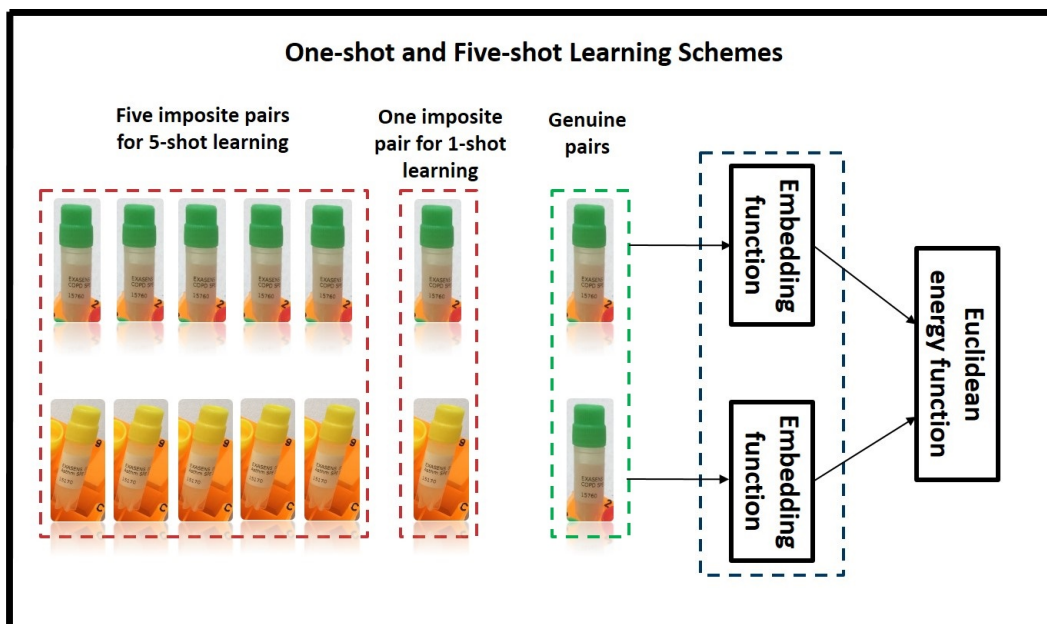


Figure 4.11: One-shot and five-shot learning schemes for training–evaluations.

SZ/SFSL_MED.

4.3.3 Results and Discussions

The initial ANN classifier, developed for the classification of COPD and HC patients, provided an average accuracy of 95% for the 5-fold cross-validations, thus making it an adequate embedding function for extracting the feature vectors of input pairs. The modeled siamese network was capable of distinguishing the genuine input pairs of COPD–COPD from the impositve pairs of COPD–HC with 100% average accuracy for the 5-fold cross-validations, thus accurately comparing their feature vectors encoded through the pre-trained embedding function. The high performance of the siamese network made the accurate distinction of COPD and asthma samples through FSL schemes possible, as presented in Table 4.3. Although all of the zero-, one-, and five-shot learning schemes provided remarkable performance for the distinction of COPD and asthma samples, the incapability of the zero-shot learning approach for distinguishing different adversarial inputs such as asthma and infected was considered the main drawback of this method from the medical perspective. However, its remarkable performance of 100% accuracy for distinguishing asthma and COPD samples, without any training, indicates its significant importance for medical applications with no available training data. On the other hand, Table 4.3 presents similar accuracies of 100% for both one-

Table 4.3: Results of zero-, one-, and five-shot learning schemes for the distinction of asthma samples from COPD and infected.

	Zero-shot	One-shot	Five-shot
COPD vs. Asthma	100%	100%	100%
Asthma vs. Infected	NA	80%	80%

and five-shot learning schemes. Apart from their high recognition capabilities, the one-shot and five-shot learning approaches are further resilient for the reliable distinction of COPD and asthma subjects upon the introduction of other adversarial inputs like infected subjects. As reported in Table 4.3, in contrast to the zero-shot learning, one-shot and five-shot learning methods were capable of distinguishing asthma and infected samples with 80% accuracies. Although the FSL models presented promising results for the recognition of asthma subjects with no prior knowledge or training, due to the small size of the scrutinized asthma dataset, we consider this work as a proof of concept, requiring further investigations in the future for comprehensive conclusions.

Generalizability to a larger population, as the main limitation with any ML study on a small-sized novel dataset, is a fundamental concern for this study, demanding extensive investigations. Nonetheless, to the best of author's knowledge, there is no other comprehensive dataset available up to date on the COPD and asthma samples, which can be used for training and evaluating introduced FSL models in this section. Therefore, this study is considered as a stepping stone to future studies in the field, while endorsing the necessity for further data collections.

Results discussed in this section demonstrated the practicality of applying FSL methods for addressing the shortcomings of ML models in applications like medicine with a few or none available data points. By taking advantage of brain-inspired algorithms such as FSL, it is possible not only to enhance the performance of conventional ML models, but also to make them further resilient against adversarial inputs. In addition, through meta-learning approaches like FSL, training ML models from scratch for every individual patient or disease is unnecessary. Furthermore, FSL methods pave the way towards the better integration of ML tools with old medical records as well as novel-complex treatments with a few data points. In addition, the main advantage of FSL-based models in medicine is their better generalization to a broader spectrum of patients or disease cases, while offering a human-like learning possibility.

FSL is capable of learning with fewer data points, thus facilitating the online learning and adaptation of ML-equipped systems like neuromorphic processors for real-world applications. The energy-efficient neuromorphic processors are expected to revolutionize the ML-based medicine in the future by bringing the data post-processing from the backend onto the chip, thus providing accurate and real-time predictions on the health status of patients. Neuromorphic-equipped medical devices better protect users' sensitive medical data without cloud communication requirements [1]. Therefore, implementation of novel meta learning algorithms, such as few-shot learning, on neuromorphic platforms will enable the rapid adaptation and real-time learning in these systems with a few data points and the least possible computation [48]. Example of such applications, where online learning and adaptation of a ML model is crucial, include autonomous driving, surgical robotics, personalized medicine, and precision diagnostic.

In the future, integration of the proposed FSL tools with the epileptic seizure prediction models will enable the better generalization of these models to a larger population of patients. In addition, the employment of canine-based models for the human epilepsy managements will be possible. Furthermore, integration of these models into the kafka framework facilitates the management of ML pipelines through data streams in a user friendly environment, which is the future work of this thesis [49]. Moreover, the future goal of this section could be to develop and deploy siamese-based FSL techniques on a neuromorphic platform for the on-chip prediction of epileptic seizure using smart healthcare wearables.

4.3.4 Conclusions and Future Work

In this section, the practicality of applying few-shot learning algorithms for addressing the shortcomings of ML models in medical applications with limited data availability was investigated. Siamese-based zero-, one-, and five-shot learning models were developed for the distinction of COPD and asthma subjects. The developed models provided high performance for the recognition of asthma samples, while making the ML-based diagnosis of COPD more resilient against adversarial inputs. Implementation of the proposed FSL models in other medical applications with limited data availability will address the generalization issues of the most ML models in this realm. The brain-inspired few-shot learning could possibly address AI's problems in medicine caused due to the lack of sufficient training data. Therefore, implementation of FSL algorithms for the epileptic seizure prediction with fewer data is the future goal of this thesis.

Bibliography

- [1] P.S. Zarrin and C. Wenger. “Pattern Recognition for COPD Diagnostics Using an Artificial Neural Network and Its Potential Integration on Hardware-Based Neuromorphic Platforms,” *Springer LNCS (ICANN19)*, Munich, Germany, September, 2019, pp. 284–288.
- [2] S. B. Baker, W. Xiang, I. Atkinson. “Internet of Things for Smart Healthcare: Technologies, Challenges, and Opportunities,” *IEEE Access*, vol. 5, pp. 26521–26544, 2017.
- [3] A.L. Fogel, J.C. Kvedar. “Artificial intelligence powers digital medicine,” *NPJ Digital Medicine*, vol. 1, no. 5, 2018.
- [4] P.S. Zarrin, F.I. Jamal, N. Roeckendorf, C. Wenger. “Development of a Portable Dielectric Biosensor for Rapid Detection of Viscosity Variations and Its In-Vitro Evaluations Using Saliva Samples of COPD Patients and Healthy Control,” *Healthcare*, vol. 7, no. 11, 2019.
- [5] C. Wenger, F. Zahari, M.K. Mahadevaiah, E. Perez, I. Beckers, H. Kohlstedt, and M. Ziegler. “Inherent Stochastic Learning in CMOS-Integrated HfO₂ Arrays for Neuromorphic Computing,” *IEEE Electron Device Letters*, vol. 40, no. 4, pp. 639–642, 2019.
- [6] N.G. Csikesz, E.J. Gartman. “New developments in the assessment of COPD: Early diagnosis is key,” *International Journal Chronic Obstructive Pulmonary Disease*, vol. 9, pp. 277–286, 2014.
- [7] E. Barreiro, A.M. Schols, M.I. Polkey, J.B. Galdiz, H.R. Gosker, E.B. Swallow, C. Coronell, J. Gea. “Cytokine profile in quadriceps muscles of patients with severe COPD,” *Thorax*, vol. 63, no. 2, 2008.

- [8] P.S. Zarrin, F.I. Jamal, S. Guha, J. Wessel, D. Kissinger, C. Wenger. “Design and Fabrication of a BiCMOS Dielectric Sensor for Viscosity Measurements: A Possible Solution for Early Detection of COPD,” *Biosensors*, vol. 8, no. 78, 2018.
- [9] P. Verdugo. “Supramolecular dynamics of mucus,” *Cold Spring Harbor perspectives in medicine*, vol. 2, p. 11, 2012.
- [10] T. Heinis, M. Schmuker. “Neuromorphic Hardware As Database Co-Processors: Potential and Limitations,” In *EDBT 2019*, Lisbon, Portugal, pp. 694–697, 2019.
- [11] D.S. Jeong, K.M. Kim, S. Kim, B.J. Choi, C.S. Hwang. “Memristors for energy-efficient new computing paradigms,” *Advanced Electronic Materials*, vol. 2, p. 9, 2016.
- [12] P. S. Zarrin, N. Roeckendorf, and C. Wenger. “In-vitro Classification of Saliva Samples of COPD Patients and Healthy Controls Using Machine Learning Tools,” *IEEE Access*, 2020.
- [13] T. Dong, S. Santos, Z. Yang, S. Yang, N.E. Kirkhus. “Sputum and salivary protein biomarkers and point-of-care biosensors for the management of COPD,” *Analyst*, 2020.
- [14] S. Mirza, R.D. Clay, M.A. Koslow, P.D. Scanlon. “COPD guidelines: a review of the 2018 GOLD report,” *Elsevier Mayo Clinic Proceedings*, vol. 93, pp. 1488–1502, 2018.
- [15] D. Price, A. Crockett, M. Arne, B. Garbe, R. Jones, A. Kaplan, A. Langhammer, S. Williams, B. Yawn. “Spirometry in primary care case-identification, diagnosis and management of COPD,” *Primary Care Respiratory Journal*, vol. 18, no. 216, 2009.
- [16] S. Haroon, R. Jordan, Y. Takwoingi, P. Adab. “Diagnostic accuracy of screening tests for COPD: a systematic review and meta-analysis,” *BMJ open*, vol. 5, no. 10, p. e008133, 2015.
- [17] S. Chiappin, G. Antonelli, R. Gatti, F. Elio. “Saliva specimen: a new laboratory tool for diagnostic and basic investigation,” *Clinica chimica acta*, vol. 383, no. 1, pp. 30–40, 2007.
- [18] M.C. Rose, J.A. Voynow. “Respiratory tract mucin genes and mucin glycoproteins in health and disease,” *Physiological reviews*, vol. 86, no. 1, pp. 245–278, 2006.

- [19] K. Wang, Y.L. FENG, F.Q. WEN, X.R. CHEN, X.M. OU, D. Xu, J. Yang, Z.P. DENG. “Decreased expression of human aquaporin-5 correlated with mucus overproduction in airways of chronic obstructive pulmonary disease,” *Acta pharmacologica sinica*, vol. 28, no. 8, pp. 1166–1174, 2007.
- [20] R.M. Effros, B. Peterson, R. Casaburi, J. Su, M. Dunning, J. Torday, J. Biller, R. Shaker. “Epithelial lining fluid solute concentrations in chronic obstructive lung disease patients and normal subjects,” *Journal of Applied Physiology*, vol. 99, no. 4, pp. 1286–1292, 2005.
- [21] R.S. Khan, Z. Khurshid, F. Yahya Ibrahim Asiri. “Advancing point-of-care (PoC) testing using human saliva as liquid biopsy,” *Diagnostics*, vol. 7, no. 3, p. 39, 2017.
- [22] P. S. Zarrin, A. Escoto, R. Xu, M. D. Naish, R. V. Patel, and A. L. Trejos. “Development of a 2-DOF sensorized surgical grasper for grasping and axial force measurements,” *IEEE Sensors Journal*, vol. 18, no. 7, pp. 2816–2826, 2018.
- [23] P.S. Zarrin, A. Escoto, R. Xu, R.V. Patel, M.D. Naish, A.L. Trejos. “Development of an optical fiber-based sensor for grasping and axial force sensing,” *IEEE International Conference on Robotics and Automation (ICRA)*, Singapore, May, 2017, pp. 939–944.
- [24] F.X. Campion, G. Carlsson, F. Francis. “Machine Intelligence for Healthcare,” Scotts Valley, CreateSpace Independent Publishing Platform, isbn=9781542924948, 2017.
- [25] T. Chen, C. Guestrin. “Xgboost: A scalable tree boosting system,” *In Proceedings of the 22nd acm sigkdd international conference on knowledge discovery and data mining*, San Francisco, USA, August, 2016, pp. 785–794.
- [26] I. Kononenko. “Machine learning for medical diagnosis: history, state of the art and perspective,” *Artificial Intelligence in medicine*, vol. 23, pp. 89–109, 2001.
- [27] F. Pedregosa, et al. “Scikit-learn: Machine learning in Python,” *Journal of machine learning research*, vol. 12, pp. 2825–2830, 2011.
- [28] R. Entezari-Maleki, A. Rezaei, B. Minaei-Bidgoli. “Comparison of classification methods based on the type of attributes and sample size,” *Journal of Convergence Information Technology*, vol. 4, no. 3, pp. 94–102, 2009.

- [29] C. Ellervik, J. Vaught. “Preanalytical variables affecting the integrity of human biospecimens in biobanking,” *Clinical chemistry*, vol. 61, no. 7, pp. 914–934, 2015.
- [30] P.S. Zarrin, N. Roeckendorf, C. Wenger. “Exasens: a novel dataset for the classification of saliva samples of COPD patients”, IEEE Dataport, 2020.
- [31] S. Aryal, E. Diaz-Guzman, D.M. Mannino. “COPD and gender differences: an update,” *Translational Research*, vol. 162, no. 4, pp. 208–218, 2013.
- [32] C.A.V. Fragoso. “Epidemiology of chronic obstructive pulmonary disease (COPD) in aging populations,” *COPD: Journal of Chronic Obstructive Pulmonary Disease*, vol. 13, no. 2, pp. 125–129, 2016.
- [33] W. Zhu, N. Zeng, N. Wang. “Sensitivity, specificity, accuracy, associated confidence interval and ROC analysis with practical SAS implementations,” *NESUG proceedings: health care and life sciences*, Baltimore, Maryland, vol. 19, p. 67, 2010.
- [34] P.S. Zarrin, R. Zimmer, C. Wenger, and T. Masquelier. “Epileptic Seizure Detection Using a Neuromorphic-compatible Deep Spiking Neural Network,” *In International Work-Conference on Bioinformatics and Biomedical Engineering (IWBBIO)*, Granada, Spain, 2020, pp. 389–394.
- [35] F. Cai, J.M. Correll, S.H. Lee, Y. Lim, V. Bothra, Z. Zhang, M.P. Flynn, W.D. Lu. “A fully integrated reprogrammable memristor–CMOS system for efficient multiply–accumulate operations,” *Nature Electronics*, vol. 2, no. 7, pp. 290–299, 2019.
- [36] P.S. Zarrin and C. Wenger. “Implementation of Siamese-based Few-shot Learning Algorithms for the Distinction of COPD and Asthma Subjects,” *Springer LNCS (ICANN20)*, Bratislava, Slovakia, 2020.
- [37] Y. LeCun, Y. Bengio, G. Hinton. “Deep learning,” *Nature*, vol. 521, pp. 436–444, 2015.
- [38] T. Ching, et al. “Opportunities and obstacles for deep learning in biology and medicine,” *Journal of The Royal Society Interface*, vol. 15, no. 141, p. 20170387, 2018.

- [39] A. Zeiaee, R. Soltani-Zarrin, S. Jayasuriya, R. Langari. “A uniform control for tracking and point stabilization of differential drive robots subject to hard input constraints,” In *Dynamic Systems and Control Conference*, Ohio, USA, vol. 57243, 2015, p. V001T04A005.
- [40] R. Soltani-Zarrin, A. Zeiaee, R. Langari, N. Robson. “Reference path generation for upper-arm exoskeletons considering scapulohumeral rhythms,” In *International Conference on Rehabilitation Robotics (ICORR)*, London, UK, 2017, pp. 753–758.
- [41] I. Kiral-Kornek. “Epileptic seizure prediction using big data and deep learning: toward a mobile system,” *EBioMedicine*, vol. 27, pp. 103–111, 2018.
- [42] V.U. Prabhu. “Few-Shot Learning for Dermatological Disease Diagnosis,” *Georgia Institute of Technology*, 2019.
- [43] P.J. Barnes. “Mechanisms in COPD: Differences from asthma,” *Journal Chest*, vol. 117, pp. 10S—14S, 2000.
- [44] D.S. Postma, K.F. Rabe. “The asthma–COPD overlap syndrome,” *New England Journal of Medicine*, vol. 373, pp. 1241–1249, 2015.
- [45] Y. Wang, J. Kwok, L.M. Ni, Q. Yao. “Generalizing from a few examples: A survey on few-shot learning,” *arXiv preprint*, 1904.05046, 2019.
- [46] A. Santoro, S. Bartunov, M. Botvinick, D. Wierstra, T. Lillicrap. “Meta-learning with memory-augmented neural networks,” *International conference on machine learning*, vol. 11, 2016, pp. 1842–1850.
- [47] H. Altae-Tran, B. Ramsundar, A.S. Pappu, V. Pande. “Low data drug discovery with one-shot learning,” *ACS central science*, vol. 3, pp. 283–293, 2017.
- [48] K. Stewart, E. Neftci, G. Orchard. “On-chip Few-shot Learning with Surrogate Gradient Descent on a Neuromorphic Processor,” *arXiv*, 1910.04972, 2019.
- [49] C. Martín, P. Langendoerfer, P.S. Zarrin, M. Díaz, B. Rubio. “Kafka-ML: connecting the data stream with ML/AI frameworks,” *arXiv preprint*, 2020.

Chapter 5

Hardware Deployment

5.1 Neuromorphic On-chip Recognition of Saliva Samples of COPD and Healthy Controls Using Memristive Devices

As extensively discussed in previous chapters, implementation of ML techniques is crucial for the effective management of COPD in home-care environments. However, shortcomings of cloud-based ML tools in terms of data safety and energy efficiency limit their integration with low-power medical devices. To address this, energy efficient neuromorphic platforms can be used for the hardware-based implementation of ML methods. Therefore, a memristive neuromorphic platform is presented in this thesis for the on-chip recognition of saliva samples of COPD patients and healthy controls. Results of its performance evaluations showed that the digital neuromorphic chip is capable of recognizing unseen COPD samples with accuracy and sensitivity values of 89% and 86%, respectively. Integration of this technology into personalized healthcare devices will enable the better management of chronic diseases such as COPD. This chapter of the thesis is based on reference [1].

5.1.1 Introduction

Among various possible methods for the early diagnosis of COPD in a PoC setup, regular screening of dielectric properties of patients' saliva has shown to provide important information on the disease status [2–5]. However, information obtained on this one single parameter, the dielectric properties of saliva, is

not sufficient by itself for providing a comprehensive diagnostic solution [6, 7]. In other words, the accurate diagnosis of the disease based on this approach is only possible by concurrent consideration of various personal–medical parameters related to patients. These parameters include demographic information of patients such as age, gender, and the smoking background. To address this issue, ML tools have been applied on the rudimentary information of the saliva properties together with the demographic parameters to identify the diagnostic status of patients in a PoC environment [6, 7].

ML tools applied on the clinical data acquired from PoC devices enable the efficient management of chronic diseases such as COPD. The scope of ML tools goes far beyond classical statistical analyses performed in medicine, providing accurate and real-time predictions on the health status of patients or the progress of their diseases [8, 9]. In addition, availability of numerous health-related data, thanks to the advancements in wearable technologies and internet-of-things, have facilitated the better integration of ML with healthcare devices in PoC environments [10]. Therefore, constant and remote monitoring of patients for the management of chronic and degenerative conditions, monitoring their rehabilitation progress, and predicting critical–emergency health conditions have become a reality [11]. For example, tracking heart activities of elderly, monitoring blood glucose levels in diabetic patients, and observing the rehabilitation progress of Parkinson’s diseased patients are all among the recent applications of ML in PoC [8, 10–13]. Moreover, by taking advantage of ML tools, valuable information can be extracted from the vast amount of user data for identifying previously unknown disease trends or diagnostic links and providing comprehensive treatment plans and recommendations for the healthcare specialists [11, 14].

Although the astonishing performance of ML for various studies, shortcomings of the cloud-based techniques have limited their real-world applications in medicine [15]. These shortcomings include data safety concerns related to securing sensitive medical data in a single database, susceptible to malicious attacks or scandals. In addition, complexities associated with cloud communications such as robustness against interference is another hurdle, requiring precise design for the short-range (device to smartphone via bluetooth) and long-range (smartphone to backend using internet) communications for transferring data from medical devices to the backend [10]. Furthermore, technical aspects of the cloud-based ML such as wide bandwidth requirements and low latency plays vital role for medical applications. For example, pre-processing and data curation—compression of the acquired data, prior to their extraction from a device towards the backend, is remarkably challenging for providing real-time information to users with the

least possible delay. Last but not least, cloud-based techniques require immense energy consumption and enormous computational power, restricting their application for low-power PoC devices [6, 16].

The abovementioned shortcomings of the cloud-based ML in healthcare can possibly be addressed using neuromorphic platforms at the edge [16, 17]. A neuromorphic platform offers a hardware-based imitation of neural networks by using actual electrical components as neurons and synapses [18]. Real-time analysis of data in a less time consuming manner with a smaller time delay is far more practical by bringing data post-processing from the backend onto a neuromorphic chip. Furthermore, securing sensitive medical data on a single chip, without cloud communications or backend storage, complies better with the patient privacy regulations. In addition, since neuromorphic platforms process data near their source, they are relatively better immune against false operations and offer a large fault tolerance for medical applications. In other words, the robustness of these technologies is vital for near-a-patient applications, where accessing a sufficient internet coverage is unfeasible. Moreover, the energy-efficient hardware-based neuromorphic systems require less computational power, making them an adequate technology for edge-computing required in PoC medical devices [19–23].

Considering remarkable advantages of neuromorphic chips, they have been recently investigated for various ML applications including in medicine. As an example, Cai *et al.* have introduced a memristor-based neuromorphic computing chip for the breast cancer data classification [17]. The developed chip demonstrated high accuracy of 94.6% for the classification of benign and malignant samples within the breast cancer screening dataset. The computationally-efficient technology has enabled the real-time processing of data with high speed and low energy consumption. Similarly, Choi *et al.* have proposed a memristor-based neuromorphic crossbar array for the online clustering of breast cancer data in an unsupervised fashion [24]. In this work, principal component analysis algorithm was implemented on the chip for effectively classifying sensory data with 97.6% accuracy. Online learning was successfully achieved in the developed memristor network, demonstrating the practicality of using neuromorphics for performing complex ML algorithms required for data-intensive tasks such as medical pattern recognition. In another study, a spiking neural network was implemented on a neuromorphic chip for the real-time discrimination of electromyography signals for the hand gesture classification [25]. The proposed low-power technique provided an accuracy of 84% for the recognition of various gestures, making it a suitable technology for remote rehabilitation and diagnostic setups required for patients with Parkinson's disease. Park *et al.* have reported

the application of memristive neuromorphic synapses as a Hardware-based Neural Network (HNN) for the Electroencephalography (EEG) signal recognition [26]. Human thought patterns related to three different vowels were recorded using EEGs, while a subject imagined speaking them. Subsequently, the proposed memristive HNN system was applied for learning and recognizing patterns of the acquired EEG signals. The developed device provided high accuracy for extracting features through the recorded EEG signals during speech imagination experiments. Apart from the mentioned biomedical applications, neuromorphic chips have been extensively used for imaging scenarios including digit recognition [27–32]. As reported by Wenger *et al.*, learning and recognition of the MNIST dataset digits have been experimentally demonstrated by taking advantage of the inherent stochasticity of CMOS-integrated memristive devices [27]. A notable recognition rate of 89%, for a MNIST subset, was achieved in this work, demonstrating the potential of the proposed Resistive Random Access Memory (RRAM) technology for performing complex ML tasks.

Although neuromorphic systems offer an alternative platform for edge-computing required for the execution of ML algorithms on portable medical devices, their time-consuming training procedure for learning complex medical patterns is a significant drawback [33, 34]. Moreover, deployment of the pre-trained sophisticated deep learning networks onto neuromorphic chips, with rudimentary network structures, leads to lower precision, increased latency, and degraded energy efficiency and accuracy [16, 35]. Therefore, development of a neuromorphic-compatible network topology is significantly important for pre-training a simulation-based Artificial Neural Network (ANN) prior to its deployment on a hardware-based neuromorphic platform. Backend training of a neuromorphic-compatible ANN, on the cloud, reduces the training time required for learning complex medical patterns; while, implementation of the pre-trained network on a neuromorphic platform enables the real-time recognition and classification of medical data on a low-power PoC device [32, 33].

In previous sections, a neuromorphic-compatible ANN was developed for the COPD pattern recognition using synthesized data [6]. However, the hardware implementation of the model on a neuromorphic platform and its *in-vitro* performance evaluation using real clinical data were missing. Therefore, the objective of this part of the thesis was to train our previously developed ANN simulation for the classification of saliva samples of COPD patients and healthy controls using real clinical data and to implement the trained ANN on IHP's memristive hardware platform for on-chip recognition. The combination of the simulation-based training and hardware-based recognition facilitates the better integration of neuromorphics with PoC

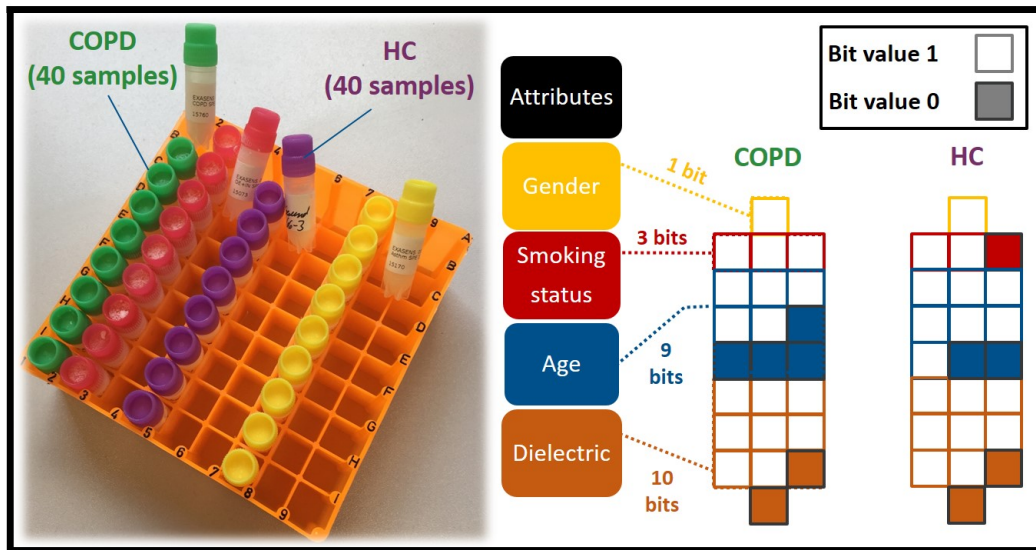


Figure 5.1: Conversion of analog attributes of Exasens dataset (gender, smoking status, age, and dielectric properties) into 23 binary bits.

medical devices, required for the management of chronic diseases such as COPD. Moreover, neuromorphic-equipped healthcare technologies provide the best platform for patients to take advantage of ML-based medicine, while having control over their medical data and privacy.

5.1.2 Materials and Methods

5.1.2.1 Data Preparation

The open access Exasens dataset, available at the UCI machine learning repository (<https://archive.ics.uci.edu/ml/datasets/Exasens>), was used in this section for training and evaluating the developed model for the classification and recognition of saliva samples of COPD patients and HC [7]. This novel dataset contains information on hundred saliva samples collected from four groups of respiratory patients including: COPD (40 samples), HC (40 samples), asthma (10 samples), and respiratory infected subjects without COPD or asthma (10 samples). The attributes of the dataset, used for the classification of subjects, include demographic information of patients (age, gender, and smoking status) as well as the dielectric properties (Minimum value for the real part of permittivity) of the characterized saliva samples for every class. For computational purposes, the non-quantitative attributes—diagnosis, gender, and smoking status—were converted into numerical values using the following labels: diagnosis (COPD (1)–HC (0)), gender (male

(1)–female (0)), smoking status (smoker (3)–ex-smoker (2)–non-smoker (1)). Subsequently, analog values of these four attributes were thresholded and converted into 23 binary bits (Gender (1), smoking status (3), age (9), dielectric permittivity (10)), as shown in Figure 5.1. Binarization of the attributes of this small-sized dataset has shown to reduce overfitting and noise, and to improve the performance of ML tools for the classification of COPD and HC samples [7, 36]. In addition, considering the small size of the investigated dataset, 80 samples for two classes of COPD and HC, 5-fold cross-validation method was implemented for the evaluation of the ANN model, thus preventing overfitting and providing reliable results. Therefore, for every cross-validation fold, the dataset was split into different test–train subsets with the ratio of 20–80%, respectively. The test-fraction, with unseen data points during model training, was considered as an external validation dataset for the evaluation of models. The data preparations and ML implementations were performed on the JupyterLab environment using Keras 2.2.5 and Scikit-learn 0.22 libraries of Python [37].

5.1.2.2 Artificial Neural Network

After data preparations, a dense ANN with one hidden-layer and one read-out layer was developed for the classification of COPD and HC samples, as shown in Figure 5.2. The input layer of the network consisted of 23 neurons, considering the binarized attributes of the dataset. To replicate the intrinsic structure of the intended neuromorphic platform, a hidden layer with 4 neurons and a sigmoid activation function was modeled. The read-out layer, with a sigmoid activation function, consisted of two neurons for the two possible classes of COPD and HC. A dropout with 20% probability was applied to the hidden-layer for the overfitting prevention. Adam optimization algorithm, with 0.0001 learning rate, and a cross entropy error function were used for training the network in the backend using the Google Colab GPU platform [38]. The developed ANN model was trained for 3000 epochs with a batch size of 10, using the train-subset of every cross-validation fold. Network parameters including weights and biases were computed and optimized during the training phase and their final analog values were recorded for every fold. Considering the fact that the intended neuromorphic chip consists of digital memristive devices, multilevel thresholding of network analog parameters into 10 levels was necessary for the deployment of the trained ANN onto the hardware platform. Therefore, calculated weights and biases of the trained ANN were thresholded into 10 levels to comply hardware requirements, as shown in Figure 5.3. For this purpose, the absolute maximum value among calculated parameters was identified and divided by five to determine the resolution of thresholding

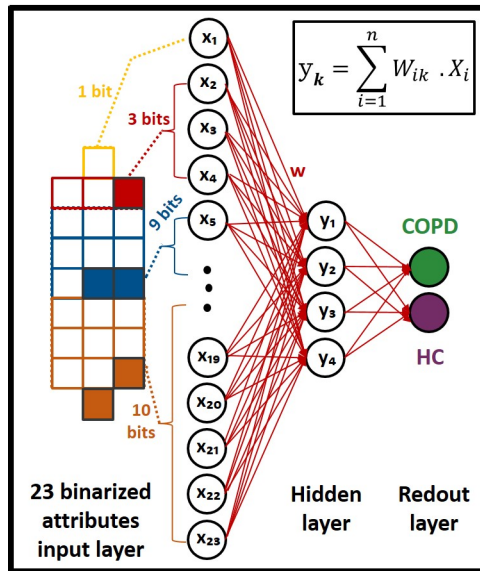


Figure 5.2: ANN simulation topology, with one hidden-layer, for the classification of saliva samples of COPD patients and HC.

levels. As shown in Figure 5.3, the calculated threshold was used with positive and negative signs for the 10-level segmentation of network parameters with positive and negative values, respectively. After calculating thresholding steps, network parameters with analog values were shifted up to the nearest threshold value (for positive levels and equivalent for negative levels), representing one digital device per level. It is noteworthy that positive and negative levels are interpreted as devices with different current directions for the hardware implementation. Finally, converted weights and biases of the network with 10-level resolution were recorded and extracted for the deployment on the memristive neuromorphic platform, as shown in Figure 5.3. All metrics and models are available in details at <https://github.com/Pouya-SZ/Bioneuromorphics>.

5.1.2.3 Hardware Implementation

The hardware implementation of the developed model was performed on amorphous HfO_2 memristors which are CMOS-integrated 4-kbit RRAM arrays fabricated using the 250 nm CMOS technology at IHP [39–41]. The integration in CMOS technology is an important step towards fully integrated neuromorphic circuits. The array consists of 64×64 memristive cells in a 1-Transistor-1-Resistor (1T-1R) configuration. The packaged chip is shown in Figure 5.4(a). Devices can be switched between two distinct states, i.e. low resistance state (LRS) and high resistance state (HRS), by the formation and dissolution of a conductive

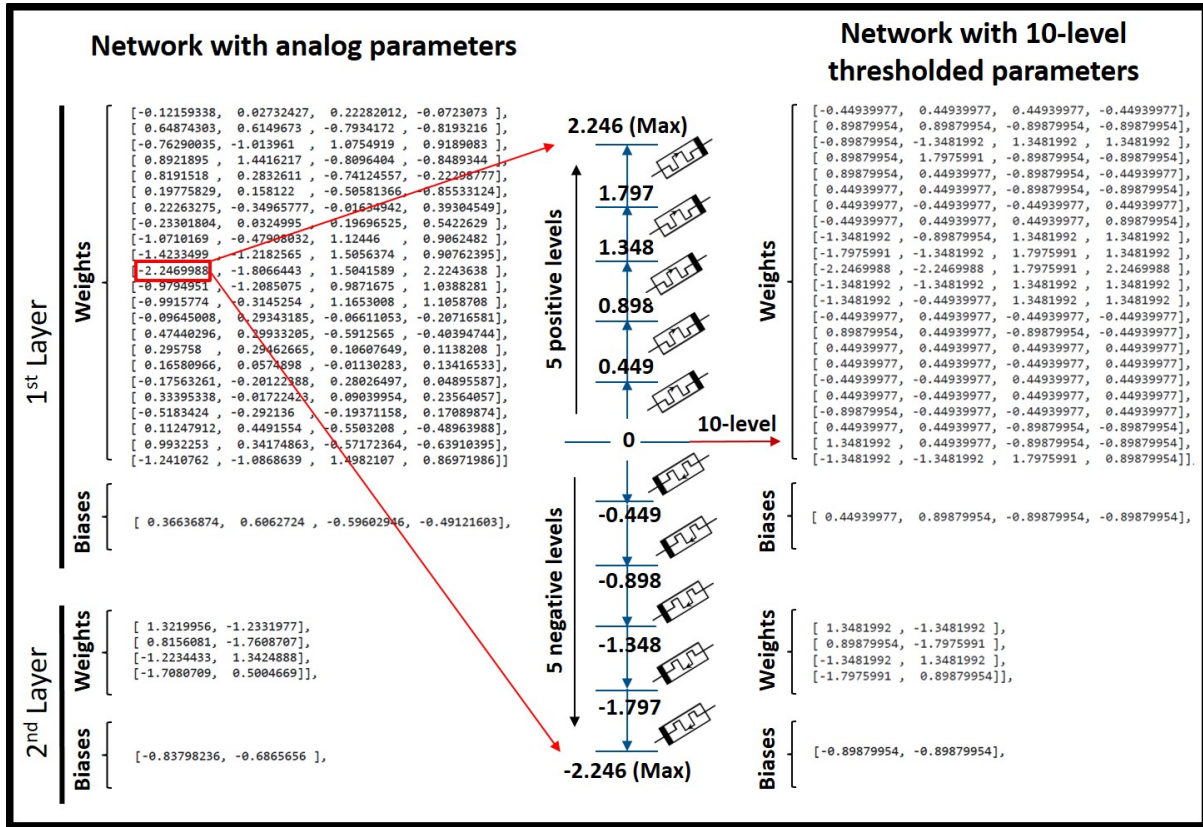


Figure 5.3: Multilevel thresholding of network analog parameters into 10 levels for complying hardware implementation requirements of the digital neuromorphic chip.

filament consisting of oxygen vacancies. Nominal read-out currents are $30 \mu\text{A}$ and $5 \mu\text{A}$ at 0.2 V for LRS and HRS, respectively. The evolution of mean read-out currents of 128 devices is shown in Figure 5.4(b). Here, two distinct states are clearly present for 1000 switching cycles. Mean read-out currents of $30.8 \mu\text{A}$ and $3.2 \mu\text{A}$ at 0.2 V for LRS and HRS, respectively, are changing marginally to $31.6 \mu\text{A}$ and $3.0 \mu\text{A}$. Mean read-out currents for different read-out voltages $V_{read} \leq 0.2 \text{ V}$ are shown in Figure 5.4(c) for 128 devices being in LRS and HRS, respectively. The resistance does not scale linearly with the voltage [39]. Using a sufficient high voltage of 1.3 V or higher leads to reliable switching to LRS while using a sufficient low voltage of -1.6 V or lower leads to reliable switching to HRS. An even better control on the switching event can be achieved by using the Incremental Step Pulse with Verify Algorithm (ISPVA), which was used in this work [42]. It should be noted that applying voltage pulses with lower absolute value of the amplitude leads to stochastic switching between resistance states, which can be exploited for stochastic learning of analog data [27]. The stochasticity in amorphous devices is lower than in polycrystalline devices. This can

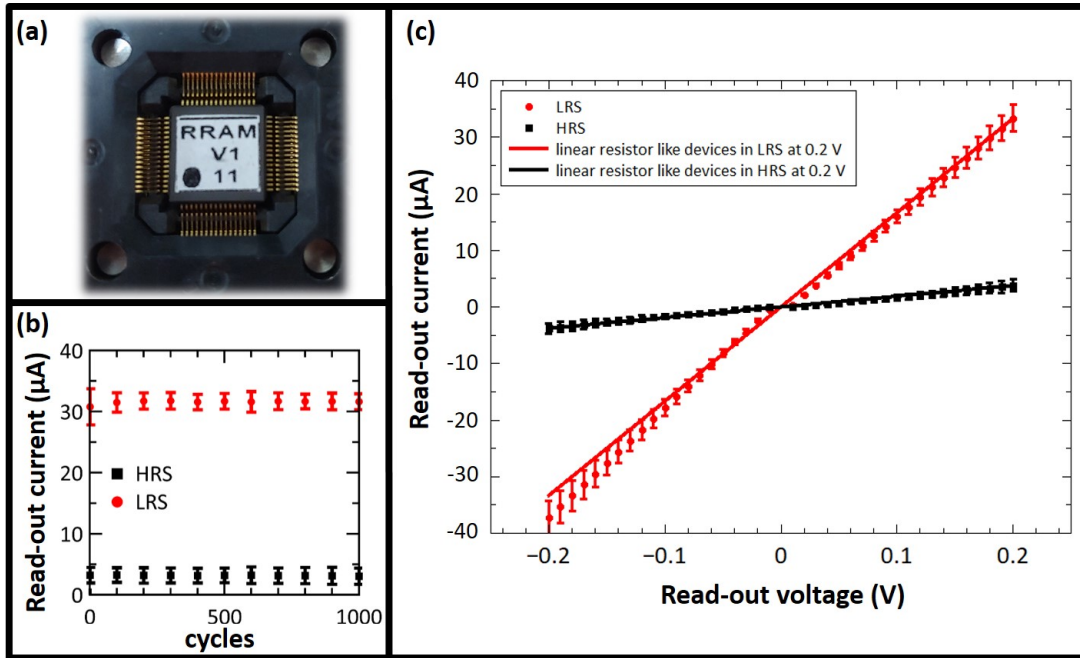


Figure 5.4: (a) 4-kbit CMOS-integrated RRAM array of IHP mounted on a PCB as synaptic weights in mixed-signal neuromorphic circuit; (b) Mean values and standard deviations of the read-out currents of 128 devices integrated in a 4-kbit chip read-out at 0.2 V for 1000 switching cycles; (c) Read-out currents dependent on the read-out voltage amplitude and polarity. Red dots and black squares denoting mean values of 128 devices in LRS and HRS, respectively, while error bars are depicting standard deviations. The solid lines are showing linear resistors with a resistance like the devices measured at +0.2 V in LRS (red) and HRS (black).

most probably be attributed to a more homogenous defect distribution in the amorphous devices [27], which is why these devices are used for the work described here. A thorough characterization of the devices in terms of switching voltages, endurance, yield and retention is given in [27].

For the deployment of the thresholded model with 10 levels, a mixed-signal neuromorphic circuit with software-based neurons and hardware synapses was used similar to those shown in [27]. The RRAM chip was connected via a standard 64 pin integrated circuit socket to a Printed Circuit Board (PCB). Visual Basic was used to simulate neurons on a conventional computer and to control the experimental setup. Furthermore, an Arduino Mega 2560 microcontroller board was used to serve the address pins of the RRAM chip. Read-out and switching pulses were applied using Agilent E5263A Source Measurement Unit (SMU).

Considering the topology of the developed ANN model (Figure 5.2) with one hidden layer and one read-out layer as well as four and two neurons per layer, respectively, 106 parameters (i.e. synaptic weights and biases) were required for linking network layers. On the other hand, since every memristive device on

the hardware represents one level of the thresholded parameters, 1060 memristive devices were required on the hardware for the implementation of the developed COPD recognition model with 10-level resolution. Resistance states of 1060 randomly chosen functional devices on a single chip were set to the HRS or LRS, respective to pre-trained weights. Every network parameter is represented by the combination of 10 devices so that the total value of the parameter is the sum of all 10 device currents read-out with voltages up to 0.2 V. Here, five devices are read-out with a positive voltage and five device are read-out with a negative voltage leading to positive and negative currents contributing to the total value of the network parameter. The minimum absolute value of one synaptic weight or bias is reached, when one device is in LRS and all other nine devices are in HRS leading to a nominal current of $1 \times 30 \mu\text{A} + 4 \times 5 \mu\text{A} - 5 \times 5 \mu\text{A} = 25 \mu\text{A}$ determined with 0.2 V. The maximum absolute value is achieved by switching all devices corresponding to the same read-out polarity to LRS while all others are in HRS. Thus, a nominal current of $5 \times 30 \mu\text{A} - 5 \times 5 \mu\text{A} = 125 \mu\text{A}$ is flowing. In between, equidistant discrete states can be achieved (shown in Figure 5.5). Devices connecting input layer and hidden layer are read-out with +0.2 V and -0.2 V, while devices connecting hidden layer and read-out layer are read-out with voltage amplitudes between -0.2 V and +0.2 V as it is explained below. This leads to a non-linear distortion of network parameters, because of the non-ohmic conduction mechanism depicted in Figure 5.4(c).

After the successful implementation of pre-trained weights on the hardware, the test-subset of data was used to evaluate the performance of the neuromorphic model for the recognition of COPD and HC samples. For the recognition of COPD samples with the mixed-signal approach, the 23 input bits of the test-subset data were applied to the simulated neurons on the input layer, as shown in Figure 5.6. Input bits with a value 1 were applied to the network by voltage pulses of ± 0.2 V (i.e. +0.2 V or -0.2 V for devices assigned to a positive or negative contribution, respectively, as explained above), while no voltage was applied for a 0 value input bit. As shown in Figure 5.6, output neurons of every subarray are perceptrons with a sigmoidal activation function, which receive the sum of current values passing through the devices connected together with a specific bias value. The read-out of device currents is done serial and they are summed up in software. A parallel read-out would require an application specific chip design. Nevertheless, a proof-of-principle for using devices in a hardware neuromorphic circuit can be given using serial read-out. These current values are normalized by the factor n to the maximum value of the pre-trained analog network to guarantee the sigmoid function is activated within a reasonable range of values. Thus, the maximum current

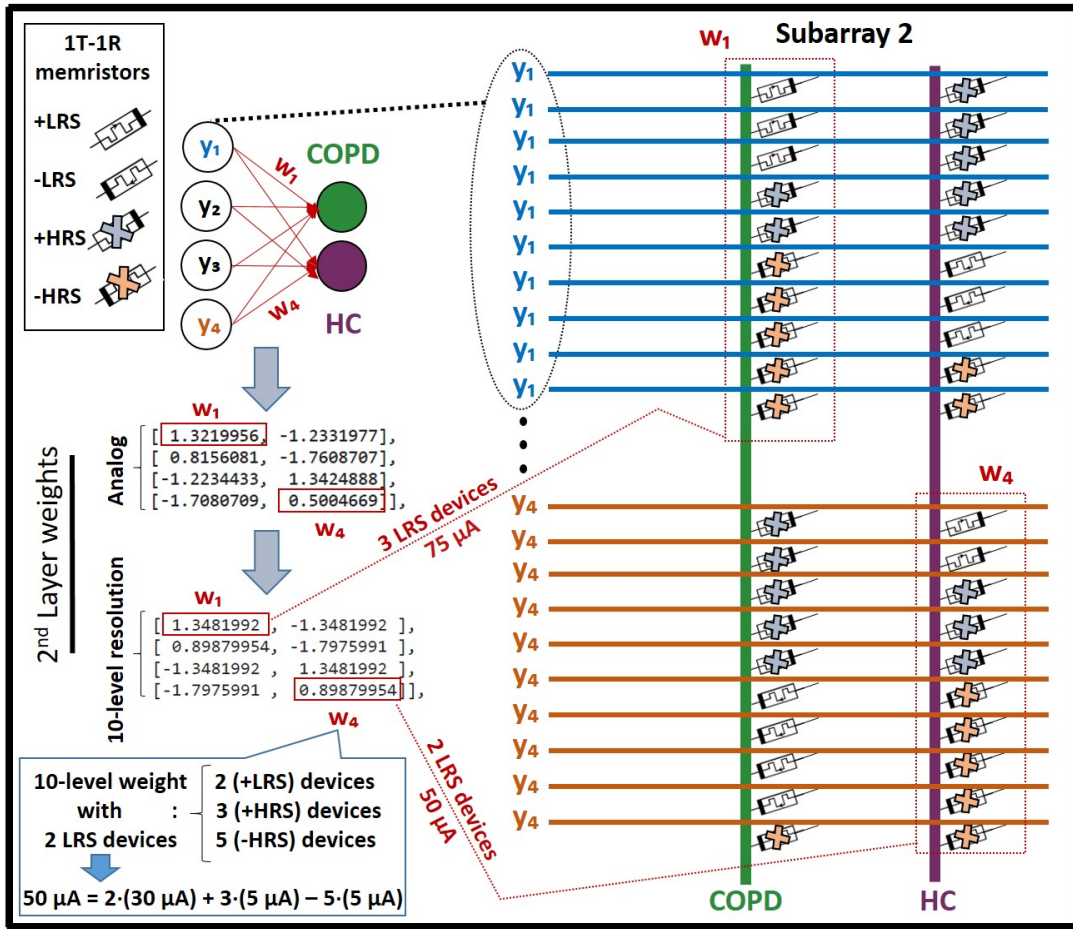


Figure 5.5: Assignment of memristive devices for the appropriate replication of simulation weights on the hardware, considering current values of 25 μA , 50 μA , 75 μA , 100 μA , and 125 μA for 1, 2, 3, 4, and 5 LRS bits (equivalent for negative bits), respectively.

of 125 μA corresponds to the maximum pre-trained analog value. An activated perceptron i of the second layer is generating an analog output signals X_i within the interval of [0, 1]. These are applied to devices connecting layer 2 and 3 as voltage pulses with amplitudes $X_i \cdot \pm 0.2$ V with a precision of 10 mV. The output values of the third layer (read-out layer) perceptrons are denoting whether a test sample belongs to COPD or HC categories. This realization is in agreement with the theory of neural networks that the weighted sum of inputs determine the value of a perceptron neuron in the subsequent layer, as demonstrated in Figure 5.2. Therefore, applying test-subsets of COPD and HC with different input patterns generated two different current values activating the read-out layer perceptrons of the neuromorphic network leading to the hardware-based recognition of these two classes.

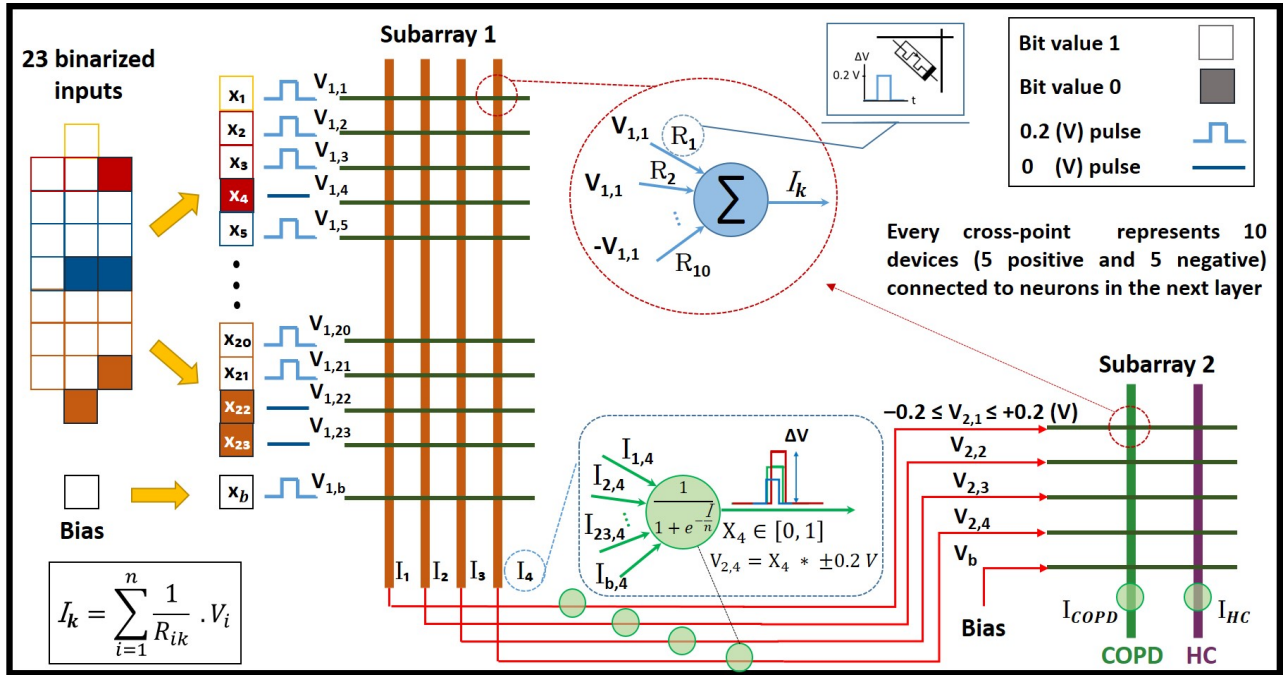


Figure 5.6: Application of 23 input bits of the test-subset data to the simulated neurons for the recognition of COPD and HC samples. Input bits with a value 1 were applied to the network by voltage pulses of ± 0.2 V (i.e. $+0.2$ V or -0.2 V for devices assigned to a positive or negative contribution, respectively), while no voltage was applied for a 0 value input bit. Output neurons of every subarray are perceptrons with a sigmoidal activation function, which receive current values as the sum of all input voltages weighted with the resistivity values of individual memristive cells. These input currents are normalized by the factor n to map them to a reasonable range of values for the activation of the perceptrons. The output of the first perceptron layer is mapped to voltage pulses with variable amplitudes.

5.1.2.4 Performance Assessment

While the train-subset of every cross-validation fold (64 data points out of overall 80) was used for training the ANN and computing the 10-level model topology, the test-subset, with 16 data points, was considered

Table 5.1: Performance of the ANN with analog parameters.

K-fold	Accuracy	Sensitivity	Specificity	Precision
Fold 1	87.5%	100%	75%	80%
Fold 2	93.75%	87.5%	100%	100%
Fold 3	81.25%	87.5%	75%	77.78%
Fold 4	93.75%	87.5%	100%	100%
Fold 5	93.75%	100%	87.5%	88.89%
Average	90%	92.5%	87.5%	89.3%

as an external validation dataset for the performance evaluation of models for the recognition of saliva samples of COPD patients and HC. Tables 5.1, 5.2, and 5.3 report the 5-fold cross-validation performance of following models, respectively: ANN with analog parameters, ANN model with 10-level resolution topology, and the HNN with 10-level resolution deployed on the memristive neuromorphic chip. The performance measures reported in these tables include accuracy, sensitivity, specificity, and precision for every cross-validation fold as well as the average of all five folds. The reported accuracy measure in these tables indicates the performance of a model for correctly recognizing unseen test data, which was calculated as the percentage of true positives (correctly identified COPD) plus true negatives (correctly identified HC) out of all assessments. The sensitivity of a model was calculated as the proportion of True Positives (TP) out of all diseased cases; while the specificity value shows the number of True Negatives (TN) over number of TNs and False Positives (FP). Precision criterion shows the ratio of true positives over true plus false positives (incorrectly identified COPD). It should be noted that the hardware realization experiments were repeated five times for every single cross-validation fold to investigate the repeatability of measurements considering undesired effects of device-to-device variability and failed switching events. Therefore, results reported in Table 5.3 represent the average of five repetition for every single cross-validation fold. In addition, Figure 5.7 demonstrates confusion matrices for a single cross-validation fold (fold-5) for the recognition of COPD and HC samples.

5.1.3 Results and Discussions

As reported in Table 5.1, the ANN simulation with analog parameters provided a high accuracy of 90% for the recognition of unseen saliva samples of COPD patients and HC. In addition, sensitivity, specificity, and precision values of 92.5%, 87.5%, and 89.3%, respectively, have been reported for its 5-fold

Table 5.2: Performance of the ANN with 10-level resolution.

K-fold	Accuracy	Sensitivity	Specificity	Precision
Fold 1	87.5%	87.5%	87.5%	87.5%
Fold 2	93.75%	87.5%	100%	100%
Fold 3	81.25%	87.5%	75%	77.78%
Fold 4	93.75%	87.5%	100%	100%
Fold 5	81.25%	75%	87.5%	85.7%
Average	87.5%	85%	90%	90.2%

cross-validation performance, making it a reliable model for the *in-vitro* diagnosis of COPD. On the other hand, Table 5.2 presents the performance assessment of the ANN simulation with the 10-level resolution topology. Although a slight performance degradation compared to its original analog structure, the ANN model with 10-level resolution provided acceptable accuracy, sensitivity, specificity, and precision values of 87.5%, 85%, 90%, and 90.2%, respectively, for the recognition of unseen samples within the test-subset. These results are along with the fact that the multilevel thresholding of a network's parameters impairs its recognition performance with respect to its resolution. In a similar manner, deployment of the model with 10-level resolution on the memristive neuromorphic platform has led to an on-chip recognition accuracy of 89%, indicating the reliability of the approach for the management of COPD in real-world applications (Table 5.3). In addition, high sensitivity, specificity, and precision values of 86%, 92%, and 92% have been reported for the on-chip recognition of 16 unseen test samples using the RRAM neuromorphic platform, making it a suitable technology for the implementation of ML techniques on low-power PoC medical devices. In particular, the network could reliably cope with the device-to-device variability of RRAM devices. Mean values of read-out currents were $3.9 (\pm 1.0) \mu\text{A}$ and $35.5 (\pm 3.7) \mu\text{A}$ for HRS and LRS devices, respectively. Additional to the device-to-device variability, failed switching events led to devices in the wrong resistance state. On average 2.68 of devices (i.e. 0.25%) were in the wrong state in each experimental run.

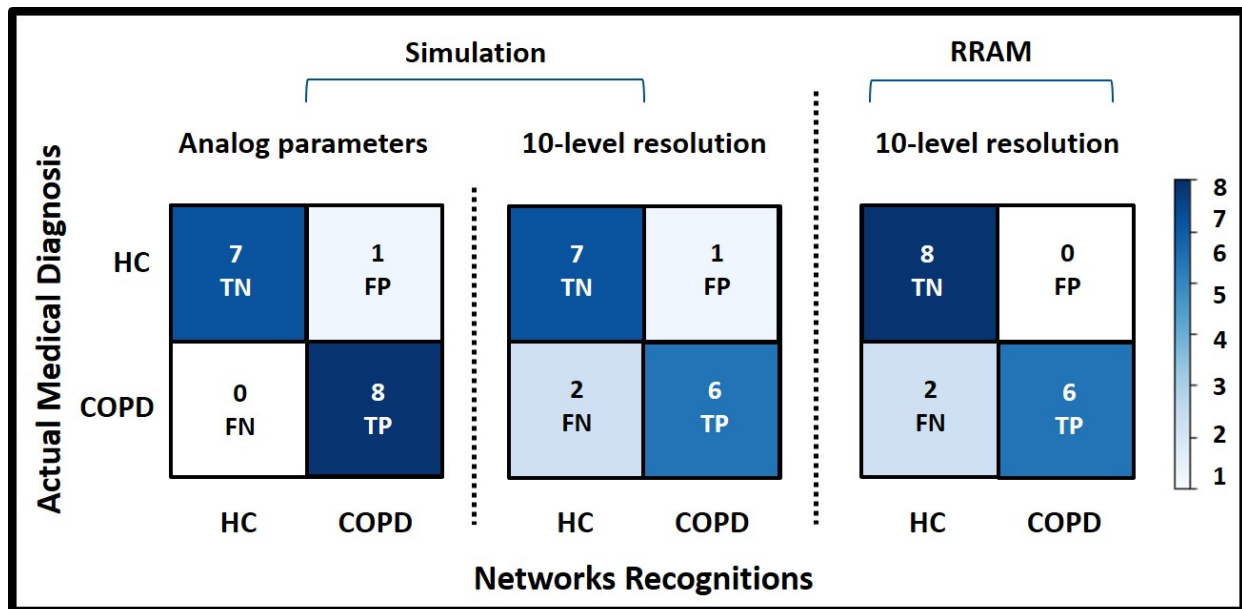


Figure 5.7: Confusion matrices for a single cross-validation fold (fold 5) for the recognition of COPD and HC samples, demonstrating the calculated sensitivity, precision, and specificity measures.

Furthermore, the non-linear response of devices connecting layer 2 and 3 to voltage pulses with amplitudes between -0.2 V and $+0.2$ V (shown in Figure 5.4(c)) did not strongly influence the accuracy. Even though all three mechanisms, i.e. device-to-device variability, failed switching events, and non-linear read-out may have affected the recognition performance of experiments, the overall average recognition rate was only slightly below the simulation with analog values. Nevertheless, in order to reduce the performance gap between the ANN simulation and its hardware-based replication on the chip, development of binary ANN models is necessary in the future [43, 44]. Alternatively, analog neuromorphic platforms, capable of replication of analog parameters on-chip, can also be used to address this issue [45].

Figure 5.7 shows the confusion matrices for the fifth cross-validation fold for the recognition of COPD and HC samples. The high accuracy, sensitivity, specificity, and precision for both simulation- and hardware-based ML models make them a promising tool for the recognition and management of COPD in PoC environments. Therefore, the acquired results illustrate the practicality of using a memristive neuromorphic platform for the on-chip recognition and classification of saliva samples of COPD patients and HC using real clinical data, which was proposed as the objective of this section.

The results reported in Tables 5.1, 5.2, and 5.3 present similar trends for all five cross-validation folds, indicating the reliability of the model performance in terms of overfitting. However, similar to any ML study on a small-sized dataset, generalizability of the presented results to a larger population of samples is the main limitation of this work, necessitating the extensive collection of data for the management of COPD. Nonetheless, to the best of author's knowledge, there is no other comprehensive dataset available up to date, which can be used for training and evaluating the proposed neuromorphic-oriented ML models for COPD detection in this work. Therefore, this study is considered as a stepping stone to future investigations in the field.

Table 5.3: Performance of the memristive neuromorphic chip.

K-fold	Accuracy	Sensitivity	Specificity	Precision
Fold 1	88%	90%	88%	88%
Fold 2	95%	88%	100%	100%
Fold 3	81%	88%	75%	78%
Fold 4	94%	88%	98%	97%
Fold 5	88%	75%	100%	100%
Average	89%	86%	92%	92%

It is noteworthy that the recognition accuracy of the neuromorphic HNN model improves with a greater number of thresholding levels, thus better replicating its original analog structure. However, a greater number of thresholding levels requires larger number of memristive devices on the hardware depending on the complexity of the original network and its number of parameters, thus restricting the resolution that can be chosen for the hardware deployment with respect to that specific neuromorphic hardware (e.g. 4096 devices for IHP's RRAM chip). In addition, greater number of devices on the hardware consume more energy, while requiring a larger chip size and a longer time span for training and executing models depending on the internal design of the chip. Therefore, the trade-off between the accuracy of models and their on-chip efficacy in terms of power consumption and chip size for various thresholding resolutions need to be taken into account for determining the most optimum resolution.

Neuromorphic platforms address the high energy consumption shortcoming of the cloud-based ML techniques for edge-computing applications. The read-out of all synaptic weights in the experiments consumed on average 614.2 (± 60.3) nJ per sample with a read-out pulse duration of 500 μs (i.e. the shortest pulse duration of the used Agilent E5263A SMU). This could be significantly reduced to 12.3 (± 1.2) nJ using 10 μs pulses, which also allows a reliable read-out of the used devices [40]. The energy efficiency of the neuromorphic systems makes them an adequate technology for the integration of ML tools with low-power PoC medical devices. Hence, additional circuitry for a complete hardware realization (e.g. the perceptrons) have to be implemented in low power electronics in the future.

As previously highlighted, for the sake of time efficacy, no learning or training was performed on the neuromorphic chip in this work. This is due to the fact that training a simulation-based model for many thousand iterations in the backend is far more practical. For instance, training the ANN model, in this study, for the classification of COPD and HC samples required an average time span of 250 seconds for 3000 learning epochs. Therefore, this work illustrates promising results for the practicality of using pre-trained neuromorphic chips in complex real-world applications, such as imaging, with time-consuming training requirements. Nevertheless, RRAM neuromorphic systems can also be used for the on-chip learning and adaptation to new input patterns by developing network structures and acquiring algorithms [27,46]. Adaptability of these chips to an individual patient data is significantly important for applications such as the epileptic seizure prediction, where developing a generalizable ML model is not possible [35]. Hence, by taking advantage of neuromorphic-based ML techniques, developing personalized solutions for the man-

agement and diagnosis of chronic diseases such as COPD is feasible.

The notable results of this section imply the feasibility of using neuromorphic-based ML techniques for the enhancement of PoC healthcare solutions for the management of COPD. The energy-efficient neuromorphic systems, used in this thesis, are expected to revolutionize the ML-based medicine in the future by bringing the data post-processing from the backend onto the chip, thus providing accurate and real-time predictions on the health status of patients. Furthermore, neuromorphic-equipped medical devices will better protect users' sensitive medical data without cloud communication requirements. Moreover, implementation of novel meta learning algorithms, such as few-shot learning, on neuromorphic platforms will enable the rapid adaptation and real-time learning in these systems with a few data points and the least possible computation [36, 47]. Example of such applications, where online learning and adaptation of a ML model is crucial, include autonomous driving, surgical robotics, personalized medicine, and precision diagnostic [47–50].

5.1.4 Conclusions and Future Work

In this section of the thesis, the concept of on-chip recognition of saliva samples of COPD patients and HC using a memristive neuromorphic platform was investigated. A hardware-friendly artificial neural network simulation was developed and trained in the backend for the classification of COPD and HC samples using real clinical data. Subsequently, analog parameters of the trained model were thresholded into 10 levels and were deployed on a memristive neuromorphic platform for on-chip recognition purposes. The neuromorphic chip with 10-level resolution provided a remarkable accuracy of 89% for the on-chip recognition of COPD and HC samples, offering an alternative approach to cloud-based ML methods required for the management of COPD in PoC environments. As the next step, a binary ANN model for the prediction of epileptic seizure will be developed and deployed on the introduced memristive neuromorphic system for the on-chip forecasting of epilepsy scenarios using low-power healthcare wearables.

Bibliography

- [1] P. S. Zarrin, F. Zahari, M.K. Mahadevaiah, E. Perez, H. Kohlstedt, and C. Wenger. “Neuromorphic On-chip Recognition of Saliva Samples of COPD and Healthy Controls Using Memristive Devices,” In *Nature Scientific Reports*, 2020.
- [2] T. Dong, S. Santos, Z. Yang, S. Yang, N.E. Kirkhus. “Sputum and salivary protein biomarkers and point-of-care biosensors for the management of COPD,” *Analyst*, 2020.
- [3] S. Mirza, R.D. Clay, M.A. Koslow, P.D. Scanlon. “COPD guidelines: a review of the 2018 GOLD report,” *Elsevier Mayo Clinic Proceedings*, vol. 93, pp. 1488–1502, 2018.
- [4] P. Soltani Zarrin, F.I. Jamal, S. Guha, J. Wessel, D. Kissinger, C. Wenger. “Design and Fabrication of a BiCMOS Dielectric Sensor for Viscosity Measurements: A Possible Solution for Early Detection of COPD,” *Biosensors*, vol. 8, no. 78, 2018
- [5] P.S. Zarrin, F.I. Jamal, N. Roeckendorf, C. Wenger. “Development of a Portable Dielectric Biosensor for Rapid Detection of Viscosity Variations and Its In-vitro Evaluations Using Saliva Samples of COPD Patients and Healthy Control,” *Healthcare*, vol. 7, no. 11, 2019
- [6] P.S. Zarrin and C. Wenger. “Pattern Recognition for COPD Diagnostics Using an Artificial Neural Network and Its Potential Integration on Hardware-Based Neuromorphic Platforms,” *Springer LNCS (ICANN19)*, Munich, Germany, September, 2019, pp. 284–288.
- [7] P. S. Zarrin, N. Roeckendorf, and C. Wenger. “In-vitro Classification of Saliva Samples of COPD Patients and Healthy Controls Using Machine Learning Tools,” *IEEE Access*, 2020.

- [8] A.L. Fogel, J.C. Kvedar. “Artificial intelligence powers digital medicine,” *NPJ Digital Medicine*, vol. 1, no. 5, 2018.
- [9] I. Kononenko. “Machine learning for medical diagnosis: history, state of the art and perspective,” *Artificial Intelligence in medicine*, vol. 23, pp. 89–109, 2001.
- [10] S. B. Baker, W. Xiang, I. Atkinson. “Internet of Things for Smart Healthcare: Technologies, Challenges, and Opportunities,” *IEEE Access*, vol. 5, pp. 26521–26544, 2017.
- [11] F.X. Campion, G. Carlsson, F. Francis. “Machine Intelligence for Healthcare,” Scotts Valley, CreateSpace Independent Publishing Platform, isbn=9781542924948, 2017.
- [12] A. Tsanas, M.A. Little, P.E. McSharry, and L.O. Ramig. “Accurate telemonitoring of Parkinson’s disease progression by noninvasive speech tests,” *IEEE transactions on Biomedical Engineering*, vol. 57, no. 4, pp. 884–893, 2009.
- [13] C.Y. Hung, W.C. Chen, P.T. Lai, C.H. Lin, and C.C. Lee. “Comparing deep neural network and other machine learning algorithms for stroke prediction in a large-scale population-based electronic medical claims database,” *IEEE Engineering in Medicine and Biology Society (EMBC)*, July, 2017, pp. 3110–3113.
- [14] P. Soltani Zarrin, A. Escoto, R. Xu, R.V. Patel, M.D. Naish, A.L. Trejos. “Development of an optical fiber-based sensor for grasping and axial force sensing,” *IEEE International Conference on Robotics and Automation (ICRA)*, Singapore, May, 2017, pp. 939–944.
- [15] Ching, T., et al. “Opportunities and obstacles for deep learning in biology and medicine,” *Journal of The Royal Society Interface*, vol. 15, p. 141, 2018.
- [16] K. Roy, A. Jaiswal, and P. Panda. “Towards spike-based machine intelligence with neuromorphic computing,” *Nature*, vol. 575, no. 7784, pp. 607–617, 2019.
- [17] F. Cai, J.M. Correll, S.H. Lee, Y. Lim, V. Bothra, Z. Zhang, M.P. Flynn, W.D. Lu. “A fully integrated reprogrammable memristor CMOS system for efficient multiplyaccumulate operations,” *Nature Electronics*, vol. 17, pp. 290–299, 2019.

- [18] G.W. Burr, et al. “Neuromorphic computing using non-volatile memory,” *Advances in Physics*, vol. 2, no. 1, pp. 89–124, 2017.
- [19] M.R. Meireles, P.E. Almeida, and M.G. Simoes. “A comprehensive review for industrial applicability of artificial neural networks,” *IEEE transactions on industrial electronics*, vol. 50, no. 3, pp. 585–601, 2003.
- [20] T. Tang, L. Xia, B. Li, R. Luo, Y. Chen, Y. Wang, and H. Yang. “Spiking neural network with rram: Can we use it for real-world application?”, *IEEE Design, Automation & Test in Europe Conference & Exhibition (DATE)*, March, 2015, pp. 860–865.
- [21] H. Ames, et al. “Persuading computers to act more like brains,” *Springer Advances in Neuromorphic Memristor Science and Applications*, pp. 37–61, 2012.
- [22] H. Zhuang, K.S. Low, and W.Y. Yau. “A pulsed neural network with on-chip learning and its practical applications,” *IEEE Transactions on Industrial Electronics*, vol. 54, no. 1, pp. 34–42, 2007.
- [23] M. Davies, et al. “Loihi: A neuromorphic manycore processor with on-chip learning.” *IEEE Micro*, vol. 38, no. 1, pp. 82–99, 2018.
- [24] S. Choi, P. Sheridan, and W.D. Lu. “Data clustering using memristor networks,” *Scientific reports*, vol. 5, p. 10492, 2015.
- [25] E. Donati, M. Payvand, N. Risi, R. Krause, and G. Indiveri. “Discrimination of EMG signals using a neuromorphic implementation of a spiking neural network,” *IEEE transactions on biomedical circuits and systems*, vol. 13, no. 5, pp. 795–803, 2019.
- [26] S. Park, et al. “Electronic system with memristive synapses for pattern recognition”, *Scientific reports*, vol. 5, p. 10123, 2015.
- [27] C. Wenger, F. Zahari, M.K. Mahadevaiah, E. Perez, I. Beckers, H. Kohlstedt, and M. Ziegler. “Inherent Stochastic Learning in CMOS-Integrated HfO₂ Arrays for Neuromorphic Computing,” *IEEE Electron Device Letters*, vol. 40, no. 4, pp. 639–642, 2019.

- [28] A. Nere, U. Olcese, D. Balduzzi, and G. Tononi. “A neuromorphic architecture for object recognition and motion anticipation using burst-STDP,” *PloS one*, vol. 7, no. 5, 2012.
- [29] M. Hansen, F. Zahari, M. Ziegler, and H. Kohlstedt. “Double-barrier memristive devices for unsupervised learning and pattern recognition,” *Frontiers in neuroscience*, vol. 11, p. 91, 2017.
- [30] M. Chu, et al. “Neuromorphic hardware system for visual pattern recognition with memristor array and CMOS neuron,” *IEEE Transactions on Industrial Electronics*, vol. 62, no. 4, pp. 2410–2419, 2014.
- [31] F. Moreno, J. Alarcón, R. Salvador, and T. Riesgo. “Reconfigurable hardware architecture of a shape recognition system based on specialized tiny neural networks with online training”, *IEEE Transactions on Industrial Electronics*, vol. 56, no. 8, pp. 3253–3263, 2009.
- [32] F. Alibart, E. Zamanidoost, and D.B. Strukov. ‘Pattern classification by memristive crossbar circuits using ex situ and in situ training,’ *Nature communications*, vol. 4, no. 1, pp. 1–7, 2013.
- [33] C. Li, et al. “Efficient and self-adaptive in-situ learning in multilayer memristor neural networks,” *Nature communications*, vol. 9, no. 1, pp. 1–8, 2018.
- [34] H. Zhuang, K.S. Low, and W.Y. Yau. “A pulsed neural network with on-chip learning and its practical applications.” *IEEE Transactions on Industrial Electronics*, vol. 54, no. 1, pp. 34–42, 2007.
- [35] I. Kiral-Kornek, et al. “Epileptic seizure prediction using big data and deep learning: toward a mobile system.” *EBioMedicine*, vol. 27, pp. 103–111, 2018.
- [36] P.S. Zarrin and C. Wenger. “Implementation of Siamese-based Few-shot Learning Algorithms for the Distinction of COPD and Asthma Subjects,” *Springer LNCS (ICANN20)*, Bratislava, Slovakia, Sep. 2020.
- [37] F. Pedregosa, et al. “Scikit-learn: Machine learning in Python,” *Journal of machine learning research*, vol. 12, pp. 2825–2830, 2011.
- [38] N. Ketkar. “Introduction to keras,” In *Deep learning with Python*, Apress, Berkeley, CA, 2017, pp. 97–111.

- [39] H.D. Kim, F. Crupi, M. Lukosius, A. Trusch, C. Walczyk, C. Wenger. “Resistive switching characteristics of integrated polycrystalline hafnium oxide based one transistor and one resistor devices fabricated by atomic vapor deposition methods,” *Journal of Vacuum Science & Technology B, Nanotechnology and Microelectronics: Materials, Processing, Measurement, and Phenomena*, vol. 33, no. 5, p. 052204, 2015.
- [40] M.K. Mahadevaiah, E. Perez, C. Wenger, A. Grossi, C. Zambelli, P. Olivo, F. Zahari, H. Kohlstedt, M. Ziegler. “Reliability of cmos integrated memristive hfo2 arrays with respect to neuromorphic computing,” In *IEEE International Reliability Physics Symposium (IRPS)*, Monterey, CA, USA, March, 2019, pp. 1–4.
- [41] V. Milo, C. Zambelli, P. Olivo, E. Pérez, M. K. Mahadevaiah, O. G. Ossorio, C. Wenger, D. Ielmini. “Multilevel HfO₂-based RRAM devices for low-power neuromorphic networks,” *APL Materials*, vol. 7, no. 8, p. 081120, 2019.
- [42] A. Grossi, C. Zambelli, P. Olivo, E. Miranda, V. Stikanov, C. Walczyk, C. Wenger. “Electrical characterization and modeling of pulse-based forming techniques in RRAM arrays,” *Solid-State Electronics*, vol. 115, pp. 17–25, 2016.
- [43] S. Yu, et al. “Binary neural network with 16 Mb RRAM macro chip for classification and online training.” *IEEE International Electron Devices Meeting (IEDM)*, December, 2016, pp. 2–16.
- [44] B. Zhuang, C. Shen, and I. Reid. “Training compact neural networks with binary weights and low precision activations,” *arXiv preprint*, 1808.02631, 2018.
- [45] M. Hansen, F. Zahari, H. Kohlstedt, et al. “Unsupervised Hebbian learning experimentally realized with analogue memristive crossbar arrays,” *Scientific Report*, vol. 8, no. 1, pp. 1–10, 2018.
- [46] C. Li, D. Belkin, Y. Li, P. Yan, M. Hu, N. Ge, H. Jiang, E. Montgomery, P. Lin, Z. Wang, W. Song. “Efficient and self-adaptive in-situ learning in multilayer memristor neural networks,” *Nature communications*, vol. 9, no. 1, pp. 1–8, 2018.
- [47] K. Stewart, E. Neftci, and G. Orchard. “On-chip Few-shot Learning with Surrogate Gradient Descent on a Neuromorphic Processor,” *arXiv*, 1910.04972, 2019.

-
- [48] P. S. Zarrin, A. Escoto, R. Xu, M. D. Naish, R. V. Patel, and A. L. Trejos. “Development of a 2-DOF sensorized surgical grasper for grasping and axial force measurements,” *IEEE Sensors Journal*, vol. 18, no. 7, pp. 2816–2826, 2018.
- [49] Y. Wang, J. Kwok, L.M. Ni, Q. Yao. “Generalizing from a few examples: A survey on few-shot learning,” *arXiv preprint*, 1904.05046, 2019.
- [50] P. S. Zarrin, R. Zimmer, C. Wenger, and T. Masquelier. “Epileptic Seizure Detection Using a Neuromorphic-compatible Deep Spiking Neural Network,” *Springer LNBI (IWBBIO20)*, Granada, Spain, 2020.

Chapter 6

Further Potential Applications

6.1 Epileptic Seizure Detection Using a Neuromorphic-compatible Deep Spiking Neural Network

This section discusses the further applications of the technology in biomedicine. For instance, the applicability of neuromorphic-based machine learning techniques for the detection of epileptic seizure has been investigated. Monitoring brain activities of Drug-Resistant Epileptic (DRE) patients is crucial for the effective management of the chronic epilepsy. Implementation of machine learning tools for analyzing electrical signals acquired from the cerebral cortex of DRE patients can lead to the detection of a seizure prior to its development. Therefore, the objective of this part was to develop a deep Spiking Neural Network (SNN) for the epileptic seizure detection. The energy and computation-efficient SNNs are well compatible with neuromorphic systems, making them an adequate model for edge-computing devices such as healthcare wearables. In addition, the integration of SNNs with neuromorphic chips enables the secure analysis of sensitive medical data without cloud computations. Results of this section are published in [1].

Introduction: Epilepsy is a common chronic neurological disorder, affecting millions of people worldwide [2]. High mortality rate of epilepsy—due to its direct and indirect consequences such as accidents, drowning, falling injuries, and sudden unexpected death due to long-term brain damages—necessitates the adequate management and monitoring of the disease for reducing its potential risks. Although the development of antiepileptic drugs have significantly improved the treatment quality of the disease, more than 30%

of patients still suffer from a particular type of epilepsy known as Drug-Resistant-Epilepsy (DRE) [2]. In the absence of a curative therapy for DRE, surgical treatment might be the only viable option for reducing the seizure frequency in patients. However, considering the complex mechanism of DRE, achieving radical improvements through surgical operations, alone, is not feasible [2]. Therefore, tracking the electrical activities of the cerebral cortex, by implanting electrode grids known as intracranial electroencephalography (iEEG) into the skull, provides important information on the treatment progress of DRE; while enabling the accurate prediction of a seizure prior to its development [3]. The availability of long duration iEEG recordings, acquired from DRE patients in clinical settings, has facilitated the adequate statistical analysis for the real-time seizure forecasting, thus transforming the epilepsy care [3, 4]. Various Machine Learning (ML) techniques, or more specifically deep learning methods, have been applied in recent studies for predicting seizures in drug-resistant epileptic patients [4, 5]. Despite the remarkable performance of the developed Deep Neural Networks (DNNs) for forecasting epileptic seizure, their implementation on the real-world mobile medical devices for point-of-care (PoC) applications is still not practical. This is due to the fact that the astonishing performance of DNNs comes at the cost of immense energy consumption and enormous computational power, thus, requiring cloud computations [4]. On the other hand, complexities associated with cloud communications such as robustness against interference, wide bandwidth requirements, low latency, and data security limit the application of DNN-based methods in sensitive fields like healthcare. On the contrary, hardware-based neuromorphic systems address these limitations by bringing the data-processing from the backend onto the chip, offering an energy-efficient platform for the real-time analysis of acquired medical data in a secure manner with less time delay [6, 7]. However, the conversion of DNN's sophisticate architecture into a rudimentary neuromorphic structure often impairs the accuracy and performance of the network [4]. As an alternative, biologically-plausible Spiking Neural Networks (SNNs) comply better with the specifications of neuromorphic systems considering their incomplex network structure [8]. Although, development of deep SNNs for performing complex tasks is still challenging (due to the discrete nature of spikes), recent attempts in using surrogate gradients for the backpropagation calculations have shown promising results for simplifying the algorithmic complexities associated with training these models [8, 9]. Therefore, the objective of this section was to develop a neuromorphic-compatible deep SNN for the epileptic seizure detection using a surrogate gradient-based learning algorithm. The implementation of the developed SNN model on IHP's HfO₂-based Resistive Random Access Memory (RRAM) neuro-

morphic chip will enable the real-time detection of diseases in the future [7]. The inherent stochasticity of CMOS-integrated RRAM devices enables the on-chip learning possibilities using various ML models including SNNs [6]. As a result, advancements in developing neuromorphic-compatible SNNs for medical applications will pave the way towards the better integration of Artificial Intelligence (AI) with PoC medical devices and biosensors [10–12]. In addition, the integration of the surrogate gradient model with novel training algorithms such as a few-shot learning, will enable the on-chip training of the SNN-based neuromorphic chips in medical applications with limited data availability [13].

Materials and Methods: The open access chronic ambulatory iEEG data, provided for the Kaggle seizure detection-prediction competition (<https://msel.mayo.edu/data.html>), were used in this study for training and evaluating the developed model. The dataset contains information on three classes of seizure (ictal), pre-seizure (preictal), and seizure-free (interictal) signals. The ictal segment of the signal is a representative of the period when a patient experiences a seizure, while the preictal segment represents the 1-hour time window prior to a seizure development. The interictal segment represents any signal period at least 4 hours before or after a seizure has been recorded. The provided data clips for the seizure prediction task were 10-minutes in duration with a sampling frequency of 400 Hz. The iEEG data were collected from canine subjects using surgically implanted electrodes with 15 channels. The similar seizure mechanism between human and dogs, make the acquired data from canine subjects very valuable for clinical applications. On the other hand, the provided data clips for the seizure detection task were 1 second in duration with a sampling frequency of 400 Hz. The iEEG data were collected from human subjects using surgically implanted electrodes with 55 channels. For training our network, 100 iEEG recordings (30–seizure (ictal) and 70–seizure-free (interictal)) of a single patient were split into the training and validation datasets with 70 to 30 percent ratios, respectively. In addition, 41 data points (27–seizure (ictal) and 14–seizure-free (interictal)) were used as the unseen test dataset for the network performance evaluations. Prior to the conversion of iEEG signals into spikes, spectrograms of the recorded data were calculated using the short-time Fourier transform in order to extract the time-frequency representations of the signals in the range of 0–200 Hz with 155 time-steps. The spectrogram transformation was done using the Scipy library of Python on the Jupyter Lab environment. As shown in Figure 6.1, a deep spiking neural network with two convolutional hidden layers was developed using the PyTorch library. The conversion of the analog iEEG spectrograms into

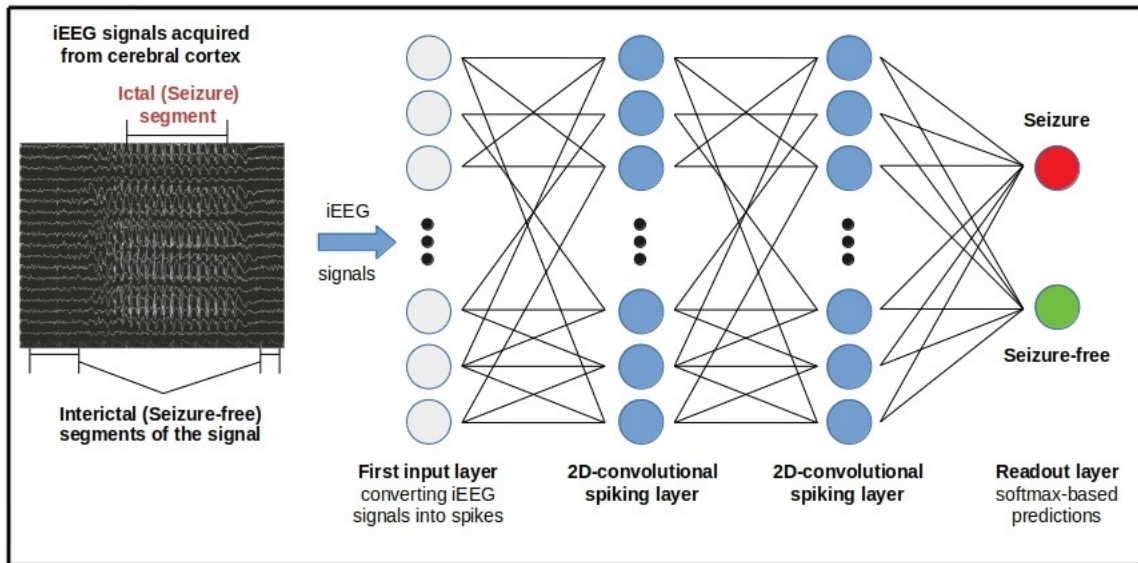


Figure 6.1: Architecture of the developed deep SNN for the epileptic seizure detection.

spikes has been done at the first input layer of the network. The weighted sum of the generated output spikes are the inputs of the following hidden layers. The readout layer with a softmax activation function has two output neurons, representing the seizure and seizure-free categories. The hidden layers are two-dimensional convolutional spiking layers with 32 neurons and a kernel size of 4×3 . It is noteworthy that, the temporal dimension of the convolution in the time-frequency domain is a representative of the propagation delays of the input spikes. Considering the discrete nature of spikes, the surrogate gradient method was used for the backpropagation calculations. For this purpose, a Sigmoid function (with a scale of 8) was used to approximate the derivative of the Heaviside step function. Rectified-Adam optimizer, with a 0.0001 learning rate, and the cross entropy error function were used for training and optimizing the network parameters. Further details of the SNN model are available at the following repository: <https://github.com/Pouya-SZ/DSC0NN>. After modeling the SNN, the pre-processed iEEG data were fed into the network for 20 training epochs with a batch size of 70. Finally, the trained network was used to predict the labels of the unseen test data.

Results and Discussions: The developed deep SNN model provided a validation accuracy of 93.3% for the epileptic seizure detection task, after 20 cycles of training. In addition, the network predicted the correct label of the unseen test signals with an accuracy of 97.6%. As illustrated in the confusion matrix of Figure 6.2(a), the SNN provided precision and sensitivity values of 100% and 96.3%, respectively, on 41 unseen

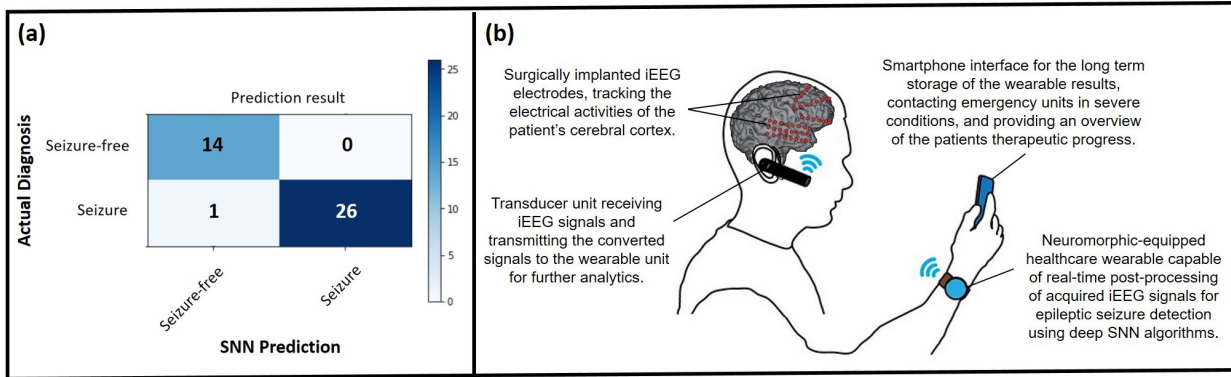


Figure 6.2: (a) Confusion matrix for the SNN performance on the unseen test data; (b) Sketch of a PoC healthcare setup for the epileptic seizure detection using a healthcare wearable equipped with neuromorphic chips and a smartphone user interface.

test data with only one false-negative prediction. The high performance of the developed SNN makes it a reliable model for edge-computing devices capable of real-time detection of seizure episodes. Figure 6.2(b) shows an example of such a wearable device which could be used as an epileptic seizure detector in a PoC setting. In such a setup, the iEEG signals acquired from patient's cerebral cortex can be transmitted by a portable transducer to the healthcare wearable such as a smart watch. The obtained data by the wearable device can be processed locally using a neuromorphic chip, prior to sending to a smartphone-based user interface for patient records.

As presented in Table 6.1, the introduced deep SNN was able to perform a complex classification task, the epileptic seizure detection, in an accuracy range comparable to the performance of the well-established DNNs. Furthermore, the biologically-inspired structure of SNNs comply better with the hardware-based neuromorphic systems, while requiring less energy and computational power, thus making them an adequate approach for edge-computing applications such as mobile medical devices. As a result, the implementation of the SNN-based ML techniques on the healthcare technologies and medical wearables will revolutionize the PoC medicine in the upcoming years.

Table 6.1: Performance of the introduced SNN compared to DNNs.

	Accuracy (%)
SNN	97.6
DNN-classifier [4]	95
Convolutional-DNN [5]	99.6

Preliminary results of the network performance for the seizure prediction task provided validation and testing accuracies of 87.5% and 93.05% , respectively. However, the repeatability of the results were questionable due to the over-fitting issue experienced during training the network. The over-fitting problem could be due to the small number of data points used for training. Moreover, the prediction task is, without a doubt, a more challenging and complex task compared to the seizure detection, considering the slight differences between two signal categories. Therefore, further investigation on a vast dataset are required for improving the network performance in the future and to make the results more generalizable and reliable. In addition, taking advantage of the phase information for the spectrogram transformation could possibly improve the network performance.

AI-equipped medical devices will bridge the gap between patients in remote locations and the medical staff by accurate monitoring of patients' health status. Moreover, AI will remarkably improve the management of chronic and degenerative conditions such as epileptic seizure by predicting the critical and emergency conditions. Additionally, collection of further health-related data from patients through edge-computing technologies, such as the one introduced in this thesis, will facilitate the statistical analysis of medical conditions with better therapeutic outcome for patients. Nonetheless, the trade-off between the mentioned benefits and the risks related to securing sensitive medical data is still a significant concern challenging governments and policy makers today. Therefore, investments for developing precise data safety regulations as well as patient-oriented secure technologies is of great importance. Among these technologies, AI-enabled neuromorphic devices will most likely provide the best platform for patients to take advantage of the AI-based medicine, while having control over their personal data and medical privacy. Therefore, the integration of the presented SNN model, for the epileptic seizure detection, on our previously developed neuromorphic platform is the future work of this thesis.

6.2 Potential Application of BiCMOS Biosensors for the Recognition of SARS-CoV-2 Through Dielectric Spectroscopy of Saliva Specimens

This section discusses the potential application of BiCMOS biosensors for the recognition of the novel coronavirus in a near-patient environment, through dielectric spectroscopy of saliva specimens. The advantages of the developed BiCMOS permittivity biosensor such as portability, low-cost, ease of operation, and

capability of rapid measurements make it a suitable technology for remote testing, required for controlling the highly transmissible coronavirus outbreak.

Introduction: Emergence of the highly transmissible novel coronavirus disease (COVID-19) has caused a worldwide pandemic with significant socio-economic impact. Severe Acute Respiratory Syndrome Coronavirus 2 (SARS-CoV-2) primarily spreads between people through close contact, leading to complications such as pneumonia [14]. In the absence of an effective vaccine or other contemporary prevention methods, rapid detection of the disease plays a pivotal role for the control of the virus spread [15]. Therefore, remote testing is necessary at outbreak hotspots such as prisons, airports, border controls, stadium entrances, drive-through testing stations, elderly houses, and hospitals for the effective identification, isolation, and contact-tracing. In addition, the best treatment outcome is possible, when patients receive appropriate medicine within the first 24–30 hours of first infection symptoms [14, 16]. However, current conventional methods used for the detection of the virus are time consuming, laborious, expensive, and require specialized facility and trained operators, thus making them inappropriate for PoC diagnosis [15, 16]. Two main types of conventional methods for the detection of SARS-CoV-2 are genetic and serological tests [15, 16]. Among serological tests, the most commonly used methods are enzyme-linked immunosorbent assay, hemagglutination inhibition assay, microneutralization–virus neutralization assay, single radial hemolysis, complement fixation assay. Serological tests characterize antibodies in bloodstream, identifying subjects who have been exposed to the virus over the course of their lives and recovered. In principal, antibodies attach themselves to specific proteins on the surface of a pathogen for disabling it. Therefore, a serological test works by using such a protein referred to as an antigen (spike protein in case of SARS-CoV-2) to capture antibodies from a blood sample. Typically, a person’s blood sample would be coated with proper antigen inside a test tube. If relevant antibodies were present, they would stick to the antigen through antigen–antibody interaction and immunocomplex-enzyme linkage, resulting in color change. Although serological tests are cheap and simple, they do not reveal any information about the current infections and they provide limited sensitivity due to cross-reaction to other types of coronaviruses. Moreover, these kinds of tests require paired serum samples, collected at the beginning of an infection and 2–4 weeks after the initial swab. Hence, results from a single serum specimen are not interpretable, making these tests unfavorable for the rapid detection of the virus in PoC [15–17]. In contrast, genetic tests identify active infections through detection of viral RNA in

Table 6.2: Available RIDTs for the PoC diagnosis of SARS-CoV-2.

Company (Author)	Test	Technology	Time (Min)	Sample
bioMérieux	BIOFIRE	serology	45	blood
Cepheid	Xpert	RT-PCR	45	nasal swab
BioMedomics	COVID19	serology	15	blood/serum
MIT	STOPCovid	CRISPR	60	nasal swab
Bosch	Vivalytic	molecular	150	blood/serum
Mesa Biotech	Accula	PCR	30	nasal swab
Abbott	ID NOW	molecular	13	nasal swab
Corman <i>et al.</i>	RdRp assay	rRT-PCR	180	nasal swab
SolGent	DiaPlexQ	RT-PCR	120	nasal swab
Roche	LightMix	qPCR	150	nasal swab

respiratory specimens. Nasal or throat swabs taken from suspected subjects are analyzed for RNAs containing SARS-CoV-2 genes. As the first step, any collected RNA from samples is copied into DNA using an enzyme called reverse transcriptase. Subsequently, the converted DNA is amplified in quantity by a process called the polymerase chain reaction. Finally, the amplified DNA is sequenced and matched against the virus' gene sequences. Reverse Transcriptase-Polymerase Chain Reaction (RT-PCR), therefore, is among the most commonly used methods in this frame, providing high specificity and sensitivity. However, the high cost and time-consuming nature of genetic tests are their main disadvantage for PoC applications. In addition, the invasive process of obtaining sputum samples or nasal swabs causes inevitable coughing in subjects, thus necessitating skilled operators with proper protection against the infection [15–17]. Apart from the two main testing methods, various technologies have been used for the development of Rapid Influenza Diagnostic Tests (RIDT), as presented in Table 6.2. Although the introduced RIDTs offer promising performance for PoC diagnosis of SARS-CoV-2, their inefficiency in terms of specificity, time, and cost of testing limit their application in the existing circumstances [15–19].

As an alternative to conventional approaches, electrochemical biosensors have long been discussed for the identification of influenza viruses through label-free DNA sensing, considering the electroactivity of DNA compounds, as reported by Palecek on the oscillographic polarography of DNA [17, 20–22]. Common electrochemical sensors used for the detection of influenza viruses are capacitive sensors, conductivity sensors, piezoelectric sensors, impedance immunosensors, and glucometers [17, 20–22]. Integrability of

these technologies into micro-scale devices is of great importance for PoC, making the diagnosis process laboratory-independent and reducing the overall testing cost and time. Similarly, Complementary Metal-Oxide Semiconductor (CMOS)-based electrochemical biosensors offer numerous advantages for PoC applications such as high accuracy, low-power consumption, rapid measurements, reliability, mass producibility, portability, low cost, operation simplicity, and compatibility with label-free measurements, thus making them a suitable technology for the detection of SARS-CoV-2 in a near-patient environment [11, 12]. Therefore, the objective of this paper was to discuss the possibility of using Bipolar CMOS (BiCMOS) biosensors for the recognition of saliva specimens contaminated by SARS-Cov-2. For this purpose, a portable BiCMOS permittivity biosensor is introduced in the next and its performance for the dielectric spectroscopy of control samples is reported. Integration of the introduced technology with advanced Machine Learning (ML) techniques could possibly enable the real-time detection of SARS-CoV-2 through characterization of saliva in PoC setup. It must be highlighted that clinical studies are yet required to investigate the diagnostic link between dielectric properties of saliva specimens and the SARS-CoV-2 virus [14, 23–25].

Results and Discussions: Although clinical experiments have yet to be performed to assess the real-world performance of the system for the recognition of SARS-CoV-2, previous studies have shown promising results for dielectric spectroscopy of saliva specimens using BiCMOS biosensors [11, 26]. Despite the fact, the high working frequency of the introduced sensor makes it suitable for the characterization of saliva samples with dominant water contents, literature studies have recommended frequency ranges of 100-500 KHz for the dielectric spectroscopy of influenza viruses [20]. Therefore, in case of an inadequate performance with clinical samples, a new design is required to tune the working frequency of the sensor into lower ranges.

As previously discussed, nasopharyngeal swab is the most commonly obtained specimen for the detection of influenza due to its high concentration of virus [23]. However, considering its invasive and uncomfortable collection procedure, it is challenging to obtain these types of swab in a safe manner without risking an operator's exposure to the infection. Therefore, it is necessary to develop novel diagnostic tools for the characterization of saliva, as an alternative with better patient compliance, for the recognition of SARS-CoV-2 in PoC [23, 24].

Previous studies on the dielectric spectroscopy of saliva using BiCMOS sensors have reported higher

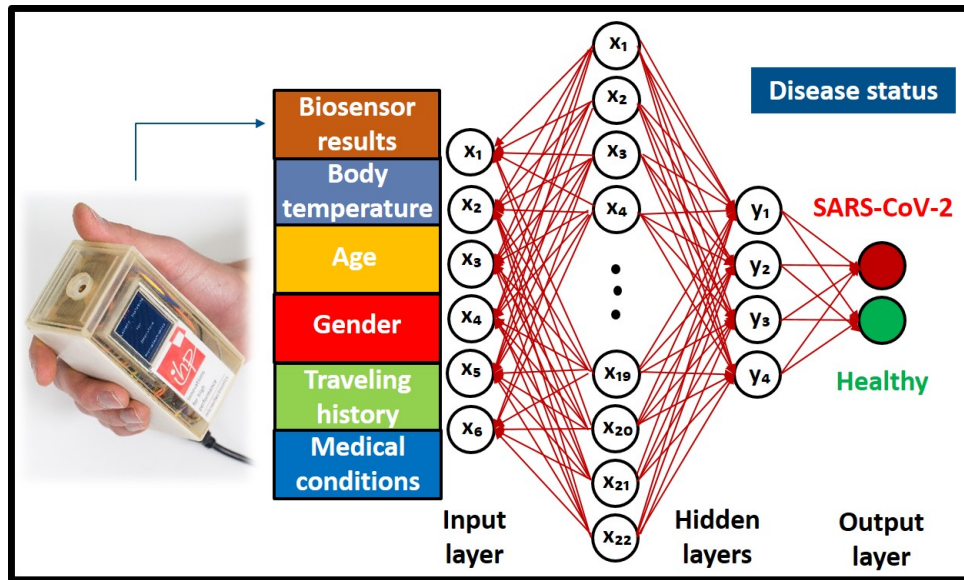


Figure 6.3: Architecture of a neural network for the classification of SARS-CoV-2.

sensitivity values compared to the sensor specificity [11]. In other words, sensor has provided more false positive results than false negative, which is significantly important for controlling virus outbreak through accurate contact-tracing and data transmission gathering. Furthermore, a highly sensitive sensor would enable the accurate exclusion of healthy subjects, thus reducing the burden on the healthcare system and lab-based testing units.

Latest studies on the mechanism of SARS-CoV-2 have highlighted the importance of demographic parameters for the effective identification and treatment of objective cases [14, 15]. These parameters include, but are not limited to, age, gender, body temperature, blood type, living district, travel history, medical conditions, etc. As a result, implementation of ML methods is necessary for the comprehensive recognition of SARS-CoV-2 in PoC by concurrent consideration of patients' demographic information together with biosensor measurements on the characterization of saliva specimens. Figure 6.3 illustrates the basic structure of a neural network for the classification of SARS-CoV-2 subjects in PoC. The importance of data analytics through ML approaches has been previously described for the recognition of diseases using biosensors [7].

Conclusions and Future Work: This section discussed the significance of using BiCMOS dielectric biosensors for the recognition of saliva samples of SARS-CoV-2 in PoC. The developed BiCMOS permit-

tivity biosensor was proposed as a potential technology for this specific application. The high performance of the biosensor as well as its portability, low cost, ease of operation, and rapid analysis makes it an adequate technology for near-patient measurements required at virus outbreak hotspots. Clinical assessments on saliva samples of COVID-19 patients are required for the assessment of the proposed approach in the future. Integration of ML techniques on the sensor output together with the demographic information of subjects can enable the effective identification and prevention of the virus spread.

Bibliography

- [1] P. S. Zarrin, R. Zimmer, C. Wenger, and T. Masquelier. “Epileptic Seizure Detection Using a Neuromorphic-compatible Deep Spiking Neural Network,” *Springer LNBI (IWBBIO20)*, Granada, Spain, 2020.
- [2] J. Sheng, S. Liu, H. Qin, B. Li, X. Zhang. “Drug-resistant epilepsy and surgery,” *Current neuropharmacology*, vol. 16, pp. 17–28, 2018.
- [3] M.J. Cook, et al. “Prediction of seizure likelihood with a long-term, implanted seizure advisory system in patients with drug-resistant epilepsy: a first-in-man study,” *The Lancet Neurology*, vol. 12, pp. 563–571, 2013. **12**, (2013).
- [4] I. Kiral-Kornek. “Epileptic seizure prediction using big data and deep learning: toward a mobile system,” *EBioMedicine*, vol. 27, pp. 103–111, 2018.
- [5] H. Daoud, M.A. Bayoumi. “Efficient epileptic seizure prediction based on deep learning,” *IEEE transactions on biomedical circuits and systems*, vol. 13, pp. 804–813, 2019.
- [6] C. Wenger, F. Zahari, M.K. Mahadevaiah, E. Perez, I. Beckers, H. Kohlstedt, and M. Ziegler. “Inherent Stochastic Learning in CMOS-Integrated HfO₂ Arrays for Neuromorphic Computing,” *IEEE Electron Device Letters*, vol. 40, no. 4, pp. 639–642, 2019.
- [7] P.S. Zarrin and C. Wenger. “Pattern Recognition for COPD Diagnostics Using an Artificial Neural Network and Its Potential Integration on Hardware-Based Neuromorphic Platforms,” *Springer LNCS (ICANN19)*, Munich, Germany, September, 2019, pp. 284–288.

- [8] E.O. Neftci, H. Mostafa, F. Zenke. “Surrogate gradient learning in spiking neural networks,” *arXiv preprint*, 190109948, 2019.
- [9] R. Zimmer, T. Pellegrini, S.F. Singh, T. Masquelier. “Technical report: supervised training of convolutional spiking neural networks with PyTorch,” *arXiv preprint*, 191119124, 2019.
- [10] P.S. Zarrin, A. Escoto, R. Xu, M. D. Naish, R. V. Patel, and A. L. Trejos. “Development of a 2-DOF sensorized surgical grasper for grasping and axial force measurements,” *IEEE Sensors Journal*, vol. 18, no. 7, pp. 2816–2826, 2018.
- [11] P.S. Zarrin, F.I. Jamal, N. Roeckendorf, C. Wenger. “Development of a Portable Dielectric Biosensor for Rapid Detection of Viscosity Variations and Its In-vitro Evaluations Using Saliva Samples of COPD Patients and Healthy Control,” *Healthcare*, vol. 7, no. 11, 2019.
- [12] P.S. Zarrin, F.I. Jamal, S. Guha, J. Wessel, D. Kissinger, C. Wenger. “Design and Fabrication of a BiCMOS Dielectric Sensor for Viscosity Measurements: A Possible Solution for Early Detection of COPD,” *Biosensors*, vol. 8, no. 78, 2018.
- [13] Stewart, K., Neftci, E. and Orchard, G: On-chip Few-shot Learning with Surrogate Gradient Descent on a Neuromorphic Processor. *arXiv preprint*, **1910**, 04972 (2019).
- [14] W.J. Guan, Z.Y. Ni, Y. Hu, W.H. Liang, C.Q. Ou, J.X. He, L. Liu, H. Shan, C.L. Lei, D.S. Hui, B. Du. “Clinical characteristics of coronavirus disease 2019 in China,” *New England journal of medicine*, vol. 382, no. 18, pp. 1708–1720, 2020.
- [15] J. Pang, M.X. Wang, I.Y.H. Ang, S.H.X. Tan, R.F. Lewis, J.I.P. Chen, R.A. Gutierrez, S.X.W. Gwee, P.E.Y. Chua, Q. Yang, X.Y. Ng. “Potential rapid diagnostics, vaccine and therapeutics for 2019 novel coronavirus (2019-nCoV): a systematic review,” *Journal of clinical medicine*, vol. 9, no. 3, p. 623, 2020.
- [16] K. Dziabowska, E. Czaczyk, D. Nidzworski. “Detection methods of human and animal influenza virus—current trends,” *Biosensors*, vol. 8, no. 4, p. 94, 2018.
- [17] L. Krejcova, D. Hynek, V. Adam, J. Hubalek, R. Kizek. “Electrochemical sensors and biosensors for influenza detection,” *Int Journal of Electrochemical Science*, vol. 7, no. 11, pp. 10779–10801, 2012.

- [18] J.S. Gootenberg, O.O. Abudayyeh, J.W. Lee, P. Essletzbichler, A.J. Dy, J. Joung, V. Verdine, N. Donghia, N.M. Daringer, C.A. Freije, C. Myhrvold. “Nucleic acid detection with CRISPR-Cas13a/C2c2,” *Science*, vol. 356, no. 6336, pp. 438–442, 2017.
- [19] V.M. Corman, O. Landt, M. Kaiser, R. Molenkamp, A. Meijer, D.K. Chu, T. Bleicker, S. Brünink, J. Schneider, M.L. Schmidt, D.G. Mulders. “Detection of 2019 novel coronavirus (2019-nCoV) by real-time RT-PCR,” *Eurosurveillance*, vol. 25, no. 3, p. 2000045, 2020.
- [20] C. Cheng, H. Cui, J. Wu, S. Eda. “A PCR-free point-of-care capacitive immunoassay for influenza A virus,” *Microchimica Acta*, vol. 184, no. 6, pp. 1649–1657, 2017.
- [21] K. Yamanaka, M. Saito, K. Kondoh, M.M. Hossain, R. Koketsu, T. Sasaki, N. Nagatani, K. Ikuta, E. Tamiya. “Rapid detection for primary screening of influenza A virus: microfluidic RT-PCR chip and electrochemical DNA sensor,” *Analyst*, vol. 136, no. 10, pp. 2064–2068, 2011.
- [22] X. Zhang, A.N. Dhawane, J. Sweeney, Y. He, M. Vasireddi, S.S. Iyer. “Electrochemical assay to detect influenza viruses and measure drug susceptibility,” *Angewandte Chemie*, vol. 127, no. 20, pp. 6027–6030, 2015.
- [23] J. Yoon, S.G. Yun, J. Nam, S.H. Choi, C.S. Lim. “The use of saliva specimens for detection of influenza A and B viruses by rapid influenza diagnostic tests,” *Journal of virological methods*, vol. 243, pp. 15–19, 2017.
- [24] J.M. Lee, E. Garon, D.T. Wong. “Salivary diagnostics,” *Orthodontics & craniofacial research*, vol. 12, no. 3, pp. 206–211, 2009.
- [25] R. Xu, B. Cui, X. Duan, et al. “Saliva: potential diagnostic value and transmission of 2019-nCoV,” *Int J Oral Sci*, vol. 12, no. 11, 2020.
- [26] P.S. Zarrin, N. Roeckendorf, C. Wenger. “Exasens: a novel dataset for the classification of saliva samples of COPD patients”, IEEE Dataport, 2020.

Chapter 7

Concluding Remarks and Future Work

7.1 Summary

The work presented in this thesis described the development of a novel AI-equipped biosensor for the management of COPD in a PoC setup. Throughout this thesis, a comprehensive literature review was performed to show the absence of an appropriate technology for the recognition of COPD in a home-care environment. Up to date, there are no commercially available technology for COPD staging in PoC, due to the shortcomings of conventional testing methods such as spirometry and complexity of tracking salivary protein biomarkers using portable devices. Therefore, the novel hypothesis of this work was to scrutinize whether the mechanical (viscosity) or electrical (dielectric) properties of saliva change upon the development of a COPD; and whether ML tools, applied on this information together with the demographic parameters, can identify the diagnostic status of patients. As a result, a portable permittivity biosensor was developed in this work and its *in-vitro* performance for the recognition of COPD samples was evaluated using saliva samples of COPD patients and healthy controls. Results of the clinical assessments were reported online in the frame of a novel dataset, Exasens, for the public use. Moreover, various ML techniques were applied on the obtained results, demonstrating the significant role of AI-based techniques for the management of COPD. The deployment of the developed ML models on a memristive neuromorphic chip has shown the practicality and importance of using neuromorphic platforms for medical applications, with strict data safety regulations.

Contributions: The work presented in this thesis shines a spotlight on the need for further investments in PoC technologies for COPD management. Nevertheless, the proposed CMOS-based biosensor, integrated with neuromorphic-compatible ML techniques, has the potential to revolutionize the management and recognition of chronic and degenerative diseases such as COPD near, or at, the point of patient care. Neuromorphic-equipped medical devices will most likely provide the best platform for patients to take advantage of the AI-based medicine, with strong data security and high privacy. The more specified contributions of this thesis are as follows:

- A BiCMOS permittivity biosensor was developed for the rapid characterization of saliva samples of COPD patients and healthy controls. The biosensor was fully integrated into a handheld device and provided promising results through clinical assessments. The capability of the biosensor to distinguish between dielectric properties of saliva samples of COPD and HC, opened up a new window into different methodologies for the early recognition of COPD. The low-cost, high accuracy and repeatability, simplified packaging, ease of cleaning, portability, and rapid detection capability of the biosensor made it a suitable technology for medical diagnostics in PoC.
- Various ML techniques including perceptron-based artificial neural networks, XGBoost, SVM, NB, and LR were applied for the *in-vitro* classification of saliva samples into COPD and HC categories. Although the XGBoost algorithm provided the best performance for classifying saliva samples in the backend, the better compatibility of ANN with the hardware implementation requirements made it a favorable model for the on-chip recognition using a memristive neuromorphic chip. Therefore, the shortcomings of cloud-based ML techniques for real-world medical applications, such data safety concerns and high computation cost, were addressed through hardware-based approaches.
- The concept of the on-chip recognition of saliva samples of COPD patients and HC using a memristive neuromorphic processor was investigated. A hardware-friendly artificial neural network simulation was developed and trained in the backend for the classification of COPD and HC samples using real clinical data. Subsequently, the trained classification model was thresholded into 10 levels and was deployed on a memristive neuromorphic processor for on-chip recognition purposes. The digital neuromorphic chip provided a remarkable accuracy for the on-chip recognition of COPD and HC samples, offering an alternative approach to cloud-based ML methods required for the management

of chronic disease in PoC environments.

7.2 Future Work

This thesis investigated the feasibility of using CMOS-based biosensors for the characterization of saliva samples of COPD patients and their on-chip recognition using neuromorphic-oriented machine learning algorithms. Several points of improvement were identified that could increase the quality of measurements and the system performance in the future. In addition, other potential applications of the neuromorphic technology in biomedicine and biomedical engineering were discussed. The following points highlight the expected developments and modifications as future work:

- As a common issue with capacitance-based sensing technologies, the vulnerability of the developed biosensor for characterizing highly water-dominated mediums such as saliva needs to be addressed in the future by enhancing the sensor design.
- Brain-inspired machine learning algorithms such as spiking neural networks, with better compatibility with neuromorphic platforms, will be developed for the COPD recognition task using the collected clinical data.
- For the better replication of simulation neural networks on neuromorphic platforms, binary ANN models will be developed and implemented for the COPD recognition task. Furthermore, possibility of using analog neuromorphic platforms, capable of replication of analog parameters on-chip, will be investigated as an alternative solution for the discussed issue.
- As a potential application for bio-neuromorphics, the proposed technology in this thesis will be used for the on-chip forecasting of epileptic seizure in a PoC environment using low-power health-care wearables. In addition, the practicality of using the developed biosensor for the recognition of coronavirus-contaminated saliva samples will be investigated in the future.

Appendix A

Technical Drawings and Expanded Views

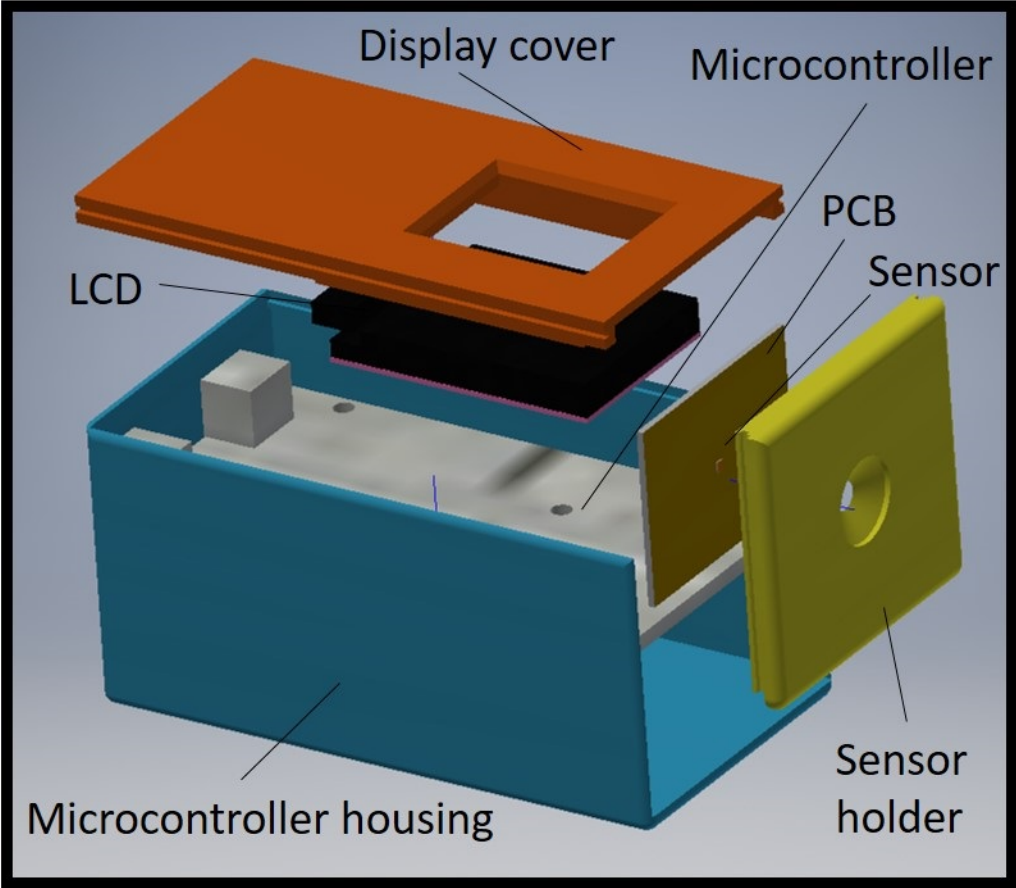


Figure A.1: Expanded view of the biosensor packaging illustrated in Fig. 3.9.

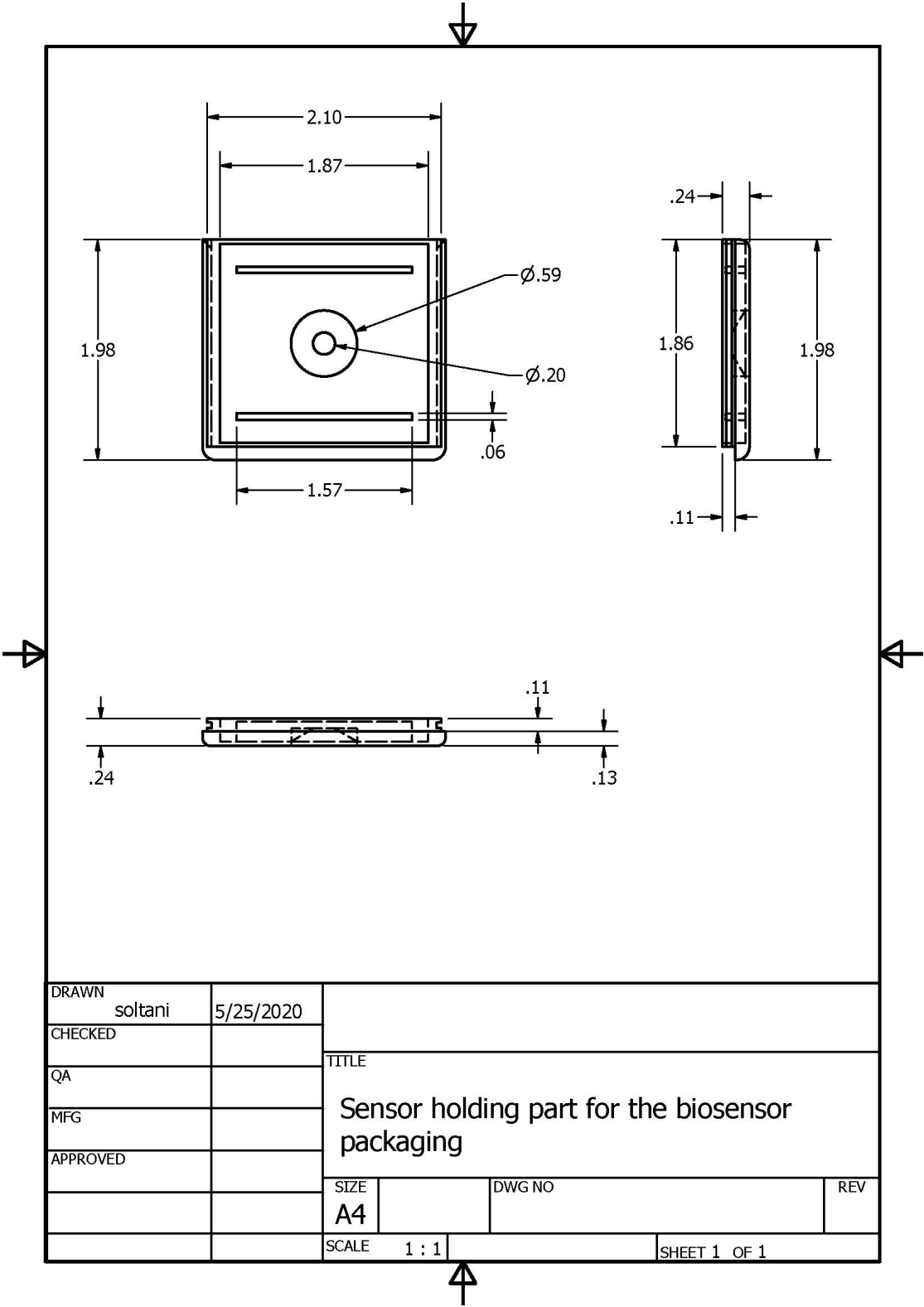


Figure A.2: Technical drawing for the sensor holding part, illustrated in Fig. 3.9.

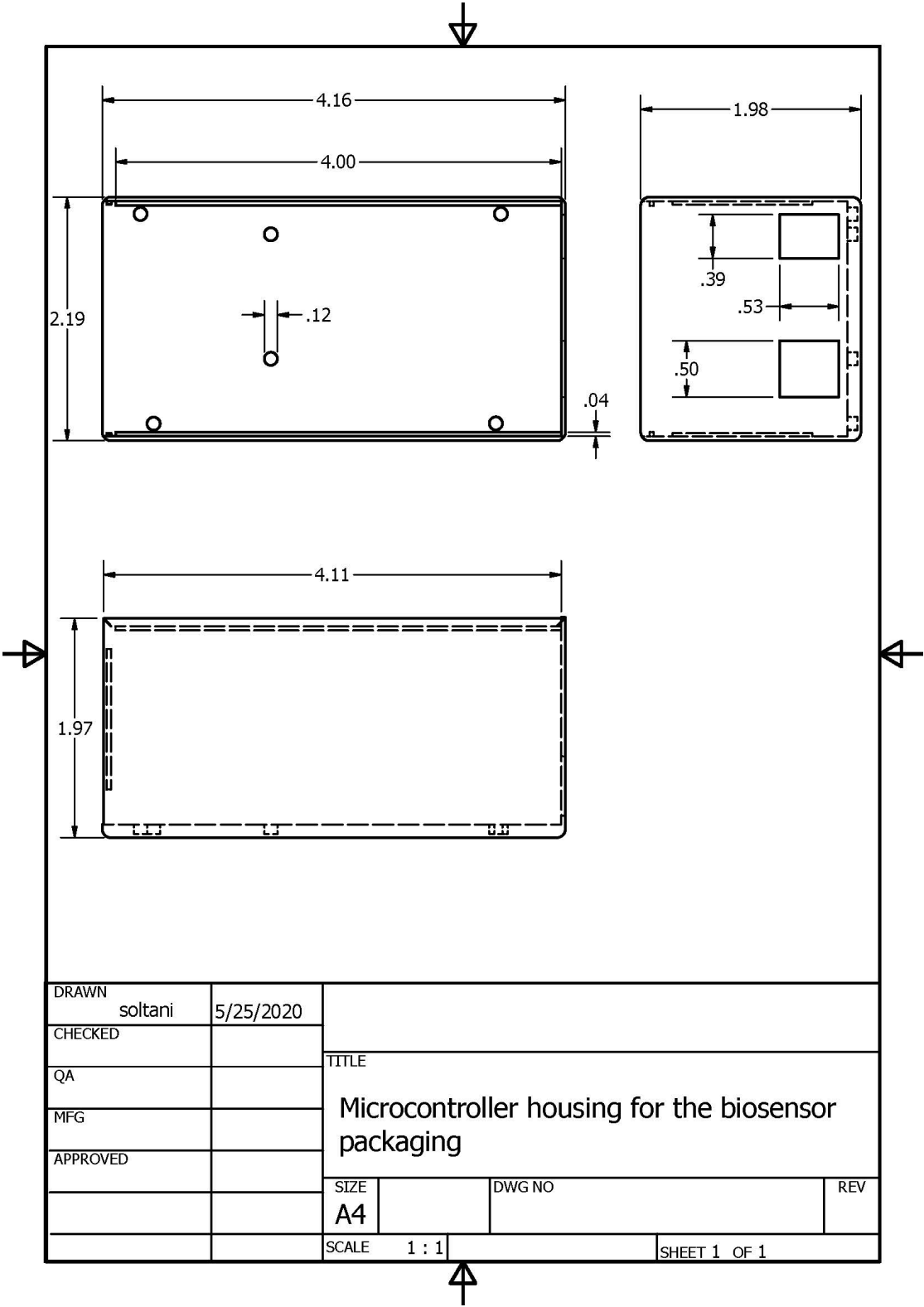


Figure A.3: Technical drawing for the microcontroller housing, illustrated in Fig. 3.9.

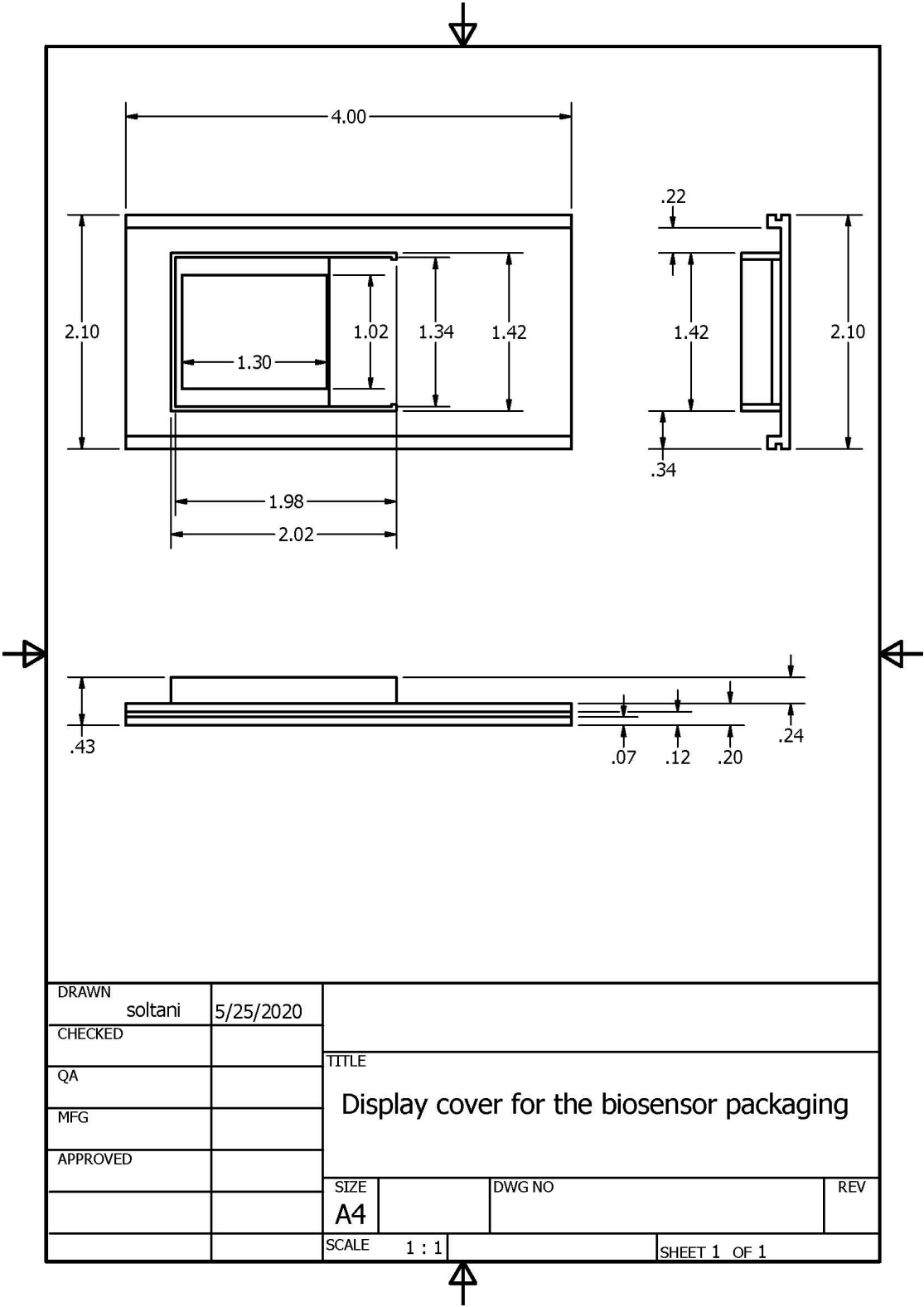


Figure A.4: Technical drawing for the display cover, illustrated in Fig. 3.9.

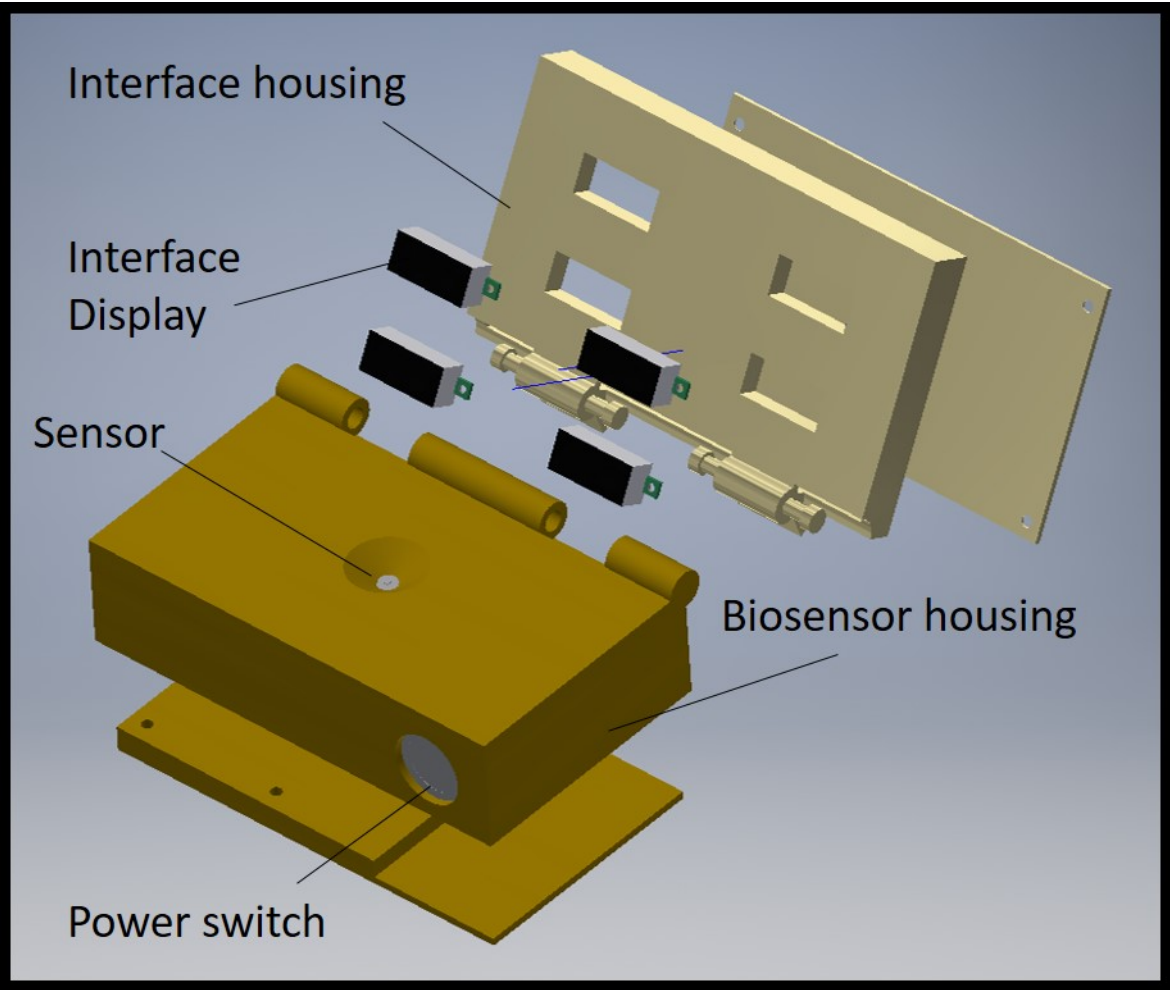


Figure A.5: Expanded view of the laptop-shaped foldable packaging illustrated in Fig. 3.10.

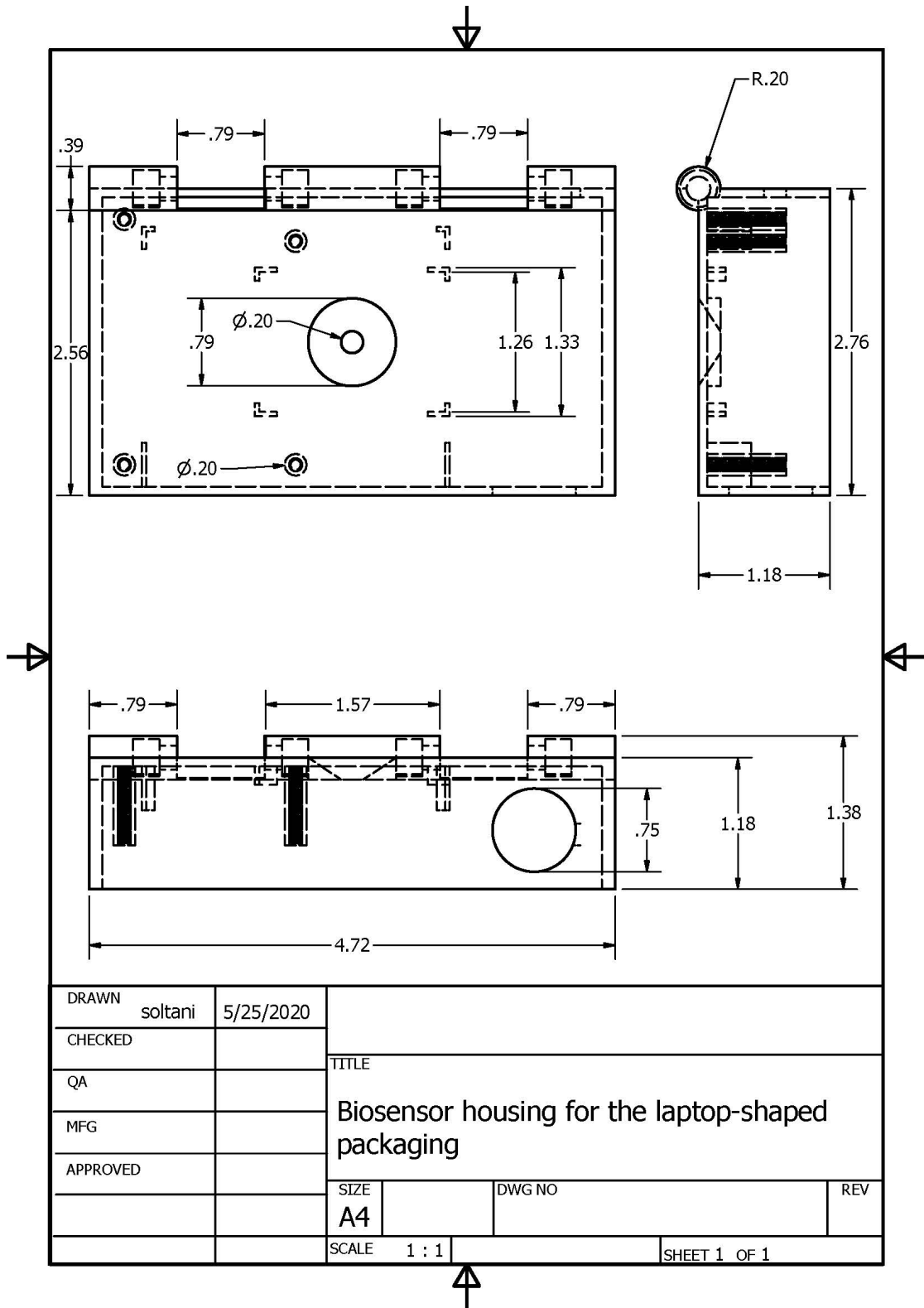


Figure A.6: Technical drawing for the biosensor housing, illustrated in Fig. 3.10.

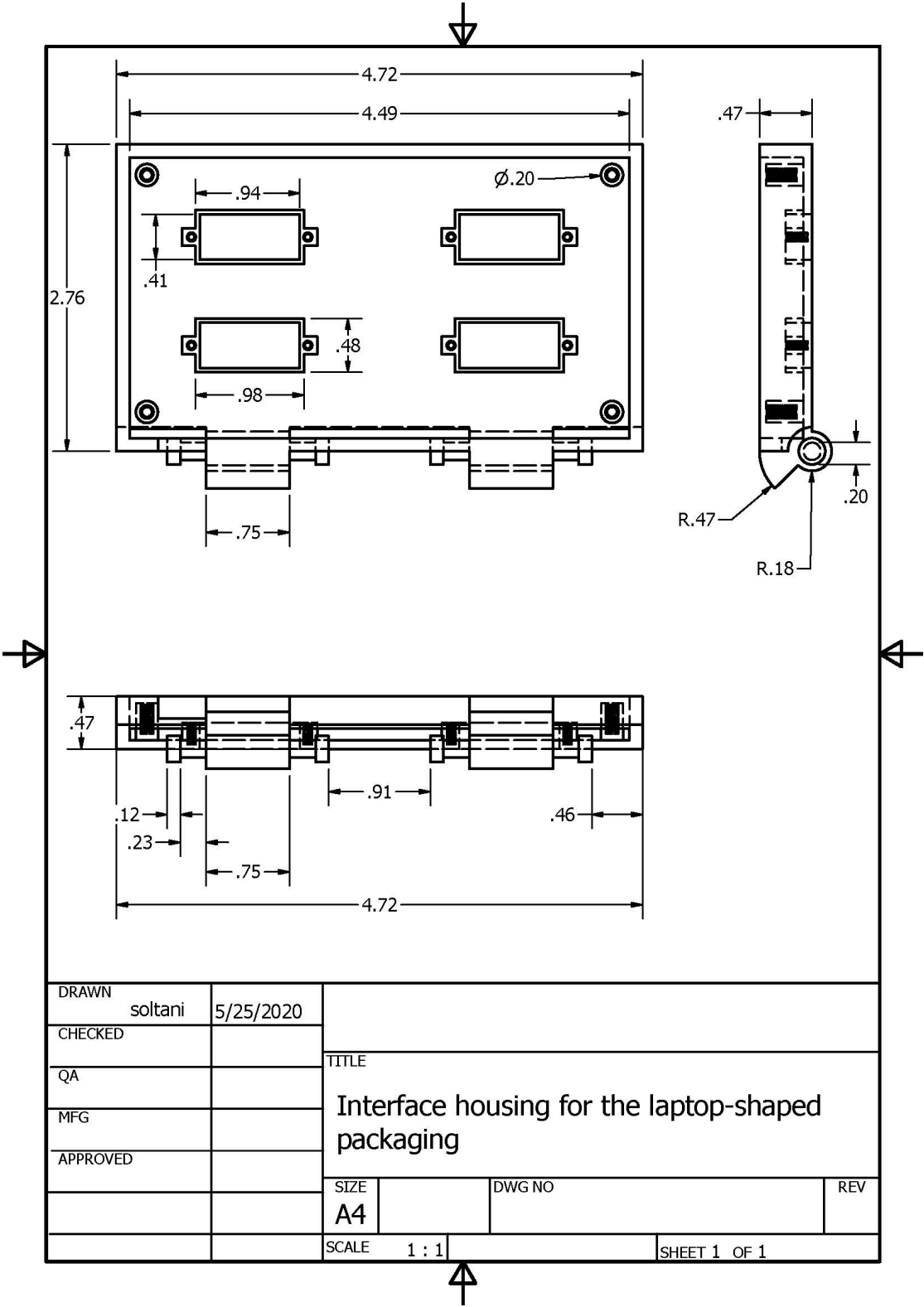


Figure A.7: Technical drawing for the interface housing, illustrated in Fig. 3.10.